Sholeh Ma'mun

Selection and Characterization of New Absorbents for Carbon Dioxide Capture

Doctoral thesis 2005:156

Faculty of Natural Science and Technology
Department of Chemical Engineering

NTNU

to

My wife, Bertha
and
My daughter, Nada

Abstract

Removal of acidic gases, in particular CO_2, is an important industrial operation. Carbon dioxide is produced in large quantities by fossil–fuel–fired power plants, steel production, the production of petrochemicals, cement production, and natural gas purification. The global climate change, where CO_2 is found to be a major contributor, is one of the most important and challenging environmental issues facing the world community. This has motivated intensive research on CO_2 capture and storage.

Carbon dioxide capture by an absorption process is one of the most common industrial technologies today. Recent economic studies (Desideri and Corbelli, 1998) indicate that the process will also remain competitive in the future. One of the key improvements under development is new, faster and more energy–efficient absorbents. A chemical to be used as a commercial absorbent must have high net cyclic capacity, high absorption rate for CO_2, and good chemical stability. Alkanolamines are the most commonly used chemical absorbents for the removal of acidic gases today.

In the first part of this thesis, an experimental screening of new absorbents for CO_2 capture was performed by absorption of CO_2 into both single absorbents and absorbent mixtures for amine–based and non–amine–based systems at 40 °C. From testing of ~30 systems, it was found that an aqueous 30 mass % AEEA {2-(2-aminoethyl-amino)ethanol} solution seems to be a potentially good absorbent for capturing CO_2 from atmospheric flue gases. It offers high absorption rate combined with high absorption capacity. In addition to AEEA, MMEA (2-(methylamino)ethanol) also needs to be considered. It could have a good potential when used in contactors where the two phases are separated, like in membrane contactors, whereas indications from the study showed foaming tendencies that will make it difficult to use in ordinary towers.

AEEA as the selected absorbent obtained from the screening tests was further investigated to determine its vapor–liquid equilibrium characteristics. The experimental and modeling study of the solubility of CO_2 in aqueous AEEA is described in the second part of the thesis. From the VLE data, it is shown that AEEA does not only offer high absorption rate combined with high absorption capacity in terms of CO_2 loading but also offers higher cyclic capacity and lower regeneration energy requirement for some cases

studied compared to MEA. In addition, a VLE thermodynamic modeling of the aqueous AEEA solution was performed by use of a modified Deshmukh–Mather model (Deshmukh and Mather, 1981) as well as NMR analyses to determine the species distribution in the liquid phase as function of CO_2 loading. A two–stage calculation was performed to model the VLE of the CO_2–AEEA–H_2O system. The first stage of the calculation was the regression of the parameters involved in the temperature dependency of the chemical equilibrium constants without binary interaction parameters taken into account. As seen from the results, the model provides a very good representation of the experimental data over a range of temperatures from 40 to 120 °C. The second regression of the VLE data was then performed to evaluate the binary interaction parameters i.e. the short–range terms in the Deshmukh–Mather model. However, only minor improvements in the overall fit were achieved.

In the last part of the thesis, an experimental kinetic study of the CO_2–AEEA–H_2O system was performed using a string of disc contactor over a range of temperatures from 32 to 49 °C for various concentrations of AEEA. The reaction mechanism used for interpretation of the kinetics was the *single step* and *termolecular mechanism* approach proposed by Crooks and Donnellan (1989) and reviewed by da Silva and Svendsen (2004). The results showed that the observed pseudo–first order rate constant is in good agreement with the equation proposed for this mechanism. In addition, the physical properties, density and viscosity, have been measured to determine the physico–chemical parameters. The solubility of N_2O in AEEA was also measured to estimate the solubility of CO_2 in AEEA solution.

Acknowledgements

Alhamdulillah, a three–year work in the field of CO_2 absorption carried out at the Department of Chemical Engineering, NTNU, Trondheim, Norway has been finished and reported in this Ph.D. thesis. I would like to express my deepest gratitude to all those people who have helped and supported me along the way.

First of all, I would like to thank my supervisor, Professor Hallvard F. Svendsen, for giving me the opportunity to join in the CO_2 research group to pursue this Ph.D. degree at the department. I would like to thank him for his supervision with his trustworthy advice and support during these years.

I would also like to thank my former supervisor, Professor Sigurd Skogestad, for giving me a chance to join in his research group, Process Control group. I would like to thank him for his supervision during the first one–and–half year of my Ph.D. study.

I wish to thank SINTEF senior scientist Olav Juliussen for his advice and his help for the experimental work, technicians Jan–Morten Roel, Dagfinn P. Tungen, and senior scientist Kai W. Hjarbo for their help on the experimental setups and the data acquisition system.

I also thank all the CO_2 research group members for the valuable discussions and suggestions. Their involvements on the work are appreciated, Dr. Karl A. Hoff on the screening tests, Dr. Jana P. Jakobsen on the VLE modeling part, and Dr. Vishwas Y. Dindore on the kinetic experimental work.

Finally, I would like to thank my family for supporting me during all the years of my studies. Special thanks go to my wife Bertha and my daughter Nada for always being there.

For the financial support, I would like to thank Indonesian government through the QUE Project, the Norwegian Research Council through the Klimatek Programme, and the European Commission through the CASTOR Integrated Project.

Contents

List of Symbols

Uppercase Latin Letters

A_γ	Debye–Hückel limiting slope [-]
B	function of temperature and dielectric constant of solvent [-]
C	concentration [mol L^{-1}]
D	diffusivity [m^2 s^{-1}]
E	enhancement factor [-]
F	objective function [-]
G	Gibbs free energy [J]
H	Henry's law constant [Pa]
Ha	Hatta number [-]
ΔH	enthalpy [kJ mol^{-1}]
I	ionic strength [mol kg^{-1}]
K	equilibrium constant [-]
N	number of component, flux [mol m^{-2} s^{-1}]
N_A	Avogadro number [6.023×10^{23} mol^{-1}]
P	total pressure [Pa]
P^o	vapor pressure [Pa]
P_w^o	saturation pressure of water [Pa]
Q	cyclic capacity [mol L^{-1}], heat duty [kJ mol^{-1}], flowrate of gas component at normal condition [NL min^{-1}]
R	universal gas constant [8.314 J mol^{-1} K^{-1}]
Re	Reynolds number ($\rho vd/\mu$)
S	entropy [J K^{-1}]
Sc	Schmidt number ($\mu/\rho D$)
Sh	Sherwood number (kl/D)
T	absolute temperature [K]
U	internal energy [J]
V	volume [L]

W	weight [kg]

Lowercase Latin Letters

a	activity, ionic size [Å], specific area [$m^2\ m^{-3}$]
c	constants [-]
c_p	specific heat [kJ $kg^{-1}\ K^{-1}$]
d	diameter [m]
e	electronic charge [1.602×10^{-19} C]
f	fugacity [Pa]
$\bar{g}$	partial molar Gibbs free energy [J mol^{-1}]
k	first-order reaction rate constant [s^{-1}]
k_G	mass transfer coefficients in gas phase [mol $m^{-2}\ s^{-1}$ Pa]
k_L	mass transfer coefficients in liquid phase [m s^{-1}]
m	molality [mol kg^{-1}], solubility of gas [-]
n	rate of mole [mol s^{-1}], number of mole [mol], Stephens-Morris constant
p	partial pressure [Pa]
pK_{a1}	protonation constant for monoprotonated AEEA [-]
pK_{a2}	protonation constant for diprotonated AEEA [-]
q	charge of particle [C]
r	distance in a vacuum medium [m], reaction rate/absorption rate [mol $L^{-1}\ s^{-1}$]
s	molar entropy [J $mol^{-1}\ K^{-1}$]
t	time [s]
v	molar volume [$m^3\ mol^{-1}$], velocity [m s^{-1}]
$\bar{v}^{\infty}$	partial molar volume at infinite dilution [$m^3\ mol^{-1}$]
v_m^0	molar volume at normal condition [22.41 NL mol^{-1}]
x	liquid–phase mole fraction [-], mass fraction [-], distance [m]
y	vapor–phase mole fraction [-]
z	absolute charge of ionic species, compressibility factor [-]

Greek Letters

α	loading [mol mol^{-1}], Stephens-Morris constant
β	parameter for the interaction of species *i* with species *j* [kg mol^{-1}]
δ	film thickness [m]
ε_o	permittivity of vacuum (8.85419×10^{-12} C^2 J^{-1} m^{-1})
ε_r	dielectric constant [-]
γ	activity coefficient [-]
Γ	wetting rate [kg m^{-1} s^{-1}]
φ	fugacity coefficient [-]
κ^{-1}	shielding length or the Debye length [m]
μ	chemical potential, viscosity [Pa s]
Θ	Poynting factor
ρ	density [kg m^{-3}]
υ	stoichiometric coefficient
ξ	extents of reaction [-]
ψ	distribution of the surface element [-]

Subscripts

$AEEAH^+$	monoprotonated AEEA
$AEEACOO^-$	carbamate of AEEA
$^+HAEEACOO^-$	protonated carbamate of AEEA
$^+HAEEAH^+$	diprotonated AEEA
$^-OOCAEEACOO^-$	dicarbamate of AEEA
b	bulk
des	desorption
G	gas phase
i	species *i*, interphase
j	species *j*, reaction *j*

L	liquid phase
LM	logarithmic mean
obs	observed
p	primary
s	secondary, solution
sens	sensible
strip	stripping
T	total
vap	vapor
w	water

Superscripts

∞	infinite dilution
0	initial condition
calc.	value calculated by model
E	excess
exp.	experimentally measured value
in	inlet
o	standard state
out	outlet

Abbreviations

AEEA	2-(2-aminoethyl-amino)ethanol
AMP	2-amino-2-methyl-1-propanol
AZ	alkazid
B	base
$BaCl_2$	barium chloride
$BaCO_3$	barium carbonate
BEA	2-(butylamino)ethanol
CO_2	carbon dioxide
CORAL	CO_2 removal absorption liquid
COS	carbon oxyxulfide

DEA	diethanolamine
DGA	diglycolamine
EMEA	2-(ethylamino)ethanol
H_2S	hydrogen sulfide
H_2SO_4	sulfuric acid
HCl	hydrochloric acid
IR	infrared
K_2CO_3	potassium carbonate
KOH	potassium hydroxide
LNG	liquid natural gas
M	molar concentration [mol L^{-1}]
MDEA	*N*-methyldiethanolamine
MEA	monoethanolamine
MMEA	2-(methylamino)ethanol
MSA	mean spherical approximation
N_2	nitrogen
NaOH	sodium hydroxide
NH_3	ammonia
NL	normal liter
NMR	nuclear magnetic resonance
NRTL	non-random two liquid
PG	Potassium glycinate
PR	Peng-Robinson
PT	potassium salt of taurine
PZ	piperazine
SAFT	statistical associating fluid theory
TEA	triethanolamine
TNO	the Netherlands Organization for Applied Scientific Research
UNIFAC	universal functional activity coefficient
UNIQUAC	universal quasi-chemical theory
VLE	vapor-liquid equilibria

CHAPTER 1

General Introduction

1.1 Background

Removal of acidic gases, e.g., carbon dioxide (CO_2), is an important industrial operation. Carbon dioxide is produced in large quantities by many important industries such as fossil–fuel–fired power plants, steel production, chemical and petrochemical manufacturing, cement production, and natural gas purification. The reasons for the CO_2 removal are traditionally technical and economical concerns. Carbon dioxide present in natural gas will reduce the heating value of the gas and as an acid component it has the potential to cause corrosion in pipes and process equipment and also, according to Astarita *et al.* (1983), CO_2 causes catalyst poisoning in ammonia synthesis. Natural gas pipe lines usually permit from 1 to 2 mol % CO_2 and sometimes as high as 5 mol % (Buckingham, 1964). In the past decades, CO_2 removal from flue gas streams started as a potentially economic source of CO_2, mainly for enhanced oil recovery (EOR) operations. Moreover, CO_2 was also produced for other industrial applications such as carbonation of brine, welding as an inert gas, food and beverage carbonation, dry ice, urea production, and soda ash industry (Rao and Rubin, 2002; Suda *et al.*, 1997). However, environmental concerns, such as the global climate change, are now focused as one of the most important and challenging environmental issues facing the world community, and have motivated intensive research on CO_2 capture and sequestration. Carbon dioxide as one of the greenhouse gases (GHG) is currently responsible for over 60% of the enhanced greenhouse effect, methane (CH_4) contributes 20%, and the remaining 20% is caused by nitrous oxide (N_2O), a number of industrial gases, and ozone. Scientific evidence now strongly suggests that increased levels of GHG may lead to higher temperature, and cause climate change on a global scale. Various climate models estimate that the global average temperature may rise by ~1.4 – 5.8 °C by the year 2100 (Williams, 2002).

A wide range of technologies currently exist for separation and capture of CO_2 from gas streams as given by Rao and Rubin (2002). Such systems have been used in the chemical industry and in the production of technical gases for industrial and laboratory use (Desideri and Corbelli, 1998). In principle, various methods could be used for the removal of CO_2. According to Shaw and Hughes (2001), several process–related factors affect the selection of the appropriate method such as CO_2 concentration in the feed stream, nature of other contaminants present in the feed stream (e.g., H_2S and water in natural gas), pressure and temperature at which the feed stream is available, product considerations, and other considerations such as geographical location which can be a significant consideration when treating natural gas, as gas wells can be remote. Figure 1-1 shows the general guidelines for selection of the CO_2 removal processes based on these considerations. It can be seen from this figure that absorption in a liquid is the most common process used in the industry for CO_2 removal today. For economic reasons, the absorbents must have a low solvent cost, a high net cyclic capacity and high reaction/absorption rate for CO_2 and must be an energy saving solvent.

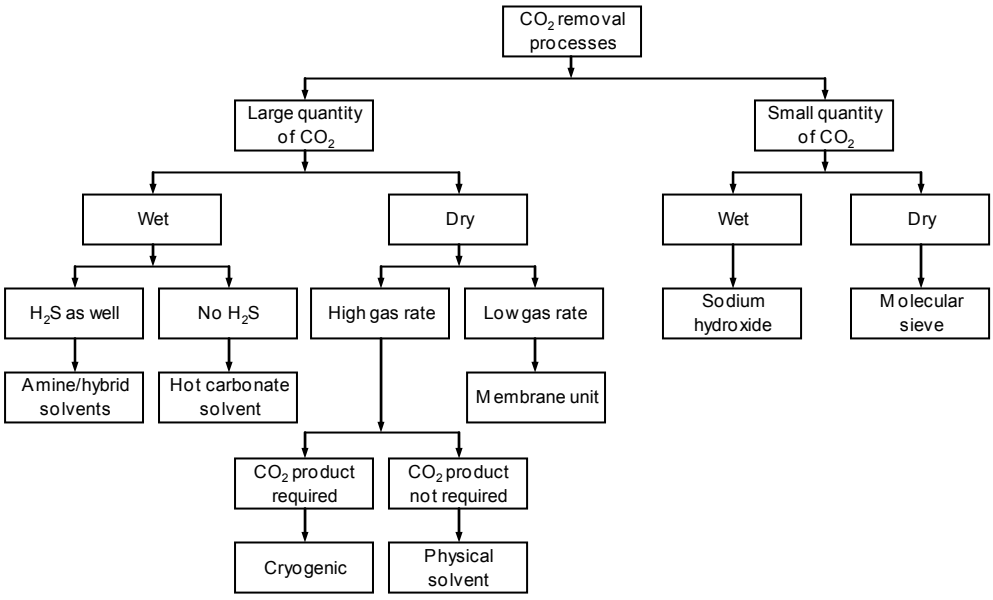

Figure 1-1. Process selection chart for the CO_2 removal processes (Shaw and Hughes, 2001).

Absorption is a separation process in which soluble components of a gaseous mixture dissolve in an absorption liquid. There are two main types of absorption processes; one

based on physical solubility (physical absorption), and the other based on chemical reactions between solute and solvent (chemical absorption). Both processes have advantages and disadvantages. The chemical absorption provides higher absorption rates and higher absorption capacity but its regeneration process normally requires more energy consumption. The regeneration process for physical absorption is easier and less energy demanding but the solvent capacity strongly depends on partial pressure. Generally the physical absorption is favorable at high partial pressures above 5 – 10 atm (Kohl and Nielsen, 1997) whereas the chemical absorption is favored at lower partial pressure. The chemical absorption is, therefore, more suitable for the CO_2 removal process from exhaust gases where the gas is typically at atmospheric pressure and containing 3 – 4 mol % CO_2 for natural gas (Poplsteinova, 2004), 10 – 14 mol % CO_2 for coal–fired power plant, and 20 – 30 mol % CO_2 in process gasses in the iron and steel–making industry.

Absorption with amine–based absorbents is the most common technology for CO_2 removal today. It is a process with considerable inherent problems, particularly when used on large gas flows, e.g., exhaust resulted from fossil–fuel–fired power stations. The processes are bulky, leading to large investment costs. They have high–energy requirements, and the absorbents in use to day are not stable and form degradation products that need to be handled particularly in processes treating oxygen (O_2) containing gases. The IEA Greenhouse Gas R&D Programme has established an international work group, the IEA GHG – CO_2 test network (www.ieagreen.org.uk), to specifically address improvements to absorption processes for CO_2 removal, and with a focus on MEA processes.

Fluor Co., one of the largest vendors of gas processing industries, has introduced commercial gas purification processes; the Econamine FG Plus^{SM} and the FLUOR Solvent processes (Reddy *et al.*, 2003; Kane and Romanow, 2003). The Econamine FG Plus^{SM}, MEA plus inhibitor–based solvent, is specially designed for removing CO_2 from low–pressure and oxygen–containing flue gas streams while the FLUOR Solvent, propylene carbonate–based solvent, for treating feed gases with high CO_2 contents (30 to 70 mol %). Benefits of the Econamine FG Plus^{SM} technology include low solvent cost, lower heat requirement and lower solvent circulation rate compared to all competing MEA–based processes. In addition, as a physical solvent, propylene carbonate has some advantages such as no heat for regeneration, nontoxic, nonfoaming, noncorrosive, and biodegradable.

The Kansai Electric Power Co. (KEPCO) and Mitsubishi Heavy Industries Ltd. (MHI) have also developed a CO_2 removal process that uses a proprietary hindered amine known as KS-1, and later KS-2, which has higher degree of steric hindrance (Mimura *et al.*, 1995 and 1997). Both KS-1 and KS-2 solvents have almost similar characteristics and, in general, their characteristics are better than that of MEA, such as higher CO_2 absorption capacity, lower heat of reaction, noncorrosive, lower regeneration energy, and very stable (may not degrade by itself), but its price is much more expensive than that of MEA as a basic solvent for the Econamine FG Plus^{SM}. A comparison of the energy consumption and amine cost for the two processes, KS-1 and Econamine FG Plus^{SM}, can be seen in Table 1-1 (Reddy *et al.*, 2003) in which KS-1 solvent is, in general, better than the Econamine FG Plus^{SM} solvent (MEA plus inhibitor). The Econamine FG Plus^{SM} process requires less than 1.5% more energy consumption and less than 1% more solvent replacement cost.

Table 1-1. Comparison of Econamine FG Plus^{SM} and KS-1

Item	Units	Econamine FG Plus^{SM}	KS-1
Energy consumption	Btu/lb CO_2	1395	1376
Solvent replacement cost	US$/Te CO_2	2.30	2.28

1.2 Scope of the Work

This work was focused on development and characterization of new absorbents for CO_2 capture. The work includes selection of new absorbents (screening tests), vapor–liquid equilibrium experiments, and kinetic study using a string of disc contactor for the selected absorbent.

1.2.1 Screening Test

The goal of this part of the work was to develop new and more acceptable solvents or solvent mixtures whose absorption rates and loading capacities, the ratio between moles of CO_2 absorbed and moles of CO_2–free absorbent used, that were higher than those of other amine or amine mixtures. The results of this work were presented in a paper entitled: “Absorption Characteristics of Solvents for Carbon Dioxide Capture” at ISSM 2003, Delft, the Netherlands in October 2003 and a refereed paper entitled: “Selection of New

Absorbents for Carbon Dioxide Capture" at GHGT–7, Vancouver, Canada in September 2004.

1.2.2 Vapor–Liquid Equilibrium: Experimental Study and Modeling

Vapor–liquid equilibrium (VLE) experiments for CO_2 in the selected absorbent from the screening tests were performed to measure the solubility of CO_2 at different temperatures ranging from 40 to 120 °C. Net cyclic capacity of the absorbent was determined from the VLE data. The results of this work were also presented at GHGT–7, Vancouver, Canada in September 2004. In addition, the VLE measurements in MEA and MDEA were also performed and the results have been published in *J. Chem. Eng. Data* 2005 entitled: "Solubility of Carbon Dioxide in 30 mass % Monoethanolamine and 50 mass % Methyldiethanolamine Solutions".

The work on thermodynamics was to develop a thermodynamic VLE model for CO_2 in the selected absorbent (AEEA). The results were presented at ECOS 2005, Trondheim, in June 2005 entitled: "Modeling of Equilibrium Solubility of CO_2 in Aqueous 30 mass % 2-(2-aminoethyl-amino)ethanol Solution" and its extended version has been accepted in *Ind. Eng. Chem. Res.* for the CO_2 Capture Special Issue in April 2006.

1.2.3 Kinetic Study

The experiments were performed in a string of disc contactor for the selected absorbent (AEEA) over a range of temperatures from 31 to 50 °C with concentrations ranging from 1.20 to 3.50 mol L^{-1}. The aim of this work was to obtain kinetic parameters, e.g., reaction rate constants as function of temperature, and the reaction mechanisms for the system observed. Additional data such as density, viscosity, and N_2O solubility in aqueous AEEA solutions were also measured to determine the physico–chemical parameters.

1.3 Outline of the Thesis

The thesis is divided into three parts according to the chronological development described above which consists of the screening tests, experimental and modeling study of the VLE, and the kinetic study.

PART I

Chapter 2 describes the selection of the absorbents for carbon dioxide capture. The selection method was based on the capacity and the rate of absorption which were determined from the absorption measurements in bubble absorbers.

PART II

Chapter 3 describes the VLE measurements which were used to validate the experimental techniques with MEA and MDEA. The results were also used to determine the cyclic capacity of the individually selected range of absorbents and to compare the cyclic capacities between the selected absorbent (AEEA) and the existing commercial absorbent (MEA). In addition, the enthalpy of solution of CO_2 in MDEA and that of in AEEA were also determined from the VLE data.

Chapter 4 presents a review of the existing thermodynamic models for the VLE of CO_2–alkanolamine–water systems and the electrolyte activity coefficient models.

Chapter 5 provides the theoretical background for the modeling of phase and chemical equilibria and for the electrolyte activity coefficients models.

Chapter 6 presents the thermodynamic model implementation for the CO_2–AEEA–H_2O system which was solved in a MATLAB code.

PART III

Chapter 7 explains the kinetic measurement in a string of disc contactor and kinetic parameter determination including a brief review of the kinetic mechanisms for the CO_2–alkanolamine–water system.

Chapter 8 summarizes the conclusions from all chapters and gives suggestions for the future work.

1.4 List of Publications

Chapter 2:

Ma'mun, S.; Svendsen, H. F.; Juliussen, O. Properties of Absorbents for Carbon Dioxide Capture. Poster presented at the 3rd Nordic Minisymposium on Carbon Dioxide Capture and Storage, October 2–3, 2003, Trondheim, Norway.

Ma'mun, S.; Svendsen, H. F.; Juliussen, O. Absorption Characteristics of Solvents for Carbon Dioxide Capture. Proc. of the 8th Indonesian Students' Scientific Meeting (ISSM), October 9–10, 2003, Delft, the Netherlands, 49–52.

Ma'mun, S.; Svendsen, H. F.; Hoff, K. A.; Juliussen, O. Selection of New Absorbents for Carbon Dioxide Capture. Proc. of the 7th International Conference on Greenhouse Gas Control Technologies (GHGT–7), September 5–9, 2004, Vancouver, Canada, refereed paper no. E3–2.

Chapter 3:

Ma'mun, S.; Nilsen, R.; Svendsen, H. F.; Juliussen, O. Solubility of Carbon Dioxide in 30 mass % Monoethanolamine and 50 mass % Methyldiethanolamine Solutions. *J. Chem. Eng. Data* **2005,** *50,* 630–634.

Chapter 6:

Ma'mun, S.; Jakobsen, J. P.; Svendsen, H. F.; Juliussen, O. Modeling of Equilibrium Solubility of Carbon Dioxide in Aqueous 30 mass % 2-(2-Aminoethyl-amino)ethanol Solution. The 18th International Conference on Efficiency, Cost, Optimization, Simulation and Environmental Impact of Energy Systems (ECOS), June 20–22, 2005, Trondheim, Norway.

Ma'mun, S.; Jakobsen, J. P.; Svendsen, H. F.; Juliussen, O. Experimental and Modeling Study of the Solubility of Carbon Dioxide in Aqueous 30 Mass % 2-(2-Aminoethyl-amino)ethanol Solution. Accepted *Ind. Eng. Chem. Res.,* the CO_2 Capture Special Issue, April 2006.

PART I

Selection of Absorbents for CO_2 Capture

CHAPTER 2

Experimental Work on Selection of Absorbents

Based on work presented at the 7th International Conference on Greenhouse Gas Control Technologies (GHGT–7), Vancouver, Canada, Sept. 5–9, 2004, refereed paper no. E3–2, at the 8th Indonesian Students' Scientific Meeting, Delft, the Netherlands, Oct. 9–10, 2003, and at the 3rd Nordic Minisymposium on Carbon Dioxide Capture and Storage, Oct. 2–3, 2003, Trondheim, Norway

This work focuses on selecting new absorbents for CO_2 capture. Absorption of CO_2 was studied at 40 °C using both single absorbents and absorbent mixtures for both amine–based and non–amine–based systems. The experimental results show that most absorbents tested have a poorer performance than MEA, but that aqueous AEEA might be a possible contender.

2.1 Introduction

A chemical that is to be used as a new commercial absorbent for removal of CO_2 will require both a high net cyclic capacity and high reaction/absorption rate for CO_2, as well as high chemical stability, low vapor pressure, and low corrosiveness. Aqueous solutions of alkanolamines are the most commonly used chemical absorbents for the removal of acidic gases (CO_2 and H_2S) from natural, refinery, and synthesis gas streams. Among them, aqueous monoethanolamine (MEA), as a primary amine, has been used extensively for this purpose especially for removal of CO_2. It has several advantages over other commercial alkanolamines, such as high reactivity, low solvent cost, low molecular weight and thus a high absorbing capacity on a mass basis, reasonable thermal stability and thermal degradation rate. The disadvantages of MEA include high enthalpy of reaction with CO_2 leading to a high desorber energy requirement, the formation of a stable carbamate and also the formation of degradation products with carbon oxysulfide (COS) or oxygen–containing gases, the inability to remove mercaptans, significant vaporization losses because of high vapor pressure, and a higher corrosivity than many other alkanolamines. Thus corrosion inhibitors are needed when used in higher concentration (Bucklin, 1982; Li and Mather, 1994; Jou *et al.*, 1995; and Liu *et al.*, 1999), as in the Fluor Econamine (30

mass % MEA) and the Econamine FG Plus^{SM} (35 mass % MEA) processes (Reddy *et al.*, 2003). Due to its wide use and advantages compared to other alkanolamines, MEA is set as a base case in this work. The absorbent property evaluated in this chapter is the absorption rate. The cyclic capacity will be determined in Chapter 3.

This work focuses on selecting new absorbents for CO_2 capture using a screening method giving the absorption rate as function of CO_2 loading, a molar ratio between CO_2 absorbed and absorbent used. The objective of the work described here is to select new and more acceptable absorbents or absorbent mixtures whose absorption rate and absorption capacity are higher than the existing ones, thereby reducing the energy consumption of the removal process.

2.2 Materials and Methods

2.2.1 Materials

The CO_2 (min. 99.99 mol %) and N_2 (min. 99.6 mol %) gases used were obtained from AGA Gas GmbH. The alkanolamines were obtained from Acros Organics and used without further purification. Those selected were monoethanolamine (MEA) – $[H_2N(CH_2)_2OH]$, 2-(ethylamino)ethanol (EMEA) – $[CH_3CH_2NH(CH_2)_2OH]$, 2-(methylamino)ethanol (MMEA) – $[CH_3NH(CH_2)_2OH]$, *N*-methyldiethanolamine (MDEA), 2-(butylamino)ethanol (BEA) – $[CH_3(CH_2)_3NH(CH_2)_2OH]$, – $[CH_3N(CH_2CH_2OH)_2]$, 2-(2-aminoethyl-amino)ethanol (AEEA) – $[H_2N(CH_2)_2NH(CH_2)_2OH]$ and the reported purities were not less than 99, 98, 99, 98.5, 98, and 97 mass %, respectively. Other absorbent chemicals tested were piperazine (PZ) – $[–NH(CH_2)_2NH(CH_2)_2–]$ (Acros Organics, min. 99 mass %), the potassium salt of taurine (PT) which was prepared by neutralizing taurine [2-aminoethanesulfonic acid – $H_2N(CH_2)_2SO_3H$] (Acros Organics, 99 mass %) with an equimolar amount of potassium hydroxide (KOH) (Merck, p.a.), the BASF ®Alkazid (AZ) (3.2 M) absorbent, and finally potassium carbonate – (K_2CO_3) (Acros Organics, p.a.).

2.2.2 Methods

The absorbent selection experiments were carried out in a screening apparatus as shown in Figure 2-1. The apparatus designed to operate at atmospheric pressure and temperatures up to 80 °C consists of six bubble absorbers, six K–type thermocouples, a HETO circulating heater (model 02 T 623), a Hartmann & Braun Uras 3G IR CO_2

analyzer, and a BRONKHORST HI–TEC $N_2/CO_2/H_2S$ mass flow controller (model E–7100). The data acquisition system uses LabVIEW. Before starting the experiment, a CO_2–N_2 gas mixture containing 10 vol % CO_2 with a flowrate of 5 NL min^{-1} was circulated through a by–pass valve to calibrate the analyzer. As the process started the by–pass valve closed automatically. The gas mixture was passed through a water saturator and then to the absorber containing 750 mL of absorbent, being either a single or mixed absorbent. The gas phase leaving the absorber was cooled and the CO_2 content directly determined by IR analysis. The temperature of the bath was maintained at 40 ± 0.1 °C.

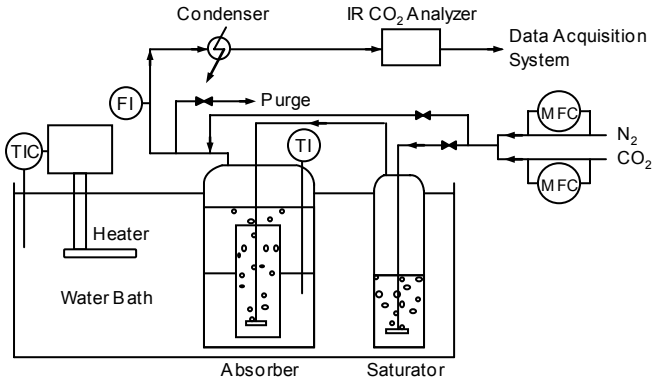

Figure 2-1. Screening apparatus for CO_2 capture.

2.2.3 Gas and Liquid Analyses

The gas CO_2 content, the temperatures, and the gas flow rates were collected by the LabVIEW data acquisition system. The process automatically terminated when the concentration of CO_2 in the outlet reached 9.5 vol % (9.5 kPa CO_2 partial pressure). After terminating the experiment, a liquid sample containing CO_2 was then analyzed by the precipitation–titration method. The liquid sample was added to a 250 cm^3 Erlenmeyer flask containing 50 cm^3 sodium hydroxide (NaOH, 0.1 mol L^{-1}) and 25 cm^3 barium chloride ($BaCl_2$, 0.5 mol L^{-1}) solutions. The amount of the liquid sample added depended on the total CO_2 content of the sample. The Erlenmeyer was heated to enhance the barium carbonate ($BaCO_3$) formation and then cooled to ambient temperature. The mixture was filtered with a 0.45 μm Millipore paper and washed with deionized water. The filter covered by $BaCO_3$ was transferred to a 250 cm^3 beaker. Deionized water, 50 cm^3, was added into the beaker and enough hydrogen chloride (HCl, 0.1 mol L^{-1}) was also added to

dissolve the $BaCO_3$ cake. The amount of HCl not used to dissolve $BaCO_3$ was then titrated with 0.1 mol L^{-1} NaOH in an automatic titrator (Metrohm 702 SM Titrino) with end point pH 5.2.

2.3 Results and Discussion

Absorption rates of CO_2 in amine–based and non–amine–based absorbents were determined by means of six lab–scale bubble absorbers as shown in Figure 2-1. The absorption rate can be calculated by Eq. (2.1) and the results are summarized in Appendix A.

$$r_{CO_2} = \frac{1}{V}\left(n_{CO_2}^{in} - \frac{x_{CO_2}^{out}\, n_{N_2}}{\left(1 - x_{CO_2}^{out}\right)} \right) \tag{2.1}$$

2.3.1 Absorption of CO_2 in Monoethanolamine Solutions

Due to its wide use and advantages compared to other alkanolamines, MEA is set as a base case in this work. Figure 2-2 shows the experimental results for 30 mass % MEA which corresponds to a molar concentration (M) of 5.0 mol L^{-1} MEA at 40 °C and indicates that the absorption rates measured vary slightly between the six absorbers. These differences are mainly caused by variations in the gas distributors used. Small differences exist which affect the number and size of bubbles produced, which again affects the absorption rate. The smaller the bubble sizes the greater the interfacial area.

To enable easy comparison to the other absorbents used, an arithmetic average of the absorption rates of CO_2 in 5.0 M MEA was taken from the results of absorber 2 and absorber 3. The reason for this was that the absorption rates of CO_2 in these two absorbers were almost identical and in addition they gave relatively high values compared to the other absorbers except for absorber 4.

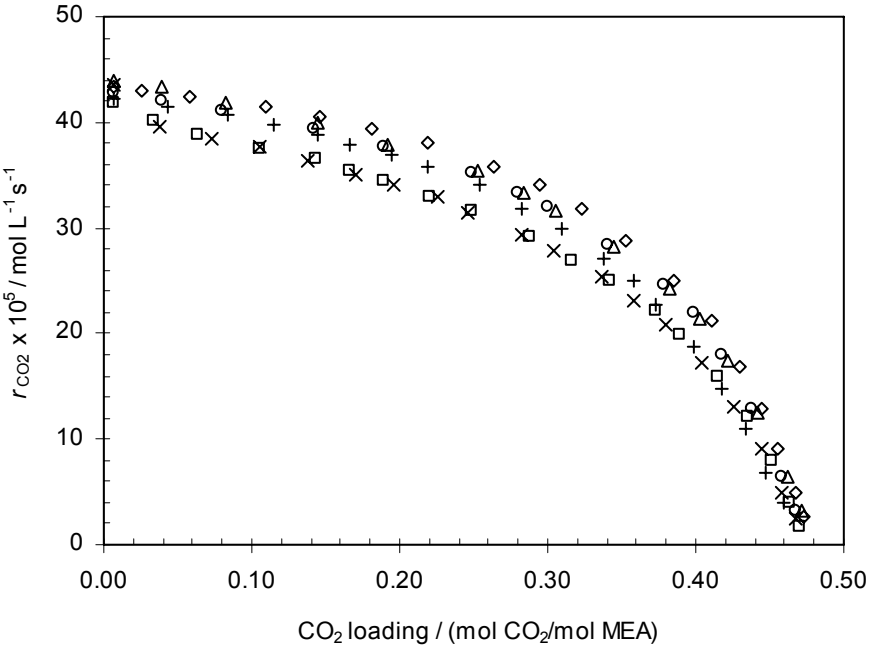

Figure 2-2. Absorption rates of CO_2 in 5.0 M MEA for various absorbers at 40 °C: □, absorber 1; ○, absorber 2; Δ, absorber 3 ; ◊, absorber 4; ×, absorber 5; +, absorber 6.

In addition to the concentration of 5.0 M MEA, the absorption rates of CO_2 were also measured at the MEA concentrations of 20 and 25 mass % which correspond to the molar concentrations of 3.3 and 4.1 M, respectively. Figure 2-3 shows the absorption rates of CO_2 at several concentrations of MEA. It can be seen from the figure that the maximum absorption rate of CO_2 in 3.3 M MEA is the lowest (41.7×10^{-5} mol L^{-1} s^{-1}) compared to the others (42.7×10^{-5} mol L^{-1} s^{-1} for 4.1 M and 43.4×10^{-5} mol L^{-1} s^{-1} for 5.0 M), but its loading capacity is slightly higher than those of 4.1 and 5.0 M MEA. However, the differences shown are within the experimental uncertainty, indicating that the rate of CO_2 absorption into MEA solution is proportional to the molar concentration. This is in accordance with the literature; see Versteeg *et al.* (1996). In addition, in the absorption processes the higher absorption rate is needed to reduce the size of the column, therefore, the concentration of 5.0 M MEA is used in this work as the base case. This is also the standard concentration used today.

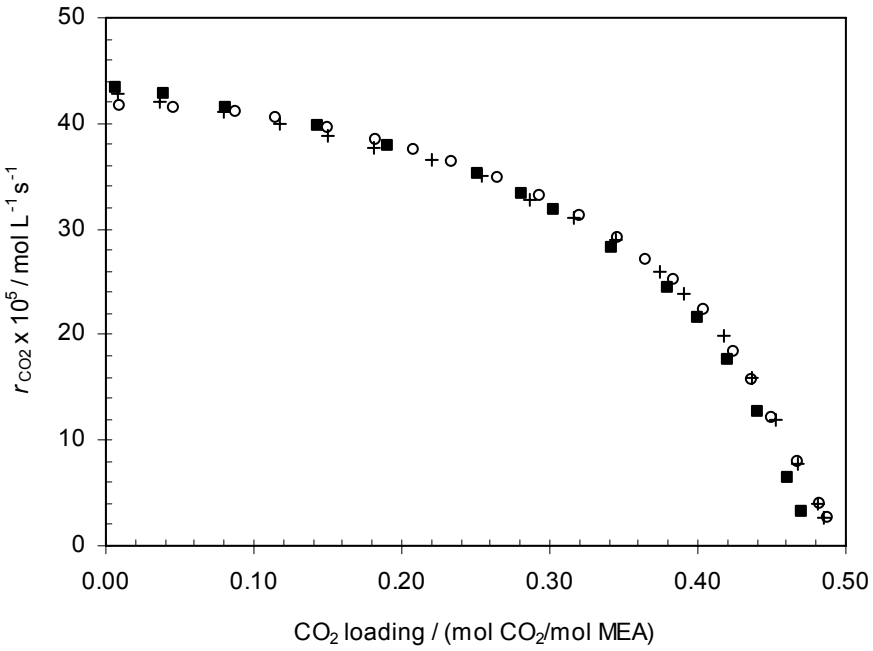

Figure 2-3. Absorption rates of CO_2 in various concentrations of MEA at 40 °C: ○, 3.3 M; +, 4.1 M; ■, 5.0 M.

2.3.2 Absorption of CO_2 in 30 mass % Alkanolamine Solutions

Absorption rates of CO_2 in amine–based absorbents and their mixtures were measured at 40 °C. To evaluate the absorption rate of CO_2 in single amine–based absorbents (e.g., MMEA, EMEA, MDEA, BEA, and AEEA), a constant mass basis, 30 mass %, was chosen for all absorbents. This implies that the molar concentrations were not the same, and generally lower than that of MEA. However, the optimal operational concentrations for these absorbents are not known a priori so a comparison based on mass fraction might be as good as one based on constant molarity. All the absorbents tested have good solubility in water. MEA, MMEA, and AEEA are miscible whereas EMEA, MDEA, and BEA are very soluble in water.

The relative performance of the 30 mass % amines can be evaluated from Figure 2-4. It should be noted that the comparison is semi–quantitative, in the sense that there is no guarantee that the bubble structure, and therefore, the gas–liquid interfacial area was exactly the same during all experiments. However, the superficial gas velocity was the same, so differences would arise mainly due to variations in interfacial tension, bubble coalescence properties, and viscosity.

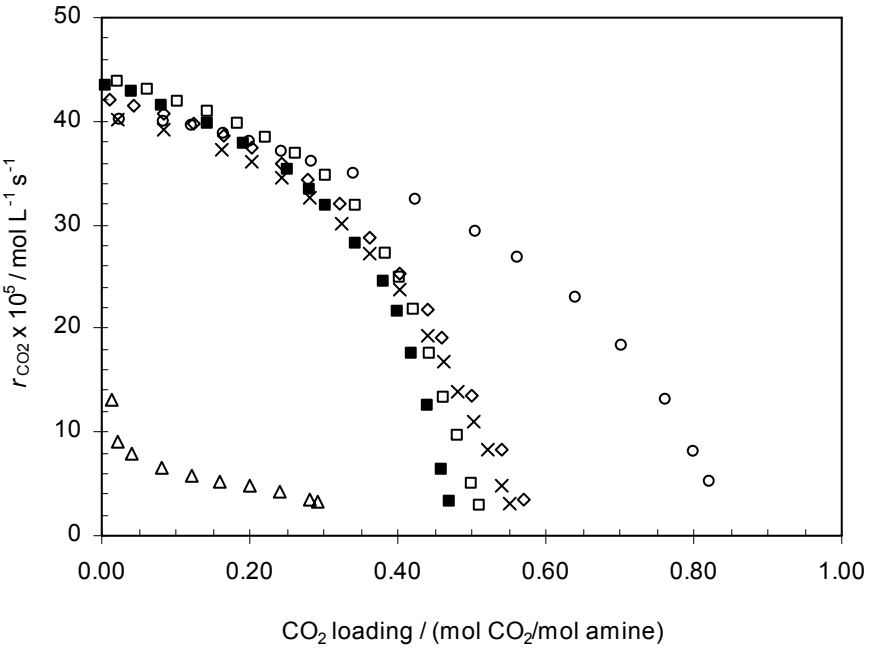

Figure 2-4. Absorption rates of CO_2 in 30 mass % alkanolamine solutions at 40 °C: ■, 5.0 M MEA; □, 4.0 M MMEA; ◊, 3.3 M EMEA; Δ, 2.6 M MDEA; ×, 2.5 M BEA; ○, 2.9 M AEEA.

In the loading range lower than 0.18 the absorption rates of CO_2 in 5.0 M MEA are generally higher than in all the other absorbents except for 4.0 M MMEA. Above ~0.32 in loading, however, the absorption rates in MEA are lower than in the other absorbents. It is also clearly shown that the absorption rates of CO_2 in MDEA are by far the lowest compared to all absorbents tested over the whole loading range. This is of course expected as a tertiary amine; MDEA lacks the extra hydrogen atom and does not form carbamate which contributes to increase the overall rate of absorption. In addition, the rapid decrease in absorption rates of CO_2 in MDEA at low loadings might indicate contamination of other amines, probably primary or secondary amines.

The homologous series of secondary amines, MMEA, EMEA, and BEA, all perform very well. MMEA has even slightly higher absorption rates than MEA at low loadings and continues to outperform MEA also for higher loadings. One should also keep in mind that MMEA has a somewhat higher molecular weight (75 vs. 61 g mol^{-1}), and therefore, a lower molar concentration. In addition, MMEA has a moderate carbamate stability resulting in increased absorbed amounts of CO_2 at low partial pressure (Suda *et al.*, 1996). Both MMEA and BEA are foaming and MMEA is in this respect much worse than BEA.

A foam inhibitor DREW 210–667 modification 1 (AMEREL 2000) was, therefore, added in this work at a quantity of 50 ppm in MMEA and also to the 2.5 M BEA solution. Normally, a foam inhibitor will have a negative impact on the mass transfer characteristics, both by reducing the interfacial area and possibly by increasing the surface resistance. MMEA could thus have an even greater potential than shown here when used in contactors where the two phases are separated, like in membrane contactors.

2.3.3 Absorption of CO_2 in Other Solutions

The absorption rates of CO_2 in other solutions were also measured such as in MDEA and its mixtures, BEA and its mixtures, the potassium salt of taurine (PT) and its mixtures, piperazine (PZ), the BASF ®Alkazid (3.2 M), and potassium carbonate. From Figures (2-5 to 2-8) it can clearly seen that the absorption rates of CO_2 in 5.0 M MEA are generally higher compared to the other absorbents for all the loading ranges except for 2.5 M PZ and for some of BEA solutions at higher loadings.

Figure 2-5 shows the absorption rates of CO_2 in MDEA and its mixtures. The mixture of 2.6 M MDEA and 0.62 M PZ gives higher absorption rates compared to other solutions of MDEA and its mixtures for the whole loading range. An addition of 0.62 M AEEA to the 2.6 M MDEA shows a larger improvement on the MDEA performance compared to additions of both MEA and BEA but the performance is still lower than that of the MDEA–PZ mixture which has almost the same absorption rates as the 5.0 M MEA at low loadings. This underlines the strong effect of PZ as a promotor.

The absorption rates of CO_2 in BEA and its mixtures can be seen in Figure 2-6. At lower loadings the absorption rates of CO_2 in 5.0 M MEA are higher than in BEA and its mixtures but the mixture of 2.6 M BEA and 1.6 M MEA surprisingly gives higher absorption rates in the high loading range. As mentioned above, the addition of some foam inhibitor will normally have a negative impact on the mass transfer characteristics. This is seen from Figure 2-6 as the addition of the foam inhibitor in the 2.5 M BEA gives lower the absorption rates compared to 2.5 M BEA without foam inhibitor. The effect of the foam inhibitor is quite strong in the low loading range, but is negligible at high loadings. This may indicate that the main effect is the interface reduction effect and that the actual transport resistance across the interface is not hindered. This will further be discussed later.

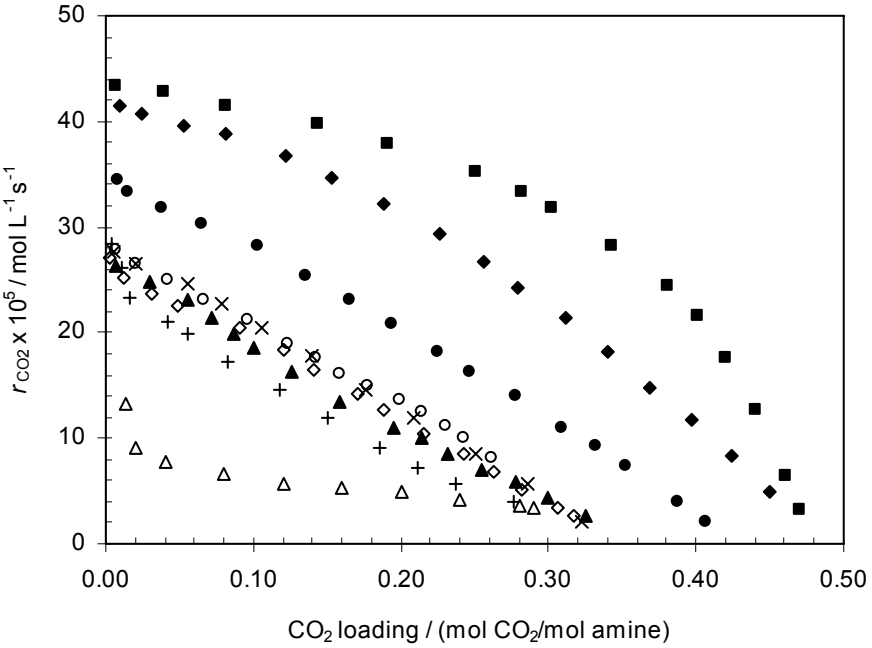

Figure 2-5. Absorption rates of CO_2 in MDEA and its mixtures at 40 °C: Δ, 2.6 M MDEA; mixtures of 2.6 M MDEA with: ◊, 0.43 M BEA; ○, 0.86 M BEA; ▲, 0.62 M MEA; ♦, 0.62 M PZ; •, 0.62 M AEEA; ×, 3.5 M with 0.62 M AEEA; +, 4.4 M with 0.62 M AEEA; ■, 5.0 M MEA.

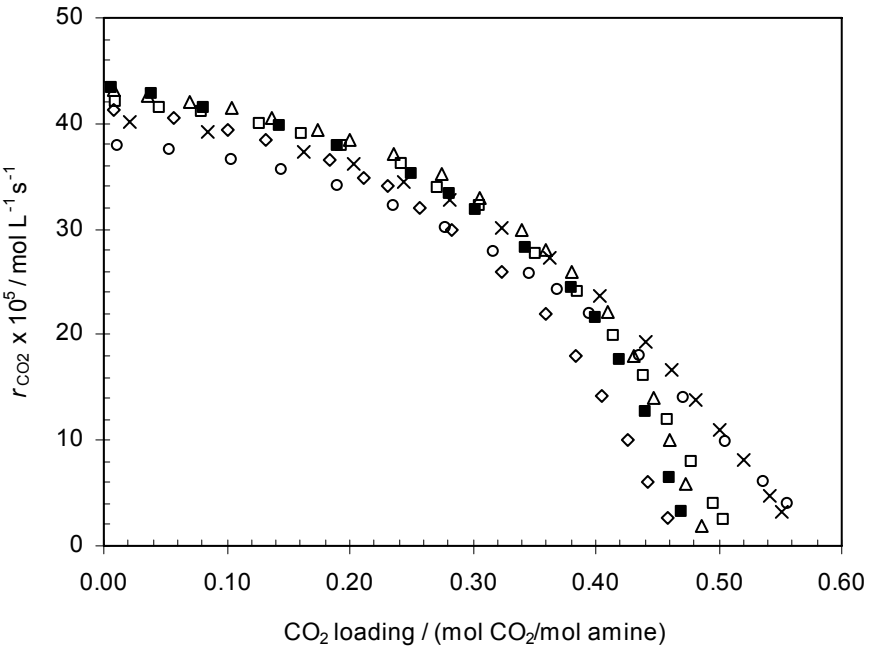

Figure 2-6. Absorption rates of CO_2 in BEA and its mixtures at 40 °C: ×, 2.5 M; □, 3.3 M; ◊, 4.1 M; Δ, 2.5 M with 1.6 M MEA; ○, 2.5 M with foam inhibitor; ■, 5.0 M MEA.

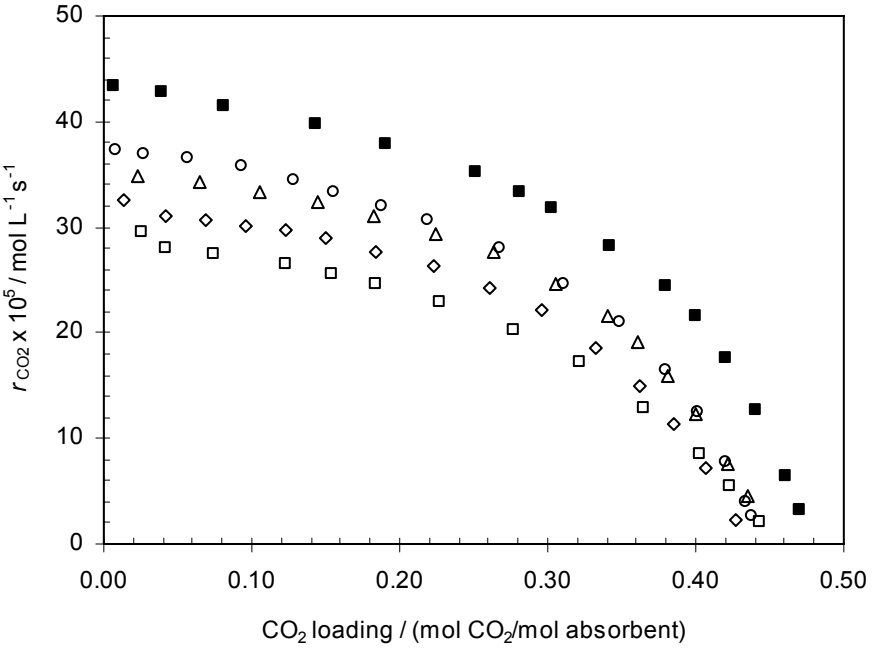

Figure 2-7. Absorption rates of CO_2 in PT and its mixture at 40 °C: □, 1.0 M; ◊, 2.0 M; Δ, 3.0 M; ○, 3.0 M with 0.62 M MEA; ■, 5.0 M MEA.

Figure 2-7 shows the absorption rates of CO_2 in PT and its mixture. From the figure it is clear that all the systems have lower performances compared to that of 5.0 M MEA. The Netherlands Organization for Applied Scientific Research (TNO) has developed and patented a range of absorbents for use in membrane contactors based on amino acid salts and given them the trade name CORAL (CO_2 Removal Absorption Liquid). These liquids are claimed to offer similar absorption characteristics as aqueous alkanolamine solutions, e.g., energy consumption and cyclic loading, better mass transfer and degradation properties, and do not wet polyolefin microporous membranes (Feron and Jansen, 1995 and 1997; Kumar *et al.*, 2002). PT is one of the suggested amino acid salts and was tested in this work at concentrations of 1.0, 2.0, and 3.0 M. Figure 2-7 shows that unlike the results from Kumar *et al.* (2002), the PT does not seem to offer better mass transfer characteristics compared to MEA. Being an inorganic acid salt, this could affect the coalescence properties of the solution. The lower mass transfer rates are, therefore, an indication, but not proof of slower kinetics than 5 M MEA. An addition of a promotor, MEA, to the 3.0 M PT just improves the performance at lower loadings. This weak effect of MEA as a promotor is in accordance with the effect with MDEA as shown in Figure 2-5 and leaves doubt us to the suitability of MEA as promotor. Increasing the concentration of

PT to above 3.0 M was found to lead to precipitation at higher loadings. Like PT, alkazid (AZ) is also an amino acid and was also tested in this work using the BASF ®Alkazid (3.2 M). As seen in Figure 2-8 its performance is also poorer than that of 5.0 M MEA. At a high loading it was found to reach a precipitation point, as also found by Hook (1997).

It is also clearly seen from Figure 2-8 that 2.5 M PZ gives higher absorption rates compared to those for all the absorbents tested, and has about the same absorption capacity for CO_2 (loading 0.82) as 2.9 M AEEA (see Figure 2-4) used in this work. BASF has successfully used PZ as a promotor in MDEA systems for high–capacity CO_2 removal in ammonia plants, LNG production, and natural gas processing, and patented it (Bishnoi and Rochelle, 2000). However, some environmental concerns have been raised about PZ based on its slow biodegradability. PZ is a diamine with two secondary amine groups. This explains its readiness to exceed 0.50 in loading. The low biodegradability, on the other hand, probably stems from its ring structure. AEEA is also a diamine, with one secondary and one primary amine group. It is a chain molecule and should, therefore, be an environmentally relatively acceptable absorbent. It is also among the amines with better absorption characteristics as it has a relatively high absorption rate (maximum rate of 40.1×10^{-5} mol L^{-1} s^{-1}) at low loading combined with a high absorption capacity for CO_2 (loading 0.82 at 9.5 kPa CO_2 partial pressure). In addition, the vapor pressure of AEEA is much lower than that of MEA, e.g., P^o_{MEA} = 15.9 kPa (Austgen, 1989) and P^o_{AEEA} = 0.969 kPa (Wilson *et al.*, 2002) at 120 °C. However, as MEA, AEEA is also corrosive (Suda *et al.*, 1997) and this may limit its usefulness. In addition to the higher absorption rate, AEEA also offers higher cyclic capacity compared to that of MEA. The cyclic capacity determination will be discussed further in Chapter 3.

In addition to the evaluation of amine–based absorbent characteristics, a non–amine–based absorbent, potassium carbonate activated by MEA, was also tested. Figure 2-8 shows the results from this work. The absorption rates of CO_2 in the 5.0 M MEA are again found to be significantly higher than those in the K_2CO_3–MEA mixture for the whole loading range. The addition of MEA as promotor increases the absorption rate of CO_2, but the effect is limited as previously found for MDEA and PT. A saddle point occurs on each curve. At this point all the MEA has reacted and only the carbonate ions are left. Even if the amount of promotor added varies, the final loadings at 9.5 kPa CO_2 partial pressure are approximately the same and ~0.45 as studied in this work.

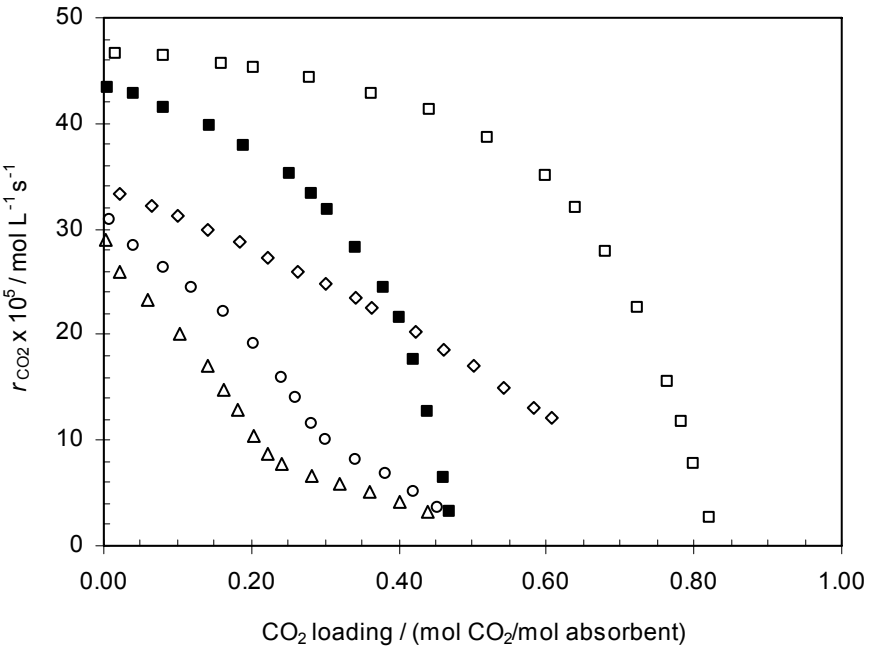

Figure 2-8. Absorption rates of CO_2 in PZ, AZ, and K_2CO_3 at 40 °C: □, 2.5 M PZ; ◊, 3.2 M AZ; ○, 1.7 M K_2CO_3 with 1.9 M MEA; Δ, 1.7 M K_2CO_3 with 1.0 M MEA; ■, 5.0 M MEA

2.4 Gas–side Mass Transfer Restrictions

In Figure 2-4, the curves show very similar values at low loadings. It indicates that the gas phase resistance might control the overall mass transfer process. This phenomenon can be explained from the two–film theory as shown in Figure 2-9 (Levenspiel, 1996).

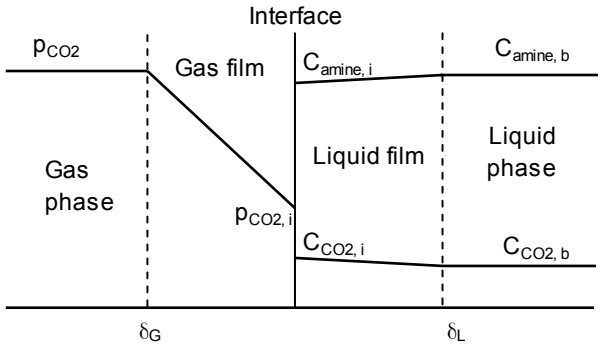

Figure 2-9. Gas–liquid reaction with gas film control.

At low loading, the concentration of amine is still high and is assumed to be constant ($C_{Amine} \approx$ constant). For a chemical absorption system, the overall absorption rate of CO_2 can be written as follows

$$-r_{CO_2} = \frac{1}{\frac{1}{k_{CO_2,G}a} + \frac{H_{CO_2}}{k_{CO_2,L}aE} + \frac{H_{CO_2}}{kC_{Amine}f_L}} p_{CO_2} \quad (2.2)$$

where a is the interfacial area and f_L is the ratio between volume of liquid and that of contactor. Since the gas film resistance is the rate determining step (RDS), $1/k_{CO_2,G}a << \left(H_{CO_2}/k_{CO_2,L}aE + H_{CO_2}/kC_{Amine}f_L\right)$, then the general rate expression reduces to

$$-r_{CO_2} = k_{CO_2,G}a\, p_{CO_2} \quad (2.3)$$

Equation (2.3) shows that at low loadings the absorption rates of CO_2 in all amines are identical. As partial pressure of CO_2 (p_{CO_2}) and the interfacial area (a) are constant during the process, the gas–side mass transfer coefficient of CO_2 ($k_{CO_2,G}$) is the only parameter taken into account. Moreover, the effect of foam inhibitor addition can also be explained with Eq. (2.3). The addition of foam inhibitor will reduce the interfacial area and thus decreases the overall absorption rate, e.g., the addition of the foam inhibitor in the 2.5 M BEA (see Figure 2-6).

2.5 Conclusions

An apparatus for rapid screening of CO_2 absorption chemicals has been developed and a range of absorbents was tested. In general, the main absorption characteristics of absorbents for CO_2 removal are the absorption rate and the absorption capacity of CO_2. The experimental results show that AEEA seems to be a potentially good absorbent for capturing CO_2 from low pressure gases according to the above criteria. It offers high absorption rate combined with high absorption capacity in terms of the CO_2 loading at 9.5 kPa CO_2 partial pressure compared to the other absorbents used in this work. The vapor pressure of AEEA is also much lower than that of MEA. In addition to AEEA, MMEA also needs to be considered. It could have a greater potential than indicated here when used in contactors where the two phases are separated, like in membrane contactors.

PART II

Vapor–Liquid Equilibria: Experiments and Modeling

CHAPTER 3

Measurements of CO_2 Solubility in Alkanolamines

Based on work published in J. Chem. Eng. Data 2005, 50, 630–634
and presented at the 7th International Conference on Greenhouse Gas Control Technologies
(GHGT–7), Vancouver, Canada, Sept. 5–9, 2004, refereed paper no. E3–2

This work focuses on the VLE experiments. The equilibrium partial pressures of carbon dioxide (CO_2) over a 30 mass % aqueous solution of monoethanolamine (MEA), a 50 mass % aqueous solution of methyldiethanolamine (MDEA), and a 30 mass % aqueous solution of 2-(2-aminoethyl-amino)ethanol (AEEA) were measured. The cyclic capacity was also determined based on the VLE data.

3.1 Introduction

As mentioned in Chapter 2 that aqueous MEA solutions have been used extensively for the gas purification processes for decades. For a high pressure CO_2 removal, Methyldiethanolamine ($CH_3N(CH_2CH_2OH)_2$, MDEA) solutions are more appropriate for this purpose. Besides, MDEA can also be used for selective removal of hydrogen sulfide (H_2S) from gas streams containing both CO_2 and H_2S. The use of MDEA solutions was first proposed by Frazier and Kohl (1950). The advantages of MDEA, a tertiary amine, over primary and secondary amines are, besides the selectivity for H_2S, a lower enthalpy of reaction with the acidic gases which leads to lower energy requirements for regeneration, lower vapor pressure of the solution, lower corrosiveness, and better thermal and chemical stability. The limitations of MDEA include slower reaction rate with CO_2 and lower absorption capacity at low concentrations of CO_2 (Jou *et al.*, 1993; Rho *et al.*, 1997).

A number of investigators have measured the solubility of CO_2 in a 30 mass % MEA at temperatures from 0 to 150 °C with partial pressures of CO_2 ranging from 0.5 Pa to 20 MPa, as shown in Table 3-1. Among the investigators, only Goldman and Leibush (1959), Lee *et al.* (1976) and Jou *et al.* (1995) measured the solubility of CO_2 in 30 mass % MEA at a regeneration temperature of 120 °C. However, there is a scarcity of data in the loading region most applicable for regenerator calculations, corresponding to partial pressures

between 5 and 200 kPa. Moreover, the data of Lee *et al.* (1976) have a consistent deviation of –0.04 mol CO_2/mol MEA compared to the data of Jou *et al.* (1995).

The solubility of CO_2 in 50 mass % MDEA has also been determined by several investigators for temperatures between 25 and 200 °C with partial pressures of CO_2 ranging from 0.07 Pa to 6.6 MPa, as shown in Table 3-1. There is, however, a great scatter in the results, and no data exist for intermediate temperatures such as 55 and 85 °C.

Table 3-1. Literature review of 30 mass % MEA and 50 mass % MDEA solubility data

Author	T/°C	p_{CO_2} /kPa
30 mass % MEA		
Mason and Dodge (1936)	0, 25, 50, 75	1.41 – 99.43
Lyudkovskaya and Leibush (1949)	25, 50, 75	255 – 4124
Goldman and Leibush (1959)	75, 100, 120, 140	0.53 – 473
Lee *et al.* (1974)	40, 100	1.15 – 6616
Lee *et al.* (1976)	25, 40, 60, 80, 100, 120	0.2 – 6616
Nasir and Mather (1977)	100	0.0005 – 0.52
Shen and Li (1992)	40, 60, 80, 100	1.1 – 1975
Jou *et al.* (1995)	0, 25, 40, 60, 80, 100, 120, 150	0.0012 – 19954
50 mass % MDEA		
Jou *et al.* (1982)[a]	25, 40, 70, 100, 120	0.00161 – 6570
Chakma and Meisen (1987)[a]	100, 140, 160, 180, 200	138 – 4930
Austgen *et al.* (1991)[a]	40	0.0102 – 93.6
Robinson (1993)	40, 70, 100, 120	146 – 5327
Rho *et al.* (1997)	50, 75, 100	0.775 – 140.3
Rogers *et al.* (1998)	40	0.00007 – 1.0018
Park and Sandall (2001)	25, 50, 75, 100	0.78 – 140.4

[a] 48.8 mass %

The solubility of CO_2 in 30 mass % AEEA, as the selected absorbent obtained from the screening tests, was also measured at temperatures from 40 to 120 °C with partial pressures of CO_2 ranging from 11 Pa to 220 kPa.

The objective of the work described here is to obtain reliable data on the solubility of CO_2 in 30 mass % MEA at the regeneration temperature of 120 °C, 50 mass % MDEA at 55, 70, and 85 °C, and 30 mass % AEEA in the most interesting loading range which could serve as a standard for use in the modeling of vapor–liquid equilibria (VLE) in MEA, MDEA, and AEEA solutions. The data points for 30 mass % MEA could also be used for validation of the experimental method.

3.2 Materials and Methods

3.2.1 Materials

Sample solutions of alkanolamines (MEA, purity >99 mass %; MDEA, purity >98.5 mass %; and AEEA, purity >97 mass %) were prepared from the received chemical from Acros Organics in mixtures with deionized water. The AEEA as received does not seem to contain any active amine impurities that significantly affect the overall absorption rate as at low loadings the absorption rates are constant indicating a well defined reaction. This is contrary to the MDEA–case, as shown in Chapter 2. The CO_2 (purity >99.99 mol %) and nitrogen (N_2) (purity >99.999 mol %) gases used were obtained from AGA Gas GmbH.

3.2.2 Methods

The equilibrium measurements were carried out in different VLE apparatuses from atmospheric to high pressures. Figure 3-1 shows the VLE apparatus for atmospheric pressure. The apparatus is designed to operate at temperatures up to 80 °C and consists of four 360–cm^3 glass flasks, a Fisher–Rosemount BINOS® 100 NDIR CO_2 analyzer, a BÜHLER pump (model P2), and two K–type thermocouples. A preloaded amine solution of 150 cm^3 was fed into flask 2. The same amount was also fed into flasks 3 and 4 while flask 1 was used as gas stabilizer. The flasks were heated by water and placed in a thermostated box with temperature measured to within ±0.1 °C. The gas phase was circulated as the temperature reached the desired level and equilibrium was obtained when the analyzer showed a constant value for the CO_2 volume percent. This took approximately 30 to 60 min. A liquid sample to be analyzed for CO_2 and amine concentrations was then withdrawn from flask 4.

The equilibrium measurements for medium pressure were carried out in a VLE apparatus with recirculation of the gas phase, as shown in Figure 3-2. The apparatus consist of three 300 cm^3 stainless steel cylinders (the equilibrium cells 1, 2, and 3) designed to operate at pressures up to 700 kPa and at temperatures up to 130 °C, a SERA (Seybert & Rahier GmbH) diaphragm pump (model ZR 408W), a KNF Neuberger compressor (Model PM 15785–145), a Bourdon pressure gauge, a Druck PTX 610 pressure transmitter with an accuracy of ±0.3% of full scale (800 kPa), four K–type thermocouples, and a Fisher–Rosemount BINOS® 100 NDIR CO_2 analyzer. The data acquisition was performed using FieldPoint FP–1000 and FP–AI–110.

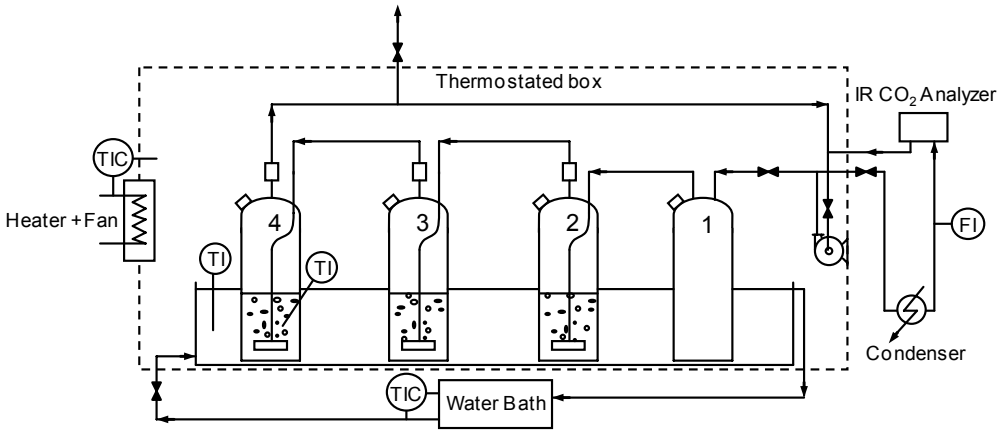

Figure 3-1. Atmospheric vapor–liquid equilibrium apparatus.

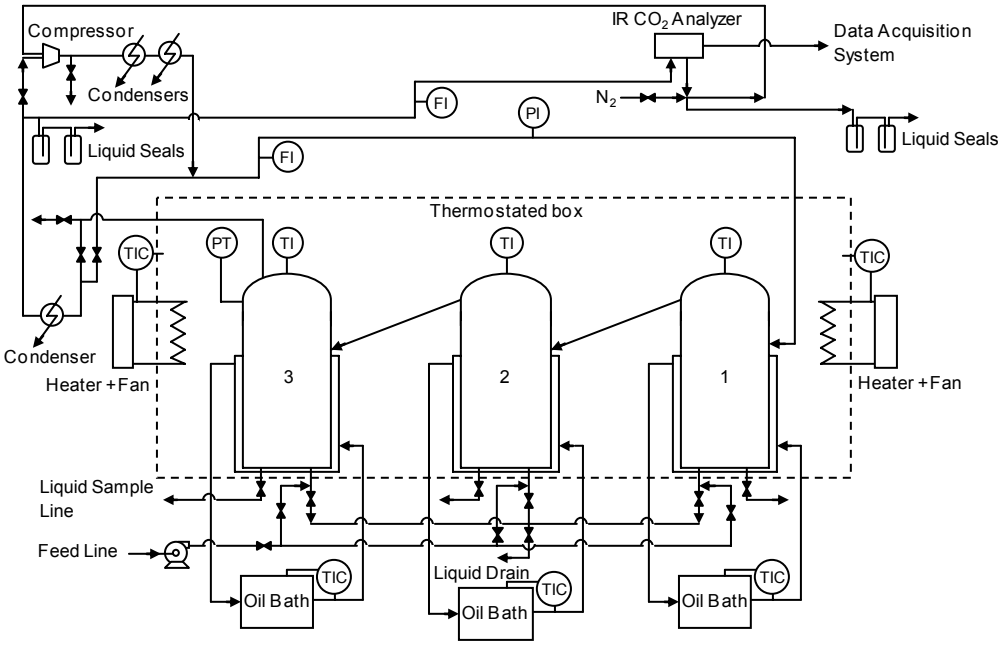

Figure 3-2. Medium pressure vapor–liquid equilibrium apparatus.

Before starting the experiment, N_2 was flushed through the apparatus to purge out the air within the cells. A preloaded 30 mass % amine solution of 200 cm^3 was then fed into cell 1, while cells 2 and 3 held 150 cm^3 each of the same solution. The cells, placed in a thermostated box, were heated by individual oil baths and the temperatures were measured to within ±0.1 °C. Typically, temperature variations during an experiment would be within ±0.5 °C. To prevent boiling and vaporization of the solvent during the heating up, the

minimum initial pressure in the cells was set to 300 kPa. As the temperature reached the desired value, the compressor increased the pressure to 700 kPa and circulated the vapor. A backpressure valve was used to maintain the pressure at 700 kPa. Equilibrium was obtained when the temperature was established at a constant value and the CO_2 concentration in the vapor phase was constant. This took ~2 – 3 h including the heating–up period. This long time for equilibration may be due to the higher amine and water vapor pressures at high temperature, and the fact that to keep the total pressure at 700 kPa, small amounts of gas had to be released to the atmosphere during equilibration. After equilibrium was reached, a liquid sample was withdrawn from cell 3 into a 75 cm^3 evacuated sampling cylinder such that the cylinder was completely filled by the liquid sample and then cooled to ambient temperature. The temperatures and pressures were automatically collected by the FieldPoint data acquisition system.

The working principle of the two VLE apparatuses described is basically the same. The vapor bleed extracted for composition measurement was cooled to 10 °C to condense water and amine, and the CO_2 content was directly determined by IR analysis. The vapor phase in the IR analyzer, therefore, consisted of N_2, CO_2, and small amounts of H_2O and amine. The concentration of CO_2 in the analyzer is then

$$y_{CO_2}^{IR} = \frac{n_{CO_2}^{IR}}{n_{CO_2}^{IR} + n_{N_2}^{IR} + n_{H_2O}^{IR} + n_{Amine}^{IR}} \tag{3.1}$$

where the n denotes molar flow and the superscript IR denotes the vapor phase in the IR analyzer. Due to the low vapor pressures of MEA and AEEA at 10 °C (P_{MEA}^{o} = 12 kPa; P_{AEEA}^{o} = 0.052 Pa) (Austgen, 1989 and Wilson *et al.*, 2002), MEA/AEEA in the vapor phase through the analyzer can be disregarded.

The circulating vapor phase in the system consisted of N_2, CO_2, and significant amounts of H_2O and amine. As noncondensable gases, the flows of CO_2 and N_2 are the same before and after the condenser. Equation (3.1) together with a mole balance will give the molar flow of CO_2 in the system

$$n_{CO_2} = y_{CO_2}^{IR}\left[n_T - \left(n_{H_2O} - n_{H_2O}^{IR}\right) - n_{Amine}\right] \tag{3.2}$$

where n_T, n_{H_2O}, and n_{Amine} respectively denote the total moles and the moles of H_2O and amine circulating in the system. The partial pressure of CO_2 can then be calculated as

$$p_{CO_2} = y_{CO_2}^{IR}\left[P-\left(p_{H_2O}-p_{H_2O}^{IR}\right)-p_{Amine}\right] \quad (3.3)$$

where P is the total pressure. The partial pressures of H_2O and MEA over the 30 mass % MEA solution were estimated using a Wilson equation (Wilson, 1964; Park and Lee, 1997), whereas a Raoult's law behavior was used to determine the partial pressures of H_2O and AEEA over the 30 mass % AEEA solution. The high total pressure has the added effect of lowering the effect on the amine and water partial pressures, and thereby improving the accuracy of the measurements.

For the medium pressure apparatus, the cooling of the gas through the IR analyzer produced ~5 mL of condensed water containing small amounts of amine during the time of equilibration. This water loss stems mainly from cell 1 where the gas enters and becomes saturated. The liquid losses of cells 2 and 3 were found to be negligible, and the sample for liquid phase analysis was taken from cell 3. Separate heating for the cells was used to obtain accurate temperature control.

Figure 3-3 shows the equilibrium apparatus for high pressure measurements. The apparatus consists of two connected autoclaves 1000 and 200 cm^3 which rotate 180^o with 2 rpm and are designed to operate up to 2 MPa at 150 °C. The instrumentations comprise a Druck PTX 610 (max 800 kPa) and a Schaevitz P 706–0025 (max 2.5 MPa) pressure transducer, and two K–type thermocouples. This apparatus was used for the MDEA tests, as the conditions ranged beyond those possible for the apparatus in Figure 3-1.

The autoclaves placed in a thermostated box were heated by an oil bath. During the heating–up period, the autoclaves were purged with CO_2 several times. The unloaded 50 mass % MDEA solution of 200 cm^3 was then injected into the smaller autoclave, and finally, CO_2 was injected to the desired pressure. Equilibrium was obtained when the temperature and pressure were constant to within ±0.2 °C and ±1 kPa. This took approximately 4 to 30 h. After equilibrium was obtained, a liquid sample was withdrawn from the smaller autoclave using a 75 cm^3 evacuated sampling cylinder where an unloaded MDEA solution of 25 cm^3 was injected into the cylinder before sampling. This was to ensure that all CO_2 in the liquid sample was totally absorbed. The cylinder was then cooled to ambient temperature. The partial pressure of CO_2 was measured by subtracting the partial pressures of H_2O and MDEA from the total pressure. As shown by Xu *et al.* (1991), it is reasonable to assume a Raoult's law behavior for the MDEA–H_2O system. The data acquisition system used was FieldPoint.

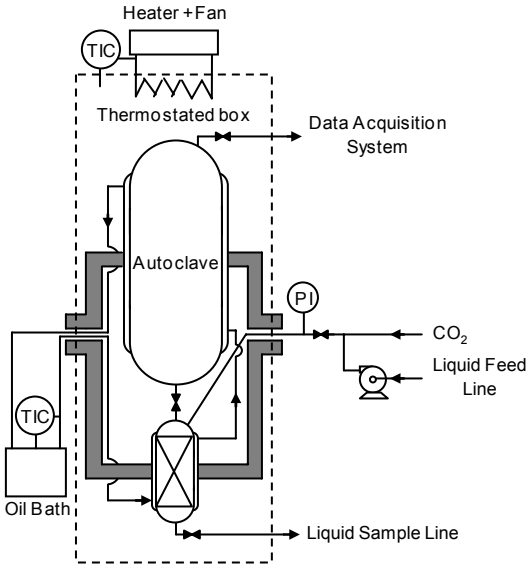

Figure 3-3. High pressure vapor–liquid equilibrium apparatus.

Liquid samples containing CO_2 were analyzed by the precipitation–titration method. The analysis procedures have been described in Section 2.2.3. Due to possible solvent losses during operation at high temperatures, the amines concentrations were determined by titration. A liquid sample of 0.5 cm^3 was diluted in 75 cm^3 deionized water and titrated with 0.1 mol L^{-1} sulfuric acid (H_2SO_4) using Metrohm 702 SM Titrino. The end point was obtained at pH 4–5. The small changes in amine concentrations due to the losses will not affect the accuracy of the measured CO_2 partial pressure, e.g., the AEEA system. The AEEA concentrations were found to be between 2.790 and 2.934 mol L^{-1} with the initial concentration of 2.936 mol L^{-1} and these concentrations were used for establishing the CO_2 loading. Since the mole fraction of AEEA is very small (approximately 0.067) and the vapor pressure is low (P^{o}_{AEEA} = 0.969 kPa at 120 ^{o}C; Wilson *et al.*, 2002), the small changes in AEEA partial pressure due to the losses will, therefore, not affect the accuracy of the measured CO_2 partial pressure data. The AEEA partial pressure contribution to the system is less than 0.01%. As AEEA, MEA was also found to have small changes in its concentrations.

3.3 Results and Discussion

Experimental solubility data for CO_2 in 30 mass % MEA/AEEA and 50 mass % MDEA solutions were measured at temperatures from 40 to 120 °C with partial pressures of CO_2 ranging from 11 Pa to 814 kPa. The MDEA and part of MEA data were measured by Nilsen (2001 and 2002). The expanded uncertainty for the temperature readings was ±0.5 °C. The uncertainties of the measured temperatures were estimated from the standard deviations and the half–width of the temperature precisions, i.e., 0.05 °C for the medium pressure VLE apparatus (Chirico, *et al.*, 2003). The experimental results are presented in Figures 3-4, 3-5, 3-6, and Appendix A respectively.

The CO_2 loading analyses were performed by using two to five parallel liquid samples each titrated for CO_2 and amine contents. The relative standard uncertainty in the loadings estimated from the standard deviation of the loading measurements was ±2%.

The CO_2 partial pressure was measured online. The IR analyzer was calibrated using the calibration gases 0.5, 5, 10, and 20 mol % CO_2 and each with a relative standard uncertainty of ±2%. The analyzer readings at equilibrium varied within the half–width of its display, with the resolution being always < ±0.5%. The estimated relative expanded uncertainty in the CO_2 content was, therefore, found to be ±2%.

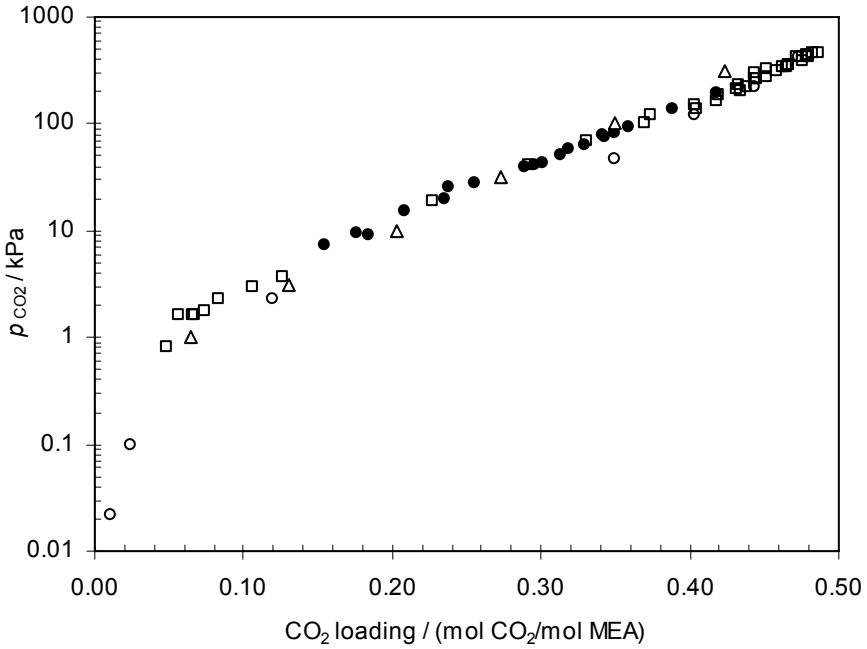

Figure 3-4. Comparison of the solubility of CO_2 in 30 mass % MEA solution at 120 °C: ●, experimental data; ○, Nilsen (2001); □, Goldman and Leibush (1959); Δ, Lee *et al.* (1976);◊, Jou *et al.* (1995).

Goldman and Leibush (1959), Lee *et al.* (1976), and Jou *et al.* (1995) have measured the equilibrium solubility for CO_2 in 30 mass % MEA solution at 120 °C. These are the only data found for this temperature. The data from this work are compared with their data. As seen from Figure 3-4, the equilibrium partial pressures of this work agree well with the data of Goldman and Leibush (1959). The data are also in good agreement with the smoothed data measurements of Lee *et al.* (1976) at loadings from (0.26 to 0.36) and those of Jou *et al.* (1995) for loadings above 0.36.

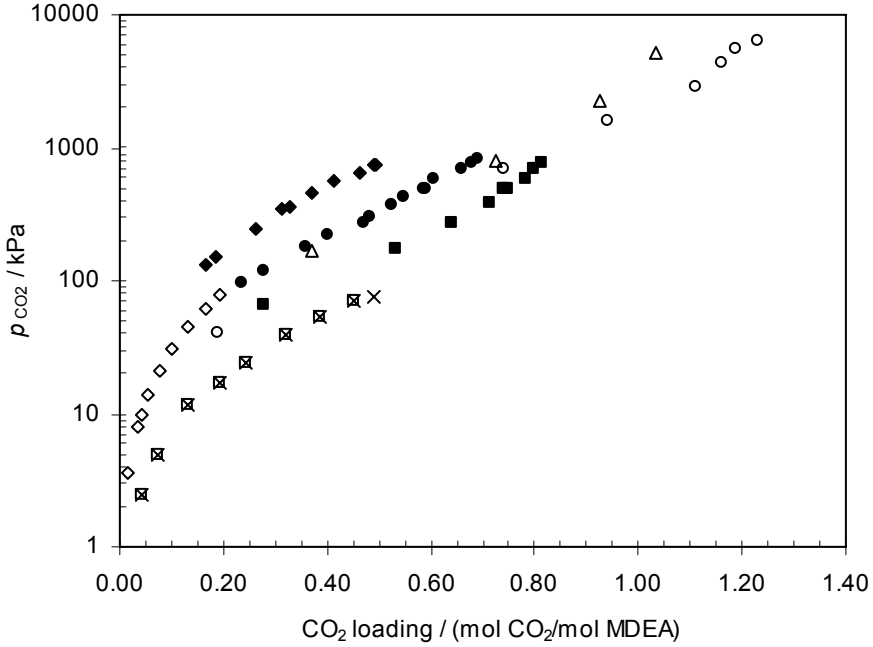

Figure 3-5. Comparison of the solubility of CO_2 in 50 mass % MDEA solution. Experimental data by Nilsen (2002): ■, 55 °C; ●, 70 °C; ♦, 85 °C. Literature data: Δ, 70 °C (Robinson, 1983); ○, 70 °C, 48.8 mass % (Jou *et al.*, 1982); □, 50 °C (Rho *et al.*, 1997); ×, 50 °C (Park and Sandall, 2001); ◊, 75 °C (Rho *et al.*, 1997; Park and Sandall, 2001).

Literature data for comparison of the equilibrium solubility of CO_2 in 50 mass % MDEA solution at the temperatures used here are limited. As seen in Figure 3-5, only at 70 °C could the data directly be compared to those of Robinson (1993). The data were also compared to those of Jou *et al.* (1982), Rho *et al.* (1997), and Park and Sandall (2001). At 70 °C, the measured CO_2 partial pressures from this work are slightly higher than the few data points of Robinson (1983). The data are also higher than those of Jou *et al.* (1982). This is natural as the concentration of MDEA used in this work is slightly higher than that used by Jou *et al.* (1982) (48.8 mass %). Rho *et al.* (1997) found that the higher the concentration of amine used, the higher the partial pressure of CO_2 measured at a fixed

temperature and CO_2 loading. The equilibrium partial pressures of CO_2 at 55 and 70 °C were then compared to those of Rho *et al.* (1997) and those of Park and Sandall (2001) but at (50 and 75) °C. The measured data at 55 °C show higher partial pressures of CO_2 compared to those of Rho *et al.* (1997) and those of Park and Sandall (2001) at 50 °C. This is natural in view of the temperature difference. Extrapolated data of Rho *et al.* (1997) and of Park and Sandall (2001) at 75 °C tend to predict higher partial pressures of CO_2 at higher CO_2 loadings compared to this work for a temperature of 70 °C. This is also reasonable because the temperature used in this work was 5 °C lower compared to the results of Rho *et al.* (1997) and those of Park and Sandall (2001).

From the screening test results in Chapter 2, AEEA seems to offer somewhat better absorption characteristics than the other absorbents tested as it shows a relatively high absorption rate combined with a high absorption capacity of CO_2. To test this absorbent further, the VLE of CO_2 into aqueous 2.9 M AEEA were, therefore, studied and measured at temperatures from 40 to 120 °C. The results are presented in Figure 3-6.

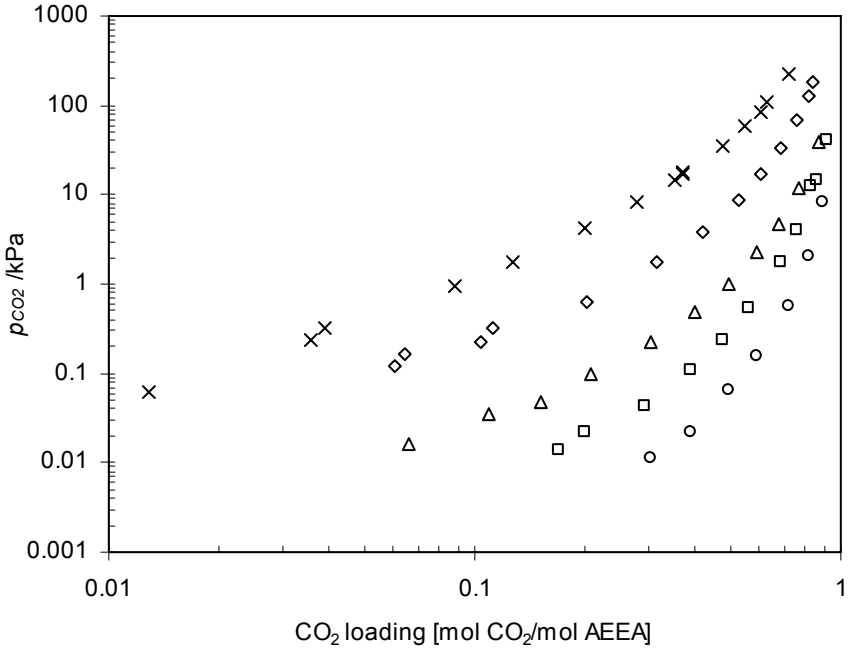

Figure 3-6. The solubility of CO_2 in 2.9 M AEEA solution: ○, 40 °C; □, 55 °C; Δ, 70 °C; ◊, 95 °C; ×, 120 °C.

3.3.1 Cyclic Capacity

A cyclic capacity of an absorption process is defined as the difference between concentrations at the absorption and stripping processes, as schematically shown in Figure 3-7 and mathematically written in Eq. (3.4).

$$Q = C_{\text{Amine}} \left(\alpha - \alpha_{\text{lean}} \right) \tag{3.4}$$

where $\alpha = \alpha_{\text{rich}}$ and α is the CO_2 loading. The maximum cyclic capacity will be achieved when the equilibrium is attained in both the absorption and stripping steps. Figure 3-8 shows comparison of the maximum/theoretical cyclic capacity of MEA and that of AEEA with applications to natural gas (e.g., 3.5 mol % CO_2), coal–fired power plants (e.g., 12 mol % CO_2), and iron and steel industries (e.g., 25 mol % CO_2). Following is an example case for the coal–fired power plant exhaust containing 12 mol % CO_2. A net CO_2 pickup of 0.369 (mol CO_2/mol amine) is indicated for a 5.0 M MEA solution at CO_2 partial pressure of 12 kPa. At the same partial pressure of CO_2, a 2.9 M AEEA, as a diamine, solution provides a net CO_2 pickup of 0.580 (mol CO_2/mol amine) which is 57 % higher than that of MEA. The maximum cyclic capacities for the three cases are summarized in Table 3-2.

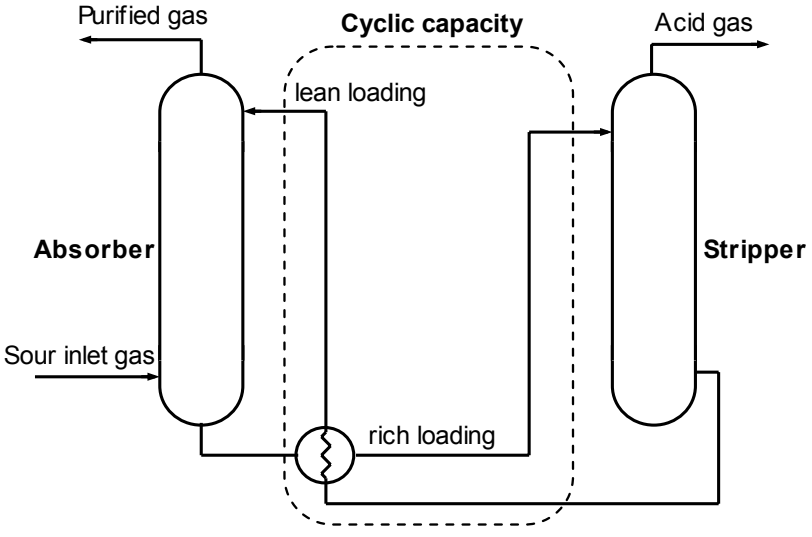

Figure 3-7. Scheme of an absorption–desorption process.

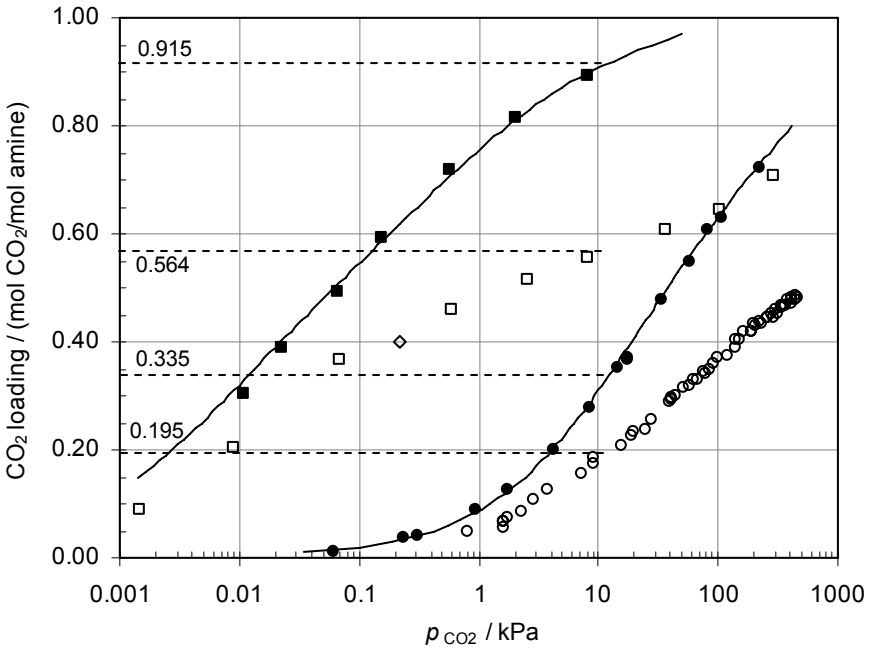

Figure 3-8. Comparison example of the cyclic capacity of MEA and that of AEEA for the coal–fired power plant exhaust. MEA: □, 40 °C (Jou *et al.*, 1995); ◊, 40 °C (This work, 2005); ○, 120 °C (Goldman and Leibush, 1959 and Ma'mun *et al.*, 2005). AEEA: ■, 40 °C; ●, 120 °C; solid lines, calculated from the VLE model.

Table 3-2. Cyclic capacities of MEA and those of AEEA for natural gas, coal–fired power plant, and iron and steel industry exhausts.

CO_2 source	MEA			AEEA		
	α_{rich}	α_{lean}	Cyclic capacity Q	α_{rich}	α_{lean}	Cyclic capacity Q
Natural gas (p_{CO2} = 3.5 kPa)	0.520	0.121	0.399	0.849	0.184	0.665
Coal–fired power plant (p_{CO2} = 12 kPa)	0.564	0.195	0.369	0.915	0.335	0.580
Iron and steel industry (p_{CO2} = 25 kPa)	0.588	0.238	0.350	0.945	0.441	0.504

α = CO_2 loading [mol CO_2/mol amine], cyclic capacity in mol CO_2/mol amine.

3.3.2 Comparison of Absorbent Performance

In addition to the higher cyclic capacity, a higher absorption rate is also important in designing an absorption column to reduce its size. Therefore, a comparison between AEEA and MEA for CO_2 recovery can be made by using a combination of the VLE data together with the absorption rate data.

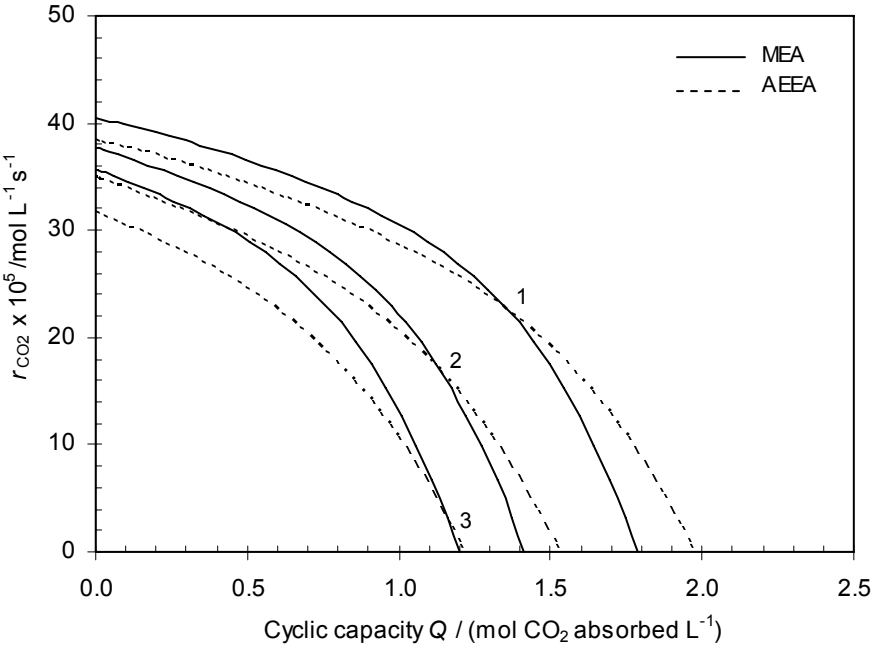

Figure 3-9. Relationship between absorption rate of CO_2 and cyclic capacity in 5.0 M MEA and 2.9 M AEEA solutions: 1, natural gas; 2, coal–fired power plant; 3, iron and steel industry.

By using Eq. (3.4) with $\alpha_{lean} \leq \alpha \leq \alpha_{max}$ and the selected lean loadings obtained from Goldman and Leibush (1959) and Ma'mun *et al.* (2005) in Figure 3-8, the comparison can be seen in Figure 3-9. The highest difference in cyclic capacity between AEEA and MEA is obtained as the loading reaches maximum (α_{max}) in which the absorption rate of CO_2 equals zero. The maximum cyclic capacity can then be calculated as a function of lean loading. The lean loading for the two absorbents is determined at a set partial pressure of CO_2. For the natural gas case, a maximum net CO_2 pickup of 1.785 M CO_2 absorbed is given by a lean MEA at loading of 0.121 which gives a CO_2 partial pressure of 3.5 kPa at 120 °C. At the same CO_2 partial pressure and temperature, the loading of lean AEEA is 0.184 with a maximum net CO_2 pickup of 1.971 M CO_2 absorbed. The difference in maximum cyclic capacity between AEEA and MEA is, therefore, 0.186 M CO_2 absorbed

for this case. This has been done for several lean loadings for coal–fired power plant and iron and steel industry as seen in Table 3-3 and Figure 3-10 where the maximum cyclic capacity is given together with the difference in cyclic capacity as a function of lean loading in one of the absorbents (MEA).

Table 3-3. Maximum cyclic capacities of MEA and those of AEEA for natural gas, coal–fired power plant, and iron and steel industry exhausts.

CO_2 source	MEA		AEEA		ΔQ_{max}
	α_{lean}	Max. capacity Q_{max}	α_{lean}	Max. capacity Q_{max}	
Natural gas (p_{CO2} = 3.5 kPa)	0.121	1.785	0.184	1.971	0.186
Coal–fired power plant (p_{CO2} = 12 kPa)	0.195	1.413	0.335	1.527	0.114
Iron and steel industry (p_{CO2} = 25 kPa)	0.238	1.198	0.441	1.215	0.017

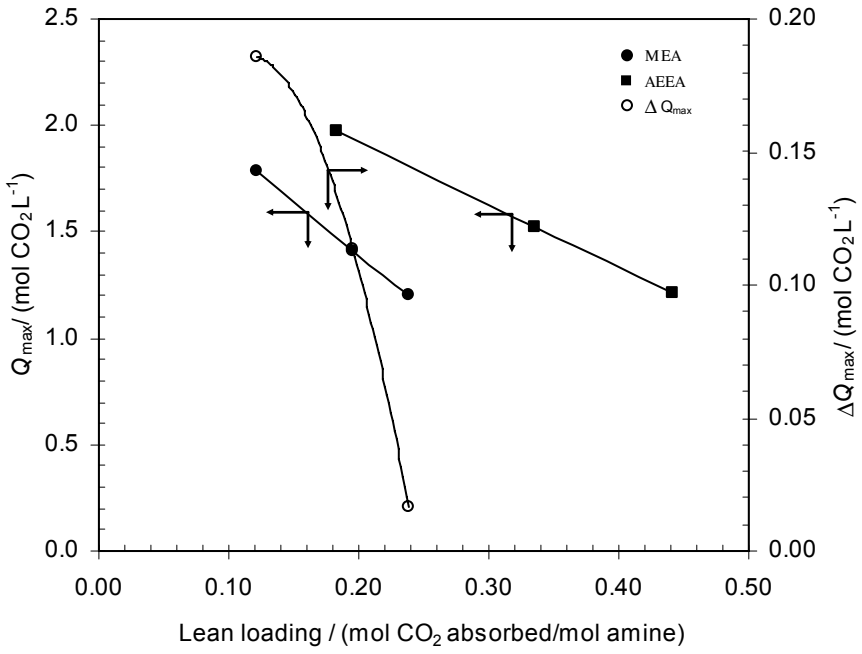

Figure 3-10. Comparison of maximum cyclic capacity in 5.0 M MEA and 2.9 M AEEA solutions with applications to natural gas, coal–fired power plant, and iron and steel industry.

In Figure 3-9, the CO_2 absorption rate is shown as function of the cyclic capacity for the two absorbents. The results indicate that at high cyclic capacities, as is normally

desired in absorption processes, AEEA seems to have better characteristics than MEA. At lower cyclic capacities, MEA is then the better choice. The region where AEEA outperforms MEA seems to increase with decreasing lean loading. In practice, the rich loading (α_{rich}) is equal to or less than α_{max}. The difference in maximum cyclic capacity at the same absorption rate will be negative at rich loadings for MEA below 0.40 and those for AEEA below 0.65 for the natural gas case. This is because the absorption rate of CO_2 in MEA is higher than for AEEA at the observed loadings. It should be noted that increasing the AEEA concentration will strengthen its case even more.

3.3.3 Enthalpy of Solution of CO_2 in MDEA and AEEA

An approximate value of the differential enthalpy of solution of CO_2 in the aqueous 50 mass % MDEA solution in such a loading was calculated by use of the following form of the Gibbs–Helmholtz equation

$$\frac{\Delta H_s}{R} = \left(\frac{\partial \ln p_1}{\partial (1/T)} \right)_{x_1} \tag{3.5}$$

where the subscript 1 refers to CO_2 and x_1 is the mole fraction or equilibrium loading of CO_2. The differential enthalpies of solution of CO_2 in the aqueous 30 mass % AEEA were also calculated by use of Eq. (3.5) for a loading range between 0.1 and 1.0. The equilibrium CO_2 partial pressures in the AEEA solution were calculated based on the VLE model in Chapter 6.

The enthalpy of solution may normally be found to be dependent on the loading. The value of ΔH_s in 50 mass % MDEA solution at a loading of 0.50 was found to be 53.4 kJ/mol CO_2. The standard uncertainty for this value was estimated to be ±5%. This value agrees well with the value 53.2 kJ/mol CO_2 (at 48.8 mass % MDEA) at a loading of 0.50 which was proposed by Jou *et al.* (1982), but is much higher than the value 30 kJ/mol CO_2 (30 mass % MDEA) at a loading of 0.51 reported by Mathonat *et al.* (1997).

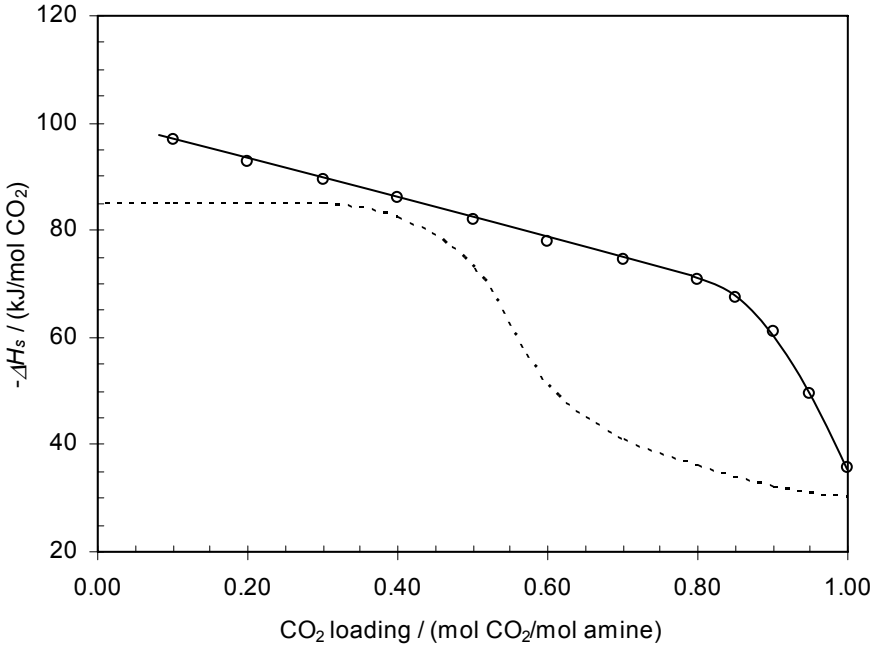

Figure 3-11. The differential enthalpy of solution of CO_2 in the aqueous 30 mass % amine solutions: solid line, AEEA; dotted line, MEA (Jou *et al.*, 1994).

Figure 3-11 shows that the enthalpies of solution of CO_2 in 30 mass % AEEA are higher than those in 30 mass % MEA (Jou *et al.*, 1994) for the whole loading range. The value of ΔH_s in 30 mass % AEEA solution at infinite dilution was found to be approximately 100 kJ/mol CO_2 which is higher 18% than that of ΔH_s at infinite dilution in 30 mass % MEA proposed by Lee *et al.* (1974), Jou *et al.* (1994), and Carson *et al.* (2000).

3.3.4 Regeneration Energy Requirement

According to Rochelle *et al.* (2002), the total energy requirement to regenerate the absorbent in a stripper consists of three elements; heat of desorption of CO_2 (Q_{des}), sensible heat of solvent to get to bottoms T (Q_{sens}), and minimum amount of heat required to maintain sufficient water vapor for stripping (Q_{strip}). This relation is mathematically expressed by

$$\begin{aligned} Q_T &= Q_{\text{des}} + Q_{\text{sens}} + Q_{\text{strip}} \\ &= \Delta H_{\text{CO}_2} + \frac{\rho c_{\text{p}} \Delta T}{\left(\alpha_{\text{rich}} - \alpha_{\text{lean}}\right) C_{\text{Amine}}} + \frac{P^{\text{sat}}_{\text{H}_2\text{O}}\left(T_{\text{top,des}}\right) x_{\text{H}_2\text{O,freebasis}}}{P^{*}_{\text{CO}_2}\left(T_{\text{top,des}} \alpha_{\text{rich}}\right)} \Delta H^{\text{vap}}_{\text{H}_2\text{O}} \end{aligned} \tag{3.6}$$

where $\Delta H_{H_2O}^{vap}$ represents heat of evaporation of water (40 kJ/mol H_2O at 100°C, Lide, 2003) and $P_{CO_2}^{*}$ is the partial pressure of CO_2 that would be in equilibrium with the rich solution at the bottom of the absorber. Q_{des} is proportional to the enthalpy of solution of CO_2 and Q_{sens} to the temperature approach in the cross exchanger and inversely proportional to the absorption capacity. Q_{strip} depends on both temperatures of absorber and stripper and CO_2 concentration in the inlet gas. Decreasing absorber temperature and increasing CO_2 concentration in the inlet gas lead to decreasing Q_{strip}. Increasing stripper temperature will also decrease Q_{strip}.

Table 3-4. The total heat duty in the reboiler for the natural gas case.

$\alpha_{lean,\ actual}$	MEA				AEEA			
	Q_{des}	Q_{sens}	Q_{strip}	Q_T	Q_{des}	Q_{sens}[a]	Q_{strip}	Q_T
0.145	85.0	50.2	102.2	237.4				
0.20	85.0	61.7	102.2	248.9				
0.221	85.0	67.5	102.2	254.7	92.7	50.7	78.7	222.1
0.25	85.0	77.7	102.2	264.9	91.5	53.8	78.7	224.0
0.30					89.5	60.2	78.7	228.4
0.35					87.5	68.3	78.7	234.5
0.40					86.0	78.9	78.7	243.6
0.45					84.0	93.4	78.7	256.1
0.50					81.9	114.5	78.7	275.1

[a] heat capacity of 30 mass % AEEA was assumed to be equal to that of 30 mass % MEA, 3.90 kJ kg^{-1} K^{-1} (Chiu *et al.*, 1999).

Q, heat duty [kJ/mol CO_2], $\alpha_{lean,\ actual} = 1.2 \times \alpha_{lean}$, $\alpha_{rich,\ MEA,\ actual} = 0.85 \times 0.520$, $\alpha_{rich,\ AEEA,\ actual} = 0.85 \times 0.849$, $T_{abs} = 40$ °C, $T_{strip,top} = 100$ °C, $T_{strip,bot} = 120$ °C.

Table 3-5. The total heat duty in the reboiler at maximum cyclic capacity for MEA and AEEA.

CO_2 source	Q_T		ΔQ_T
	MEA	AEEA	
Natural gas (p_{CO2} = 3.5 kPa)	237.5	222.1	15.4
Coal–fired power plant (p_{CO2} = 12 kPa)	200.8	179.6	21.2
Iron and steel industry (p_{CO2} = 25 kPa)	187.8	209.0	–21.2

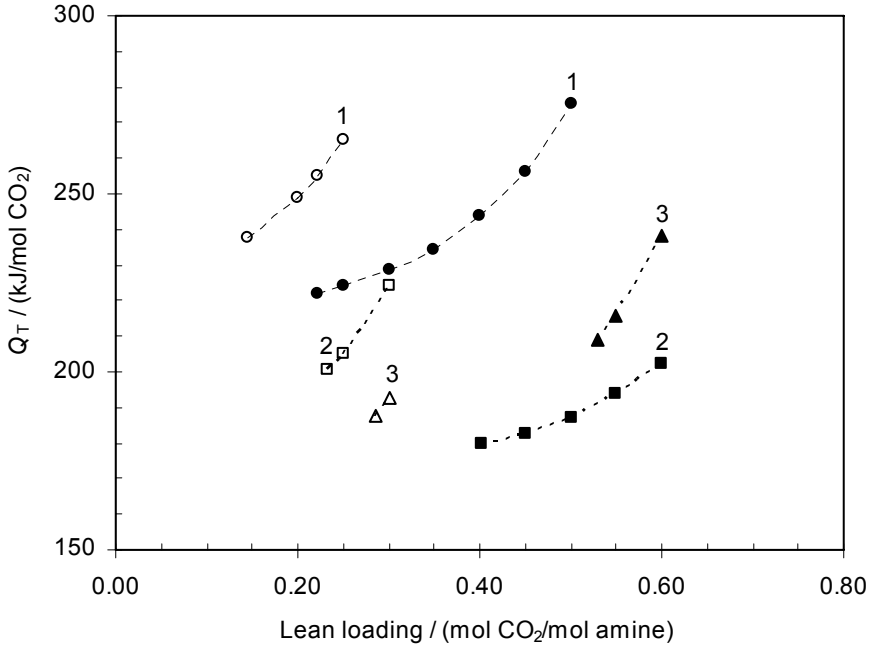

Figure 3-12. Comparison of the total heat duty in the reboiler: 1, natural gas (○, MEA; •, AEEA); 2, coal–fired power plant (□, MEA; ■, AEEA); 3, iron and steel industry (Δ, MEA; ▲, AEEA).

In the case of natural gas with CO_2 content of 3.5 mol %, the comparison of the total heat duty in the reboiler (Q_T) as a function of lean loadings is summarized in Table 3-4. The total heat duty in the reboiler was found to be mainly from Q_{des} and Q_{strip} at low lean loadings. Figure 3-12 shows Q_T for the three cases. In general, at high absorption capacities, AEEA surprisingly gives lower Q_T than MEA. Despite the heat of solution of CO_2 in AEEA is higher, but its Q_{strip} is much lower than that MEA. At maximum cyclic capacity, Q_T for AEEA in the natural gas case is found to be lower, approximately 7%, than that for MEA. Table 3-5 summarizes the results for different inlet gas CO_2 concentrations for the cases.

For economic reason, a lower energy consumption for regeneration process of an absorbent is a must. From the case study mentioned, the results indicate that at high absorption capacities and at medium partial pressure of CO_2 (p_{CO_2} = 12 kPa), AEEA seems to have lower total energy requirement for regeneration process than MEA.

3.4 Conclusions

The vapor–liquid equilibrium data of CO_2 in 30 mass % MEA solution were measured at 120 °C, in 50 mass % MDEA solution at 55, 70, and 85 °C, and in 30 mass % AEEA solution from 40 to 120 °C, respectively. The VLE data of MEA, MDEA, and AEEA should be useful for the absorber/desorber design using these amines to remove CO_2. The VLE data could also serve as a standard for use in the modeling of VLE in MEA, MDEA, and AEEA solutions. The VLE model for AEEA will be discussed further in Chapter 6.

From the study case, AEEA seems to have better performances than MEA. In addition to the high absorption rate, AEEA also offers high cyclic capacity. The regeneration energy requirement for AEEA is much lower than that for MEA at the partial pressure of CO_2 around 12 kPa.

CHAPTER 4

Review on VLE Models

The acid gas sweetening processes have been studied for decades. A large number of publications on experimental data, model development, and plant operation can be found in the literature. The goal of the present chapter is to give a brief review on the thermodynamics and VLE models for the acid gas–alkanolamine–water systems which have been proposed in the literature and reviewed by several authors (Austgen, 1989; Lee, 1996; Hoff, 2003; and Poplsteinova, 2004). The review is summarized in Table 4-1.

Table 4-1. Literature review of the VLE models for the acid gas–alkanolamine–water systems

Author	Experimental condition	VLE model
Mason and Dodge (1936)	- Acid gas: CO_2 - Amine: MEA (0.5, 2.0, 5.0, 9.5, 12.5 N), DEA (0.5, 2.0, 5.0, 8.0 N), and TEA (0.5, 1.0, 2.0, 3.5, 5.0 N) - Temp.: 0 to 75 °C	A plain curve–fitting approach
Atwood *et al.* (1957)	- Acid gas: H_2S - Amine: MEA (5, 15, 20, 30 mass %), DEA (10, 25, 50 mass %), TEA (15, 20, 30, 50 mass %) - Temp.: 27 to 71 °C	Using mean ionic activity coefficient approach which was assumed to be equal for all ionic species
Danckwerts and McNeil (1967)	- Acid gas: CO_2 - Amine: MEA 2 M and DEA 2 M - Other: NH_3 2 M - Temp.: 18 °C	- Adopting van Krevelen *et al.* (1949) approach: apparent equilibrium constants, no activity coefficients, ionic strength dependence - Limitation: ionic strength is insufficient to determine the concentration dependency of the equilibrium constants
Klyamer *et al.* (1973)	Modeling work with application to CO_2–MEA/DEA–H_2O systems	Using Atwood *et al.* (1957) approach to generalize model for H_2S–CO_2–ethanolamine–water system

Table 4-1. (continued)

Author	Experimental condition	VLE model
Edwards *et al.* (1975, 1978)	Modeling work with application to aqueous solutions containing volatile weak electrolytes, e.g., NH_3, CO_2, H_2S, SO_2, and HCN	- More rigorous than earlier models - Activity coefficient was adopted from Guggenheim (1935) - Valid for low concentrations of the electrolytes (10^{-4} to 1 or 2 molal) - Replacing Guggenheim's equation with the Pitzer expression (Pitzer, 1973) to extend the range of validity of the model up to 20 molal (Edwards *et al.*, 1978)
Kent and Eisenberg (1976)	Modeling work with application to H_2S/CO_2–MEA/DEA–H_2O systems	- Modifying Danckwerts–McNeil approach: Henry's law to correlate vapor–liquid equilibrium for the acid species, activity and fugacity coefficients taken to be unity. - Validation: reasonable predictions in some commercial absorbers - Limitation: could not accurately predict the concentration of each species and unsuccessful for tertiary amines because of no carbamate formation
Deshmukh and Mather (1981)	Modeling work with application to H_2S/CO_2–MEA–H_2O systems	- Applying the Guggenheim extension of the Debye–Hückel theory (Debye and Hückel, 1923) - Binary interaction parameters were fitted for H_2S/CO_2–MEA–H_2O systems - Valid up to an ionic strength of 5 molal - Very popular and widely used in industrial application
Austgen *et al.* (1989, 1991)	- Acid gas: CO_2, H_2S - Amine: 2.5 M MEA, 4.28 M MDEA, 2.0 M MDEA + 2.0 M MEA, 2.0 M MDEA + 2.0 M DEA - Temp.: 40 and 80 °C	- Proposing a complex model - Activity coefficients: adopting the electrolyte–NRTL theory by Chen *et al.* (1982) and Chen and Evans (1986) - Fugacity coefficients: the Soave–Redlich–Kwong equation of state - Binary and ternary interaction parameters were fitted to the binary (amine–water) and ternary (acid gas–amine–water) data - The carbamate equilibrium constant was treated as an adjustable parameter

Table 4-1. (continued)

Author	Experimental condition	VLE model
Weiland *et al.* (1993)	Modeling work with application to H_2S/CO_2–MEA/DEA/DGA/MDEA–H_2O systems	- Applying the Deshmukh–Mather model to several alkanolamines - A new set of parameters were obtained by regression - The commercial *ProTreat* code (www.ogtrt.com/protreat-r.htm) was developed based on the Deshmukh–Mather model
Li and Mather (1994)	Modeling work with application to CO_2–MEA–MDEA–H_2O system	- Similar to the model by Edwards *et al.* (1975, 1978) by applying the new Pitzer equation (Clegg and Pitzer, 1992) - Limitations: low pressure range application because of neglecting the non–ideality in the gas phase; unreliable at very low and very high loadings because the carbonate and free CO_2 species were not considered
Kritpiphat and Tontiwachwuthikul (1996)	Modeling work with application to CO_2–AMP–H_2O systems	- Modifying Kent–Eisenberg model: apparent equilibrium constants for all reactions as well as for the Henry's constant - Sensitivity analysis result: the apparent constants of amine protonation, dissociation and physical solubility of CO_2 were the most significant parameters
Lee (1996)	Modeling work with application to H_2S/CO_2–alkanolamines–water and Hydrocarbon–CO_2–alkanolamines–systems	- Combining the mean spherical approach (MSA) from ionic solution theory of statistical mechanics with the UNIFAC group contribution method of Wu and Sandler (1991) for polar solvents - Fugacity coefficients: Peng–Robinson equation of state
Posey *et al.* (1996)	Modeling work with application to MDEA–CO_2–,MDEA–H_2S–, and DEA–H_2S–H_2O systems	- Explicit relationship to calculate acid gas partial pressure using single combined chemical and phase equilibrium constant which is a function of temperature, loading of acid gas, and concentration of amine - Useful for quick desktop calculations and checking the consistency of experimental data

Table 4-1. (continued)

Author	Experimental condition	VLE model
Kuranov *et al.* (1997)	Modeling work with application to CO_2/H_2S–MDEA–H_2O system	- Using electrolyte equation of state based on a lattice theory - Activity coefficients in liquid and vapor phases: using the modified hole group–contribution model (HM) by Smirnova and Victorov (1987) for molecular fluid and the modified Debye–Hückel approximation by Pitzer (1973)
Button and Gubbins (1999)	Modeling work with application to CO_2–MEA/DEA–H_2O system	Using the original form of the Statistical Associating Fluid Theory (SAFT) by Huang and Radosz (1990, 1991) consisting of terms for repulsion, dispersion, chain formation, and association
Vallée *et al.* (1999)	Modeling work with application to CO_2/H_2S–DEA–H_2O system	Adopting the electrolyte equation of state by Fürst and Renon (1993)
Bishnoi (2000)	- Acid gas: CO_2 - Amine: 0.6 M PZ, 4.28 M MDEA, 0.6 M PZ + 4 M MDEA - Temp.: 40 and 70 °C	- Using the same model as that of Austgen (1989)
Kaewsichan *et al.* (2001)	Modeling work with application to CO_2–H_2S–MEA–MDEA–H_2O system.	- Activity coefficients: similar approach based on the electrolyte–UNIQUAC model by Sander *et al.* (1986) - Fugacity coefficients: Soave–Redlich–Kwong equation of state
Solbraa (2002)	- Acid gas: CO_2 - Amine: MDEA - Temp.: 25 and 40 °C	Adopting the electrolyte equation of state (ScRK–EOS) based on the model developed by Fürst and Renon (1993) and the electrolyte CPA–EOS
Poplsteinova (2004)	Modeling work with application to CO_2–MEA/MDEA–H_2O system	- Activity coefficients: combining the group contribution method UNIFAC approach by Lee (1996) with the extended Debye–Hückel approach by Deshmukh and Mather (1981) - Fugacity coefficients: Peng–Robinson equation of state - Applicability: a wide range of loadings and temperatures

CHAPTER 5

Thermodynamic Framework

5.1 Introduction

The present chapter is intended to provide the reader a brief review of some of the thermodynamic concepts regarding relations between chemical potential, fugacity, activity coefficients, and excess Gibbs energy functions that have been applied to this work to model the vapor–liquid equilibria (VLE) of the weak electrolyte system of CO_2–alkanolamine–water. All of the information contained here can be found in various thermodynamics textbooks, e.g., Prausnitz *et al.* (1999), Elliott and Lira (1999), Smith *et al.* (2001) etc.

In aqueous solution, volatile electrolytes exist in ionic and molecular forms. At ordinary temperature and pressure, only the molecular form exists in the vapor phase. The CO_2–alkanolamine–water system is one of the examples of weak electrolyte reactive systems. When CO_2 is absorbed into an alkanolamine solution, the chemical reactions result in a complex mixture of volatile molecular species and nonvolatile ionic species. Calculation of VLE requires simultaneous solution of phase–equilibrium equations for the molecular species, chemical–equilibrium equations for the liquid phase, and material balances. The coupling between phase and chemical equilibria is schematically illustrated in Figure 5-1 (Edwards *et al.*, 1975).

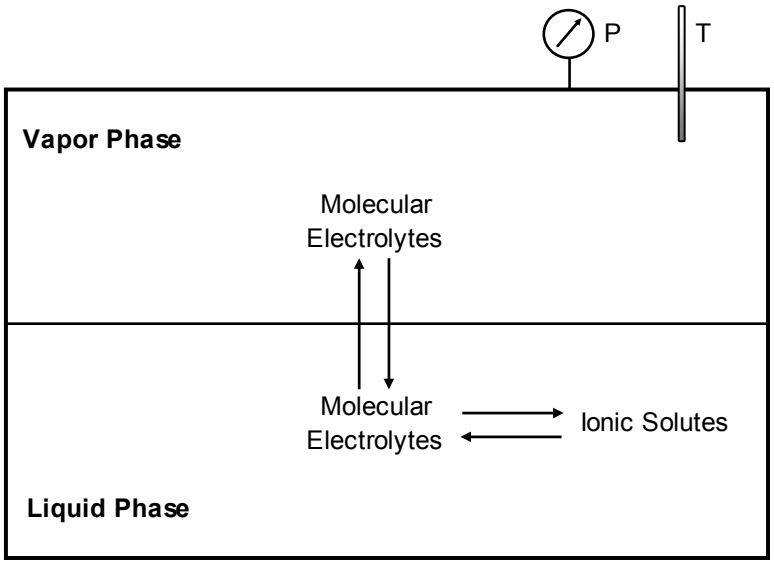

Figure 5-1. Schematic representation of vapor–liquid equlibria for an aqueous weak electrolyte solution.

5.2 Conditions of Equilibrium

A closed homogeneous system is one with uniform properties throughout without exchanging matter inside the system with its surrounding, although it may exchange energy. The number of moles of each component in a closed system not undergoing chemical reaction is, therefore, constant. A thermodynamic equilibrium is reached when interactions of the system with its surroundings in the form of heat transfer and work of volumetric displacement is reversible at a constant temperature and pressure. The general condition of thermodynamic equilibrium can then be written as a combined statement of the first and the second laws of thermodynamics (Prausnitz, 1999)

$$dU = TdS - PdV \tag{5.1}$$

where dU, dS, and dV are, respectively, small changes in internal energy, entropy, and volume of the system. The first terms on the right (TdS) is the heat absorbed by the system and the second term (PdV) is the work done by the system. Entropy, S, and volume, V, are the independent variables for the system.

By interchanging both T and S and P and V in Eq. (5.1) so as to use T and P as the independent variables, Gibbs free energy, G, is then defined as

$$G \equiv U - TS - (-PV) \tag{5.2}$$

which gives

$$dG = -SdT + VdP \tag{5.3}$$

in which at constant T and P indicated as subscripts below, Eq. (5.3) reduces to

$$\left(dG\right)_{T,P} = 0 \tag{5.4}$$

Equation (5.4) shows the *thermodynamic equilibrium* condition for a closed homogeneous system at constant T and P in which the Gibbs free energy reaches its minimum.

Consider a closed heterogeneous system, made up of two or more phases with each phase treated as an open system within the overall closed system. There is mass and heat transfer between the various phases in the system. At thermal and mechanical equilibrium, temperature and pressure are uniform throughout the entire heterogeneous closed system by neglecting surface forces, semipermeable membranes, and electric, magnetic, or gravitational forces. These conditions of phase equilibrium for the heterogeneous closed system consisting of π phases and N components can be summarized as follows:

$$T^1 = T^2 = ... = T^\pi \tag{5.5}$$

$$P^1 = P^2 = ... = P^\pi \tag{5.5}$$

$$\mu_i^1 = \mu_i^2 = ... = \mu_i^\pi \qquad i = 1, 2, ..., \mathrm{N} \tag{5.7}$$

where μ_i is chemical potential which is equal to the partial molar Gibbs free energy $\overline{g}_i$ and is defined as:

$$\mu_i = \left(\frac{\partial G}{\partial n_i}\right)_{T,P,n_{j\neq i}} \tag{5.8}$$

Chemical potential is a difficult thermodynamic variable to use in the real world because only relative values of this variable can be computed. It is, therefore, desirable to express the chemical potential in term of a new thermodynamic variable called fugacity, f_i, that might be more easily identified with physical reality. It was G. N. Lewis (Prausnitz *et al.*, 1999) who first defined a relation between the chemical potential and the fugacity for an isothermal change for any component in any system, solid, liquid, or gas, pure or mixed, ideal or not,

$$\mu_i - \mu_i^{\circ} = RT \ln \frac{f_i}{f_i^{\circ}}, \quad (\widehat{f}_i, \text{ for a mixed system}) \tag{5.9}$$

where μ_i° and f_i° are arbitrary, but not independent, values of the chemical potential and fugacity of component *i* for some chosen reference state. Substituting Eq. (5.9) into Eq. (5.7), expression of phase equilibrium at constant and uniform values of the system and pressure is therefore,

$$f_i^1 = f_i^2 = ... = f_i^{\pi} \qquad i = 1, 2, ..., \mathrm{N} \tag{5.10}$$

for all species. Equation (5.10), sometimes referred to as the *isofugacity* condition, has been widely used for phase equilibrium calculations.

5.3 Partial Molar Gibbs Free Energy

An open system can exchange matter as well as energy with its surroundings. The number of moles of each component in the system is not constant. Therefore, the Gibbs free energy *G*, one of the extensive properties of the system, can be transformed from a function of temperature, pressure, and the number of moles of each component:

$$G = G\left(T, P, n_1, n_2, ..., n_{\mathrm{N}}\right) \tag{5.11}$$

where N is the number of components. The total differential of *G* is then

$$dG = \left(\frac{\partial G}{\partial T}\right)_{P,n} dT + \left(\frac{\partial G}{\partial P}\right)_{T,n} dP + \sum_{i=1}^{\mathrm{N}} \overline{g}_i dn_i \tag{5.12}$$

At constant temperature and pressure Eq. (5.12) reduces to

$$dG = \sum_{i=1}^{\mathrm{N}} \overline{g}_i dn_i \tag{5.13}$$

where

$$\overline{g}_i \equiv \left(\frac{\partial G}{\partial n_i}\right)_{T,P,n_{j \neq i}} \tag{5.14}$$

The Gibbs free energy is related to the partial molar Gibbs free energy $\overline{g}_1, \overline{g}_2, ..., \overline{g}_{\mathrm{N}}$ by Euler's theorem:

$$G = \sum_{i=1}^{N} \bar{g}_i n_i \tag{5.15}$$

Differentiation of Eq. (5.15) gives

$$dG = \sum_{i=1}^{N} \bar{g}_i dn_i + \sum_{i=1}^{N} n_i d\bar{g}_i \tag{5.16}$$

in which the Gibbs–Duhem equation will later be derived from this equation.

The definition of a partial molar property is applicable only to extensive properties (volume V, internal energy U, enthalpy H, entropy S, Helmholtz energy A, and Gibbs free energy G) differentiated at constant temperature and pressure. For example, the total volume of a mixture is related to the partial molar volumes by a summation.

5.4 Chemical Potential

As mentioned before, the chemical potential is a difficult thermodynamic variable to use in the practical world because one cannot compute its absolute value but only its change accompanying any arbitrary change in the independent variables temperature, pressure, and composition. For a pure substance i, the chemical potential is related to the temperature and pressure by the differential equation

$$d\mu_i = -s_i dT + v_i dP \tag{5.17}$$

where s_i is the molar entropy

$$s_i = \left(\frac{\partial \mu_i}{\partial T}\right)_P \tag{5.18}$$

and v_i the molar volume

$$v_i = \left(\frac{\partial \mu_i}{\partial P}\right)_T \tag{5.19}$$

Integrating and solving μ_i at some temperature T and pressure P yields

$$\mu_i(T,P) = \mu_i(T^o,P^o) - \int_{T^o}^{T} s_i dT + \int_{P^o}^{P} v_i dP \tag{5.20}$$

where superscript o refers to some arbitrary reference state.

The chemical potential can be defined as the derivative of the extensive thermodynamic properties (*U*, *H*, *A*, and *G*) with respect to the amount of the component under consideration. Equation (5.8) shows the expression of the chemical potentials in terms of the Gibbs free energy. The equilibrium condition in terms of the chemical potentials at constant temperature and pressure can be written as

$$dG = \sum_{i=1}^{N} \mu_i dn_i = 0 \tag{5.21}$$

Since the chemical potential cannot directly be used in the real world, suitable expressions relating the chemical potential to more convenient quantities are needed. In the following paragraphs the fugacity and activity concepts that might be more easily identified with physical reality will be presented.

5.5 Fugacity and Fugacity Coefficient

The concept of fugacity was introduced to real gases to obtain a relation for the chemical potential that might be analogous to the simple relation for ideal gas. At constant temperature *T*, the relation of the chemical potential in Eq. (5.20) reduces to

$$\mu_i = \mu_i^{o} + \int_{P^{o}}^{P} v_i dP \tag{5.22}$$

Substituting the ideal–gas equation

$$v_i = \frac{RT}{P} \tag{5.23}$$

and integrating the Eq. (5.22) from the standard state pressure P^{o} to a system pressure *P* give the final expression for the chemical potential at temperature *T* and pressure *P*:

$$\mu_i - \mu_i^{o} = RT \ln \frac{P}{P^{o}} \tag{5.24}$$

Equation (5.24) shows the change in the abstract thermodynamic quantity μ as a simple logarithmic function of the physical real quantity, pressure. However, this relation is valid only for pure, ideal gases. To obtain a broader application (e.g., any system, solid, liquid, or gas, pure or mixed, ideal or not), the fugacity must be introduced instead of pressure as written in Eq. (5.9).

For a pure, ideal gas, the fugacity is equal to the pressure, and for a component *i* in a mixture of ideal gases, it is equal to its partial pressure p_i. At very low pressures for all systems, pure or mixed, the gas behaves like an ideal gas and the fugacity must, therefore, be equal to the partial pressure as defined by the limit

$$\lim_{P\to 0}\frac{f_i}{y_i P}=1 \tag{5.25}$$

where y_i is the mole fraction of *i*. The dimensionless ratio between the fugacity and the partial pressure is called the fugacity coefficient,

$$\varphi_i=\frac{f_i}{y_i P} \tag{5.26}$$

The chemical potential in terms of the fugacity coefficient can then be expressed as

$$\mu_i-\mu_i^{\circ}=RT\ln y_i P+RT\ln\varphi_i \tag{5.27}$$

There are two ways to calculate the fugacity coefficient of a species either in a pure or mixed gas. The fugacity coefficient relations in terms of *P* and *T*, volume–explicit, and in terms of *V* and *T*, pressure–explicit, are respectively (Beattie, 1949; Prausnitz *et al.*, 1999):

$$RT\ln\varphi_i=RT\ln\frac{f_i}{y_i P}=\int_0^P\left[\left(\frac{\partial V}{\partial n_i}\right)_{T,P,n_{j\neq i}}-\frac{RT}{P}\right]dP \tag{5.28}$$

$$RT\ln\varphi_i=RT\ln\frac{f_i}{y_i P}=\int_V^{\infty}\left[\left(\frac{\partial P}{\partial n_i}\right)_{T,V,n_{j\neq i}}-\frac{RT}{V}\right]dV-RT\ln z \tag{5.29}$$

where $z=Pv/RT$ is the compressibility factor of the mixture. For a mixture of ideal gases, $\varphi_i=1$. Because volumetric properties of fluids are usually and more simply expressed by an equation of state that is pressure–explicit, it is more convenient to calculate thermodynamic properties in terms of independent variables *V* and *T* as written in Eq. (5.29).

5.6 Activity and Activity Coefficient

The activity, *a,* of component *i* at some temperature, pressure, and composition is defined as the ratio of the fugacity of component *i* at these conditions to the fugacity of component *i* in the standard state. The activity of a substance gives an indication of how active a substance is relative to its standard state.

$$a_i(T,P,x) \equiv \frac{f_i(T,P,x)}{f_i(T,P^{\circ},x^{\circ})} \tag{5.30}$$

where superscript o refers to some arbitrary reference state, arbitrary specified pressure and composition. Substituting Eq. (5.30) in to Eq. (5.9) yields a relation between the chemical potential and the activity.

$$\mu_i - \mu_i^{\circ} = RT \ln a_i \tag{5.31}$$

The activity coefficient γ_i is defined as the ratio of the activity of component *i* to its concentration, usually the mole fraction

$$\gamma_i \equiv \frac{a_i}{x_i} \tag{5.32}$$

5.6.1 Excess Gibbs Free Energy

Excess functions are the excess of thermodynamic properties of solutions compared to those of an ideal solution at the same condition of temperature, pressure, and composition. For an ideal solution all excess functions are zero. A general excess function is defined as

$$e^{\mathrm{E}} = e^{\mathrm{real}} - e^{\mathrm{ideal}} \tag{5.33}$$

The excess Gibbs free energy as an important excess function is defined by

$$G^{\mathrm{E}} \equiv G_{(\text{actual solution at } T,P, \text{ and } x)} - G_{(\text{ideal solution at same } T,P, \text{ and } x)} \tag{5.34}$$

For phase–equilibrium thermodynamics, the partial molar excess Gibbs free energy is the most useful partial excess property because it is directly related to the activity coefficient. The relation between partial molar excess Gibbs energy and the activity coefficient for a component *i* in solution at constant temperature and pressure is

$$\bar{g}_i^{\mathrm{E}} = \bar{g}_{i(\mathrm{real})} - \bar{g}_{i(\mathrm{ideal})} = RT\left[\ln f_{i(\mathrm{real})} - \ln f_{i(\mathrm{ideal})}\right] \tag{5.35}$$

and finally

$$\bar{g}_i^{\mathrm{E}} = RT \ln \gamma_i \tag{5.36}$$

Equation (5.36) can be rewritten as

$$g^{\mathrm{E}} = RT \sum_{i=1}^{\mathrm{N}} x_i \ln \gamma_i \tag{5.37}$$

where g^{E} is the molar excess Gibbs free energy.

5.7 Normalization of Activity Coefficient

It is convenient to define the activity coefficient in such a way that for an ideal solution or an ideal solution containing solid or gaseous solutes, the activity coefficient is equal to unity. Therefore, the activity coefficient may be normalized in three different ways.

5.7.1 Convention I

The most common reference state is the pure component at the same temperature and pressure as the system observed. Therefore, this convention leads to an ideal solution in the sense of Raoult's law and is normally used when all components, both solutes and solvent of the solution in their pure states, are liquids at the system temperature and pressure. The activity coefficient of each component *i* then approaches unity as its mole fraction approaches unity at the system temperature and the system reference pressure. Thus, the normalization of the activity coefficient for each component *i* is

$$\mu_i = \mu_i^{\circ} + RT \ln \gamma_i x_i \qquad \gamma_i \to 1 \quad \text{as} \quad x_i \to 1 \tag{5.38}$$

Since this normalization holds for all components, solute and solvent, this convention is called the symmetric convention for normalization in which the activity coefficients are said to be symmetrically normalized.

5.7.2 Convention II

For some systems, e.g., a solution containing components that alone would be solid or gaseous at the system temperature and pressure; it is not convenient to use the Convention I to normalize the activity coefficients of the components.

In this convention, the reference state for the solvent is the same as that adopted under Convention I in which the reference state is that of the pure solvent at the system temperature and pressure. However, the reference state for the solute is the hypothetical state of pure solute found by extrapolating its chemical potential to infinite dilution at the system temperature and reference pressure. This convention, therefore, leads to an ideal dilute solution in the sense of Henry's law. The normalization of the activity coefficients for the solvent and solute considered under Convention II is

$$\mu_s = \mu_s^{\circ} + RT \ln \gamma_s x_s \qquad \gamma_s \to 1 \quad \text{as} \quad x_s \to 1 \tag{5.39}$$

$$\mu_i = \mu_i^{\circ} + RT \ln \gamma_i^{*} x_i \qquad \gamma_i^{*} \to 1 \quad \text{as} \quad x_i \to 0 \tag{5.40}$$

where the subscripts *s* and *i* refer to solvent and solute respectively. Because solvent and solute are not normalized in the same way, this gives the unsymmetric convention for normalization and the superscript asterisk (*) on the activity coefficient for the solute is then introduced to indicate that the activity coefficient of this solute approaches unity as its mole fraction approaches zero.

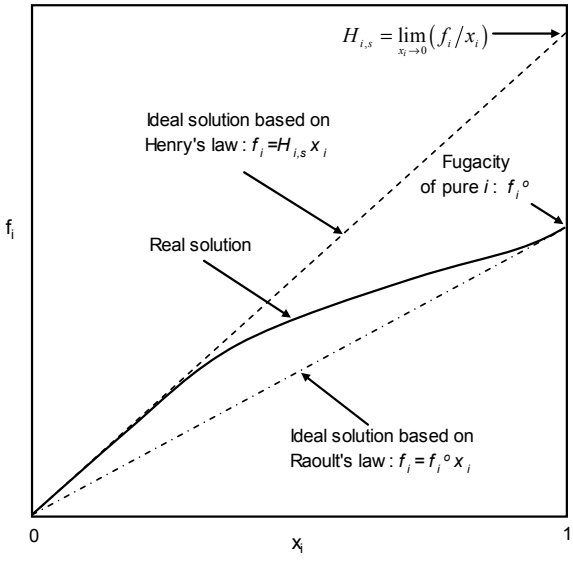

Figure 5-2. Normalization of activity coefficients based on pure fugacity reference state and infinite dilution reference state

5.7.3 Convention III

For solutions containing solid, e.g., salts and polymers, the concentrations are often measured on the molality scale m (moles of solute/1000 g of solvent) and activity coefficients of these solutes are defined based on the molality scale. It is more convenient to use the molality scale because it does not require density data. The reference state for the solvent is the same as that considered under Convention I or II; the state of pure solvent at the system temperature and pressure. The reference state for the solute is the same as that considered under Convention II. Based on this convention, the chemical potentials and the activity coefficients for solvent and solute can be expressed as

$$\mu_s = \mu_s^{\circ} + RT \ln \gamma_s x_s \qquad \gamma_s \to 1 \quad \text{as} \quad x_s \to 1 \tag{5.41}$$

$$\mu_i = \mu_i^{\Delta} + RT \ln \gamma_i^{\Delta} m_i \quad \gamma_i^{\Delta} \to 1 \quad \text{as} \quad m_i \to 0 \tag{5.42}$$

where Δ superscript denotes the molality concentration scale.

5.8 Chemical Equilibrium

In a chemically reacting system with R stoichiometric equations the number of moles are related to the extents of reaction ξ_j by

$$n_i = n_i^{\circ} + \sum_{j=1}^{\mathrm{R}} \upsilon_{ij} \xi_j \quad i = 1, 2, ..., \mathrm{N} \tag{5.43}$$

where υ_{ij} is the stoichiometric coefficient of species i in reaction j, and n_i° is a reference amount of species i. Using Eq. (5.43) the Gibbs free energy can then be expressed as a function of temperature, pressure, and R extents of reaction:

$$G = G(T, P, \xi_1, \xi_2, ..., \xi_R) \tag{5.44}$$

The condition of chemical equilibrium is found when the Gibbs free energy reaches its minimum at constant T and P with respect to the R independent extents of reaction.

$$\left(\frac{\partial G}{\partial \xi_j} \right)_{T, P, \xi_{k \neq j}} = 0 \quad j = 1, 2, ..., \mathrm{R} \tag{5.45}$$

Equation (5.45) can be written in terms of number of moles by use of the chain rule for differentiation as

$$\left(\frac{\partial G}{\partial \xi_j}\right)_{T,P,\xi_{k\neq j}} = \sum_{i=1}^{\mathrm{N}} \left(\frac{\partial G}{\partial n_i}\right)_{T,P,n_{k\neq i}} \left(\frac{\partial n_i}{\partial \xi_j}\right)_{\xi_{k\neq j}} \qquad j = 1,2,...,\mathrm{R} \tag{5.46}$$

Differentiation of Eq. (5.43) with respect to the extents of reaction leads to

$$\left(\frac{\partial n_i}{\partial \xi_j}\right)_{\xi_{k\neq j}} = \upsilon_{ij} \tag{5.47}$$

Combining Eqs. (5.45), (5.46), (5.47), and (5.8) finally gives

$$\sum_{i=1}^{\mathrm{N}} \upsilon_{ij}\mu_i = 0 \quad j = 1,2,...,\mathrm{R} \tag{5.48}$$

Equation (5.48) is the classical form of the equilibrium conditions which was derived in terms of chemical potentials. However, the chemical equilibrium is traditionally expressed by the chemical equilibrium constant.

For a single chemical reaction, substitution of Eqs. (5.31) and (5.32) into Eq. (5.48) for any reaction *j* yields

$$\sum_{i=1}^{\mathrm{N}} \upsilon_{ij}\mu_i^{\circ} + RT\sum_{i=1}^{\mathrm{N}} \upsilon_{ij} \ln \gamma_i x_i = 0 \tag{5.49}$$

where the summations are over all N components of the system. Another expression of Eq. (5.49) is

$$\ln\left[\prod_{i=1}^{\mathrm{N}} (\gamma_i x_i)^{\upsilon_i}\right] = -\frac{1}{RT}\sum_{i=1}^{\mathrm{N}} \upsilon_{ij}\mu_i^{\circ} \tag{5.50}$$

A thermodynamic equilibrium constant can be defined as

$$\ln K_j = \left(\frac{-\Delta G_j^{\circ}}{RT}\right) \tag{5.51}$$

where ΔG_j° is the standard Gibbs free energy change for the reaction *j* at a given temperature and defined reference state. In terms of the reference chemical potential, ΔG_j° can be expressed as

$$\Delta G_j^{\circ} = \sum_{i=1}^{\mathrm{N}} \upsilon_{ij}\mu_i^{\circ} \tag{5.52}$$

Combining Eqs. (5.50), (5.51), and (5.52) yields

$$K_j = \prod_{i=1}^{N} (\gamma_i x_i)^{\upsilon_{ij}} = \prod_{i=1}^{N} a_i^{\upsilon_{ij}} \tag{5.53}$$

Equation (5.53) represents a nonlinear algebraic equation of the chemical equilibrium constant relating the standard state Gibbs free energy change of reaction to the activities of various species participating in the chemical reaction *j*.

5.9 Phase Equilibrium

The condition of phase equilibrium in a closed heterogeneous system at constant pressure and temperature is given by Eq. (5.10). For a vapor–liquid multicomponent system, Eq. (5.10) can be expressed as

$$\hat{f}_i^{\mathrm{V}}(T,P,y) = \hat{f}_i^{\mathrm{L}}(T,P,x) \qquad i = 1,2,...,\mathrm{N} \tag{5.54}$$

where $\hat{f}_i^{\mathrm{V}}$ and $\hat{f}_i^{\mathrm{L}}$ are the fugacities of component *i* in the vapor phase and liquid phase respectively, *y* and *x* are mole fractions for the vapor and liquid phases.

Inserting Eqs. (5.26), (5.30), and (5.32) into Eq. (5.54) yields

$$\varphi_i(T,P,y)\, y_i P = \gamma_i(T,P,x)\, x_i f_i^{\mathrm{oL}}(T) \tag{5.55}$$

where φ_i and γ_i are the fugacity coefficient and activity coefficient respectively, and f_i^{oL} is some reference fugacity that may be taken from the Conventions mentioned previously. The reference fugacity for a solvent may follow the Convention I and is specified to be the saturation pressure of the solvent at the system temperature

$$f_s^{\mathrm{oL}}(T) = P_s^{\mathrm{o}}(T)\, \varphi_s^{\mathrm{o}}(T) \tag{5.56}$$

Substituting Eq. (5.56) into Eq. (5.55) yields the vapor–liquid equilibrium expression for the solvent

$$\varphi_s(T,P,y)\, y_s P = \gamma_s(T,P,x)\, x_s P_s^{\mathrm{o}}(T)\, \varphi_s^{\mathrm{o}}(T) \tag{5.57}$$

For a gaseous solute *i*, the reference sate fugacity will follow the Convention II and the vapor–liquid equilibrium expression is, therefore, defined as

$$\varphi_i(T,P,y)\, y_i P = \gamma_i^*(T,P,x)\, x_i H_i^{\infty}(T) \tag{5.58}$$

where H_i^{∞} is the Henry's constant of the solute at infinite dilution.

5.10 Poynting Factor

A correction term used to relate fugacities at different pressures is called the Poynting factor written as

$$\Theta = \frac{f_2(T, P_2)}{f_1(T, P_1)} \tag{5.59}$$

Combining Eqs. (5.20) and (5.31) at constant temperature with pressure change from P_1 to P_2 yields

$$RT\left(\ln \frac{f_2(T, P_2)}{f_1(T, P_1)}\right) = \int_{P_1}^{P_2} v_i dP \tag{5.60}$$

Rearranging Eq. (5.60) results in the general expression for the Poynting factor as follows

$$\Theta = \exp\left(\int_{P_1}^{P_2} \frac{v_i dP}{RT}\right) \tag{5.61}$$

By use of Eqs. (5.57) and (5.58) together with the Poynting factor, the vapor–liquid expressions at the system temperature and pressure for the solvent and solute can respectively be defined as

$$\varphi_s(T, P, y)\, y_s P = \gamma_s(T, P, x)\, x_s P_s^{\circ}(T)\, \varphi_s^{\circ}(T) \exp\left\{\frac{v_s\left(P - P_s^{\circ}\right)}{RT}\right\} \tag{5.62}$$

and

$$\varphi_i(T, P, y)\, y_i P = \gamma_i^*(T, P, x)\, x_i H_i^{\infty}(T) \exp\left\{\frac{\bar{v}_i^{\infty}\left(P - P_s^{\circ}\right)}{RT}\right\} \tag{5.63}$$

where v_s and $\bar{v}_i^{\infty}$ are respectively partial molar volume for solvent *s* and that for molecular solute *i* at infinite dilution in the solvent and H_i^{∞} is the Henry's law constant.

5.11 The Gibbs–Duhem Equation

The Gibbs–Duhem equation is a thermodynamic consistency relation for a heterogeneous system that combined both for experimental data evaluation and theory

development. At internal equilibrium, a heterogeneous system will have a total of $\mu + 2$ variables consisting of temperature, pressure, and μ chemical potentials of each component present in the system. Only μ +1 are independent variables and the last variable is a dependent variable calculated in such a way that the Gibbs–Duhem equation is satisfied. The Gibbs–Duhem equation is derived by inserting Eq. (5.16) into Eq. (5.12).

$$\left(\frac{\partial G}{\partial T}\right)_{P,n} dT + \left(\frac{\partial G}{\partial P}\right)_{T,n} dP - \sum_{i=1}^{\mathrm{N}} \bar{n}_i dg_i = 0 \tag{5.64}$$

5.12 Activity Coefficient of Electrolyte Solution: Debye–Hückel Limiting Law and its Development

The first significant achievement for activity coefficient expression in dilute electrolyte solutions was made by Debye and Hückel (1923). Modifying that activity coefficient expression was made by several authors such as Guggenheim (1935), Bromley (1973), and Pitzer (1973). An overview of the Debye–Hückel limiting law given here is based on the description by Prausnitz *et al.* (1999).

The activity coefficients of ions in an electrolyte solution strongly depend on concentrations and the number of charges of ions. This dependence can be expressed in terms of *ionic strength* of the solution, *I*, defined by

$$I = \frac{1}{2}\sum_{i}^{\mathrm{N}} m_i z_i^2 \qquad i = 1, 2, ..., \mathrm{N} \tag{5.65}$$

where z_i is the charge on ion *i* and m_i its molal concentration.

Due to their velocities, molecules have kinetic energy and they also have potential energy as a result of their positions relative to one another. Consider two spherically symmetric molecules with different charges of magnitudes q_i and q_j separated by the distance *r* in a vacuum medium, the potential energy Γ shared by these two charged molecules or ions is

$$\Gamma_{ij} = \frac{q_i q_j}{4\pi\varepsilon_{\mathrm{o}} r} = \frac{z_i z_j e^2}{4\pi\varepsilon_{\mathrm{o}} r} \tag{5.66}$$

where z_i and z_j are the ionic valences, ε_{o} is the permittivity of vacuum (8.85419×10^{-12} C^2 J^{-1} m^{-1}), and *e* is the electronic charge (1.60218×10^{-19} C). For a medium other than vacuum, Eq. (5.66) becomes

$$\Gamma_{ij} = \frac{z_i z_j e^2}{4\pi\varepsilon r} \tag{5.66a}$$

where ε is the absolute permittivity defined by $\varepsilon = \varepsilon_o \varepsilon_r$; ε_r is the dielectric constant or permittivity relative.

Equation (5.66) shows that the potential energy of interaction varies inversely with the first power of distance (r^{-1}). A shielding effect between anion and cation will produce a decrease in their attractions. To account for this effect, the Debye–Hückel theory shows that r^{-1} should be multiplied by a "damping factor",

$$r^{-1} \rightarrow (r^{-1})\exp(-r\kappa) \tag{5.67}$$

where κ^{-1} is the *shielding length* or the *Debye length* defined by

$$\kappa^{-1} = \left(\frac{\varepsilon RT}{2\rho_s N_A^2 e^2 I}\right)^{1/2} \tag{5.68}$$

where ρ_s is the solvent density and N_A is the Avogadro's number. From Eq. (5.68), it is clearly seen that the Debye length decreases with rising concentration (ionic strength).

Using well–established concepts from classical electrostatics, Debye and Hückel derived a simple expression for the molar activity coefficient γ_i of an ion with charge z_i in a dilute solution:

$$\ln \gamma_i^{(c)} = -z_i^2 \frac{e^2 N_A}{8\pi\varepsilon RT}\kappa \tag{5.69}$$

Since there is no significant difference between molarity and molality for dilute aqueous solutions near ambient temperature, for a nonvolatile solute, it is convenience to use the activity coefficient in the molality scale,

$$\ln \gamma_i^{(m)} = -A_\gamma z_i^2 I^{1/2} \tag{5.69a}$$

where constant A_γ is given by

$$A_\gamma = \left(\frac{e^2}{\varepsilon RT}\right)^{3/2} \frac{N_A^2}{8\pi}(2\rho_s)^{1/2} \tag{5.70}$$

Equations (5.69) and (5.69a) give the activity coefficients of ions, not of electrolytes in an electrically–neutral solution. In the experiment, the mean ionic activity coefficient

$\gamma_{\pm}^{(m)}$ is, however, the quantity usually measured. For a 1-1 electrolyte solution, it is defined by

$$\gamma_{\pm}^{(m)} = -A_{\gamma} \left| z_{+} z_{-} \right| I^{1/2} \tag{5.71}$$

where $\left| z_{+} z_{-} \right|$ is the absolute value of the product of the charges. Equation (5.71) is called as the *Debye–Hückel limiting law* which is useful for interpreting the properties of electrolyte solutions.

The Debye–Hückel equation is applicable only to very dilute solutions (typically, for ionic strengths up to 0.01 mol kg^{-1}). For concentrated electrolyte solutions, several semi–empirical corrections to the Debye–Hückel limiting law have been proposed such as follows

$$\ln \gamma_{\pm} = -\frac{A_{\gamma} \left| z_{+} z_{-} \right| I^{1/2}}{1 + I^{1/2}} + bI \tag{5.72}$$

where *b* is an adjustable parameter. This extended Debye–Hückel equation is only valid up to an ionic strength of ~1 mol kg^{-1} which is still much lower than that of many practical industrial applications. When ion concentrations are low, the average distance between ions is large; therefore, only long–range electrostatic forces are important. As ion concentrations rise, ions begin to interact also with hard–core repulsive forces and with short–range (van der Waals) attraction forces. Based on this, later models try to consider the short–range interactions by combining binary and sometimes ternary interaction parameters in their equations.

The mean ionic activity coefficient correlation for an electrolyte solution has been proposed by Guggenheim (1935) based on the combination of an extended Debye–Hückel equation, to account for long–range ion–ion interactions, with a second order virial expansion term, to account for various short–range forces between ions of opposite charge,

$$\ln \gamma_{\pm} = -\frac{A_{\gamma} \left| z_{+} z_{-} \right| I^{1/2}}{1 + I^{1/2}} + \frac{2\nu_{-}}{\nu_{-} + \nu_{+}} \sum_{+} \beta_{+,-} m_{+} + \frac{2\nu_{+}}{\nu_{-} + \nu_{+}} \sum_{-} \beta_{+,-} m_{-} \tag{5.73}$$

where ν_{+} and ν_{-} are number of cations and anions of the electrolyte, $\beta_{+,-}$ is interaction coefficient between cation and anion at a given temperature.

Bromley (1973) also proposed a semi–empirical equation for representing the mean activity coefficient of a single electrolyte or mixed electrolytes in water. The mean ionic activity coefficient correlation for a single salt solution is defined by,

$$\ln \gamma_{\pm} = -\frac{A_{\gamma}\left|z_{+}z_{-}\right| I^{1/2}}{1+I^{1/2}} + \frac{(0.06+0.60\beta\left|z_{+}z_{-}\right| I}{\left(1+\dfrac{1.5I}{\left|z_{+}z_{-}\right|}\right)^{2}} + \beta I \tag{5.74}$$

β is taken as a constant, approximated as the sum of individual ion β values. However, the constant is only applicable to ~0.1 molal (Bromley, 1972).

Pitzer (1973) presented an excess Gibbs energy model based on a reformulation and extension of Guggenheim's equation in which the ion–ion short range interactions are important and are dependent on the ionic strength. The excess Gibbs energy for an electrolyte solution containing w_s kilograms of solvent, with molalities of solute species m_i, m_j…, is given by

$$\frac{G^{\mathrm{E}*}}{RTw_{\mathrm{s}}} = f(I) + \sum_{i}\sum_{j} m_i m_j \lambda_{ij}(I) \sum_{i}\sum_{j}\sum_{k} m_i m_j m_k \Lambda_{ijk} + \ldots \tag{5.75}$$

where function $f(I)$, representing long–range electrostatic forces and including the Debye–Hückel limiting law, depends on ionic strength I, temperature, and solvent properties. $\lambda_{ij}(I)$ represents the short–range interaction between two solute particles in the solvent and Λ_{ijk} terms account for three–body ion interactions which are important only at high salt concentration.

Consider an electrically neutral electrolyte $M_{v+}X_{v-}$ be dissociated in a high–dielectric–constant like water,

$$\mathrm{M}_{v+}\mathrm{X}_{v-} \rightleftarrows v_{+}\mathrm{M}^{z+} + v_{-}\mathrm{X}^{z-} \tag{5.76}$$

For this solution containing n_{s} moles of solvent and n_{MX} moles of completely dissociated electrolyte, the mean ionic activity coefficient of the model of Pitzer is then expressed as

$$\begin{aligned} \ln \gamma_{\pm}^{(\mathrm{m})} &= \frac{1}{\left(v_{+}+v_{-}\right)RT}\left(\frac{\partial G^{\mathrm{E}*}}{\partial n_{\mathrm{MX}}}\right)_{P,T,n_{\mathrm{s}}} \\ &= \left|z_{+}z_{-}\right| f^{\gamma} + m\left(\frac{2v_{+}v_{-}}{v_{+}+v_{-}}\right) B_{\mathrm{MX}}^{\gamma} + m^{2}\left(\frac{2\left(v_{+}v_{-}\right)^{3/2}}{v_{+}+v_{-}}\right) C_{\mathrm{MX}}^{\gamma} \end{aligned} \tag{5.77}$$

where f^{γ} and B^{γ}_{MX} are ionic strength dependence and C^{γ}_{MX} depends on triple–ion interactions which is important at high concentration (usually higher than 2 mol kg^{-1}), see Prausnitz *et al.* (1999).

The *ion–interaction model* of Pitzer has achieved wide acceptance and has been applied successfully in such industrial processes such as solubilities of atmospheric gases in seawater and equilibria of multicomponent brines with solid phases (Prausnitz *et al.*, 1999).

Deshmukh and Mather (1981) applied the Guggenheim extension of the Debye–Hückel (1923) theory to acid gas–alkanolamine–water solution. The model became very popular among chemical engineers. The coefficient activity expression used in this work is analogue to the one of the Deshmukh–Mather (1981) model but formulated in terms of molar concentration.

$$\ln \gamma_i = \frac{-2.303 A_{\gamma} z_i^2 I^{1/2}}{1 + BaI^{1/2}} + 2\sum_{j \neq w} \beta_{ij} m_j \quad \text{w} = \text{water} \tag{5.78}$$

CHAPTER 6

Modeling of CO_2 Solubility in Aqueous AEEA Solution

Based on work presented in ECOS 2005, Trondheim, Norway, June 20–22, 2005 and accepted in Ind. Eng. Chem. Res. for the CO_2 capture special issue, April 2006

This work focuses on the experimental determination and thermodynamic modeling of the solubility of carbon dioxide (CO_2) in an aqueous solution of 30 mass % 2-(2-aminoethyl-amino)ethanol (AEEA), with AEEA being a potentially new solvent for postcombustion CO_2 capture by absorption. The vapor–liquid equilibrium (VLE) experiments were performed over a range of temperatures from 40 to 120 °C and for partial pressures of CO_2 ranging from 0.01 to 220 kPa. The results obtained were then modeled by use of a modified Deshmukh–Mather thermodynamic model. The model provides a very good representation of the experimental data over the whole temperature range. In addition, ^{1}H and ^{13}C 1D NMR spectra were acquired for species identification and quantitative analysis of the major species distribution. The predicted speciation was also found to be in agreement with the speciation from the NMR data. Protonation constants (pK_a) for AEEA were obtained by titration.

6.1 Phase and Chemical Equilibria

CO_2–AEEA–H_2O is a reactive system, and the VLE model, therefore, involves simultaneous solutions of phase and chemical equilibria. The chemistry of the system is very complex, because AEEA is a diamine containing one secondary and one primary amine group. This gives rise to a large number of possible chemical reactions and formed species. In analogy to what is known for the speciation of piperazine (Bishnoi and Rochelle, 2000), the following 14 species are considered, and later confirmed by NMR, to exist in the liquid phase: AEEA, $AEEAH^+$, $^+HAEEAH^+$, $AEEACOO^-_p$, $AEEACOO^-_s$, $^+HAEEACOO^-_p$, $^+HAEEACOO^-_s$, $^-OOCAEEACOO^-$, CO_2, HCO_3^-, $CO_3^=$, H_2O, H_3O^+, and OH^-. Here, subscripts p and s denote bonding to the primary and secondary amine group respectively.

A series of physical and chemical reaction equilibria for the CO_2–AEEA–H_2O system can be written as follows:

$$CO_{2\,(g)} \rightleftharpoons CO_{2\,(l)} \tag{6.1}$$

The considered equilibrium reactions that take place in the liquid phase are
Dissociation of water

$$2H_2O \rightleftharpoons H_3O^+ + OH^- \tag{6.2}$$

Dissociation of carbon dioxide

$$CO_{2\,(l)} + 2H_2O \rightleftharpoons HCO_3^- + H_3O^+ \tag{6.3}$$

Dissociation of bicarbonate ion:

$$HCO_3^- + H_2O \rightleftharpoons CO_3^= + H_3O^+ \tag{6.4}$$

Dissociation of monoprotonated AEEA:

$$AEEAH^+ + H_2O \rightleftharpoons AEEA + H_3O^+ \tag{6.5}$$

Dissociation of diprotonated AEEA:

$$^+HAEEAH^+ + H_2O \rightleftharpoons AEEAH^+ + H_3O^+ \tag{6.6}$$

Formation of carbamates:

$$AEEA + CO_{2\,(l)} + H_2O \rightleftharpoons AEEACOO_p^- + H_3O^+ \tag{6.7}$$

$$AEEA + CO_{2\,(l)} + H_2O \rightleftharpoons AEEACOO_s^- + H_3O^+ \tag{6.8}$$

Dissociation of protonated carbamates:

$$^+HAEEACOO_p^- + H_2O \rightleftharpoons AEEACOO_p^- + H_3O^+ \tag{6.9}$$

$$^+HAEEACOO_s^- + H_2O \rightleftharpoons AEEACOO_s^- + H_3O^+ \tag{6.10}$$

Formation of dicarbamate:

$$\begin{aligned} AEEACOO_p^- + AEEACOO_s^- + 2CO_{2\,(l)} + 2H_2O \\ \rightleftharpoons {}^-OOCAEEACOO^- + 2H_3O^+ \end{aligned} \tag{6.11}$$

According to Eq. (5.53), the corresponding chemical equilibrium constants for the reactions in Eqs. (6.2) – (6.11) in terms of activity coefficients γ_i and mole fractions x_i can be rewritten as

$$K_j = \prod_i a_i^{\nu_{ij}} = \prod_i \left(\gamma_i x_i\right)^{\nu_{ij}} \quad j = 1, 2, ..., R \tag{6.12}$$

Additional equations are needed to fully determine the system and resolve for all species concentrations. The following total mass balance expressions in terms of mole fraction *x* were used:

$$\sum_i x_i = 1.0 \tag{6.13}$$

mass balance for AEEA,

$$\begin{aligned} C_{\mathrm{T}}^{\mathrm{o}}\, x_{\mathrm{AEEA}}^{\mathrm{o}} = C_{\mathrm{T}}\, (&x_{\mathrm{AEEA}} + x_{\mathrm{AEEAH^+}} + x_{^+\mathrm{HAEEAH^+}} + x_{\mathrm{AEEACOO_p^-}} \\ &+ x_{\mathrm{AEEACOO_s^-}} + x_{^+\mathrm{HAEEACOO_p^-}} + x_{^+\mathrm{HAEEACOO_s^-}} + x_{^-\mathrm{OOCAEEACOO^-}}) \end{aligned} \tag{6.14}$$

mass balance for CO_2,

$$\begin{aligned} C_{\mathrm{T}}^{\mathrm{o}}\, x_{\mathrm{CO_2}}^{\mathrm{o}} = C_{\mathrm{T}}\, (&x_{\mathrm{CO_2}} + x_{\mathrm{HCO_3^-}} + x_{\mathrm{CO_3^=}} + x_{\mathrm{AEEACOO_p^-}} + x_{\mathrm{AEEACOO_s^-}} \\ &+ x_{^+\mathrm{HAEEACOO_p^-}} + x_{^+\mathrm{HAEEACOO_s^-}} + 2x_{^-\mathrm{OOCAEEACOO^-}}) \end{aligned} \tag{6.15}$$

and electroneutrality.

$$\begin{aligned} x_{\mathrm{H_3O^+}} + x_{\mathrm{AEEAH^+}} + 2x_{^+\mathrm{HAEEAH^+}} = &x_{\mathrm{OH^-}} + x_{\mathrm{HCO_3^-}} + 2x_{\mathrm{CO_3^=}} \\ &+ x_{\mathrm{AEEACOO_p^-}} + x_{\mathrm{AEEACOO_s^-}} + 2x_{^-\mathrm{OOCAEEACOO^-}} \end{aligned} \tag{6.16}$$

Equations (6.12) – (6.16) represent a system of 14 equations that are solved simultaneously to obtain the equilibrium composition of the liquid phase. As seen from the reactions (6.2) – (6.11), the number of moles in solution does not change, apart from the free CO_2 which is in very low concentration (approximate maximum 10^{-2} mol L^{-1} at a high loading). The volume of the solution also changes very little. On the basis of density measurements, the change was found to be <1.5% at high loadings. Therefore, the assumption of constant molar concentration has been used.

According to the phase equilibrium condition, the fugacities in the vapor and liquid phase are equal. The equilibrium condition for volatile solutes (e.g., CO_2) were based on the infinite dilution reference state and defined by Eq. (5.63).

$$\varphi_i y_i P = \gamma_i^* x_i H_i^{\infty} \exp\left\{\bar{v}_i^{\infty}\left(P - P_{\mathrm{w}}^{\mathrm{o}}\right)/RT\right\} \tag{6.17}$$

The Henry's law constant for CO_2 at infinite dilution in water was taken from Chen *et al*. (1979) and the partial molar volume of CO_2 was substituted by the molar volume and taken from Brelvi and O'Connell (1972). For the solvent (water), the vapor–liquid equilibrium is given by Eq. (5.62),

$$\varphi_w y_w P = \gamma_w x_w P_w^o \varphi_w^o \exp\left\{v_w \left(P - P_w^o\right)/RT\right\} \tag{6.18}$$

The fugacity coefficients φ_i for all volatile components were calculated by the Peng–Robinson equation of state (Peng and Robinson, 1976).

6.2 Activity Coefficient Model

The activity coefficients in this work were calculated using an adaptation of the Deshmukh–Mather model (Deshmukh and Mather, 1981). This model has been chosen because it is more rigorous than the simple approaches, e.g., those by Kent and Eisenberg (1976), and is capable of predicting reasonable species concentrations. Yet, algebraically, it is simple enough to be computationally efficient for whole column and plant calculations where the equilibrium calculation has to be performed maybe 10^5 to 10^6 times. More complex models such as the electrolyte–NRTL or the electrolyte–UNIFAC/UNIQUAC models are more expensive computationally (Weiland *et al.*, 1993) without seeming to offer any better fit to VLE data or species concentrations. In the Deshmukh–Mather model, the activity coefficients of the species in the liquid phase are calculated using the extended Debye–Hückel equation as written in Eq. (5.78).

$$\ln \gamma_i = \frac{-2.303 A_\gamma z_i^2 I^{1/2}}{1 + B a_i I^{1/2}} + 2\sum_j \beta_{ij} m_j \tag{6.19}$$

The first term of this equation represents the electrostatic forces and the second term represents the short–range van der Waals forces. A_γ (the Debye–Hückel limiting slope) and B are functions of temperature and the dielectric constant of the solvent. I is the ionic strength and is defined as a function of the charge number on the ion z_j and the molality m_j as written in Eq. (5.65).

$$I = \frac{1}{2}\sum_j m_j z_j^2 \tag{6.20}$$

The quantity a_i represents the effective diameter of the ion i. Because of a lack of information, it is usually set to a constant default value of 4 Å for all ions, although it would be different for different ions and would possibly also be a function of the solvent composition and the ionic strength (see Robinson and Stokes, 1959). AEEA is considered

to be a solute, and the reference state is infinite dilution in water. The activity coefficients obtained by Eq. (6.19) are molality based and have to be transformed to the molar fraction concentration scale on which the equilibrium constants were defined.

Simplifications were made for the Deshmukh–Mather model in which the value of the Debye–Hückel limiting slope at 25 °C in water was used ($A_{\gamma,25^\circ C}$ = 0.509) and the product Ba_i was set equal to 1.3 ($B_{25^\circ C}$ = 0.3286, a_i = 4 Å) since the model for the calculated CO_2 partial pressure showed little sensitivity to the temperature variation in A and B. The constants A_γ and B are given as functions of temperature in Manov *et al.* (1943). In addition, the second term of the extended Debye–Hückel equation representing the short–range van der Waals forces was disregarded in the first stage of the work. This implies that, initially, the activity coefficient model did not contain any regression parameters. In the second stage, when considering the ionic interaction parameters, interactions with the solvent (water) were also taken into account. This is contrary to the original Deshmukh–Mather model.

6.3 Thermodynamic Parameters

The thermodynamic parameters needed for the model are the equilibrium constants for all chemical reactions, the parameters in the activity coefficient model, and the Henry's law constant for CO_2 in pure water. The temperature dependency of the equilibrium constants and the Henry's law constant can be expressed in the form

$$\ln K \text{ or } \ln H = c_1 + c_2/T + c_3 \ln T + c_4 T \tag{6.21}$$

The coefficients c_1 – c_4 for all reactions and the Henry's law constant are summarized in Table 6-1. For Eq. (6.2), the equilibrium constant of water is originally given by Olofsson and Hepler (1975) and later used by Weiland *et al.* (1993) as:

$$\begin{aligned}\ln K_w = &-328379.9/T - 4229.195 \ln T + 20501.02448 + 22.4345T \\ &- 2.985025\times10^{-2}T^2 + 2.649539\times10^{-5}T^3 - 1.05965\times10^{-8}T^4\end{aligned} \tag{6.22}$$

which is valid for the temperatures from 0 to 145 °C. For the reactions in Eqs. (6.3) and (6.4), the equilibrium constants were taken from Edwards *et al.* (1978). The protonation constants for tdreaction (6.5) and (6.6) were determined from separate titration

experiments. For the reactions in Eqs. (6.7) – (6.11), the coefficients were determined by regression of the VLE data with the model.

6.4 Parameter Regression

As mentioned above, the parameters regressed in this model were first those in the temperature dependency of the equilibrium constants for the reactions in Eqs. (6.7) – (6.11). The β parameters of the Deshmukh–Mather model were set to zero, i.e., the short–range terms were neglected. This was done because the equilibrium constants for Eqs. (6.7) – (6.11) were not known from independent experiments and, therefore, needed to be determined as model parameters by regression of VLE experimental data. Later, the sensitivity of the parameters of the activity coefficient model was also tested. However, only a few of the parameters β showed significant sensitivity. These were regressed in a second stage where the equilibrium constants were set to the expressions obtained by the first fitting. This procedure should ideally be repeated to also obtain better fits for the equilibrium constants. However, as will be seen, only one fitting was necessary. The regression was performed by using Modfit, an in–house MATLAB computer program for parameter estimation. The regression method used was the Levenberg–Marquardt minimization with the normalized objective function as given by

$$F = \sum_{i=1}^{n} \left(\frac{p_{CO_2}^{exp.} - p_{CO_2}^{calc.}}{p_{CO_2}^{exp.}} \right)^2 \tag{6.23}$$

The criterion used was the relative error between the calculated and experimental values of the CO_2 partial pressures.

6.5 Results and Discussion

6.5.1 pK_a Determinations

Protonation constants of AEEA were measured over a range of temperatures from 20 to 60 °C. The results are given in Table 6-2 and Figures 6-1 and 6-2. The pK_a values for higher temperatures were extrapolated from the data obtained. AEEA is a diamine with one primary and one secondary amine group and will, therefore, have two equilibrium points

(EPs) corresponding to the formation of monoprotonated and diprotonated AEEA. Figure 6-1 shows the titration curves where the two end points are clearly visible. The protons will associate with both the primary and secondary amine group in a certain ratio which cannot be determined from the experiment, but it will probably be 80–90% with the primary group in the first protonation stage. The first protonation constant (K_{AEEAH^+}) in the model {see Eq. (6.5)} is, however, an overall constant for both the first protonation on either the primary or secondary amine group. Similarly, the diprotonated AEEA ($^+HAEEAH^+$) will then form from primary or secondary monoprotonated AEEA ($AEEAH^+_p$ and $AEEAH^+_s$). The second protonation constant ($K_{^+HAEEAH^+}$) is, therefore, an overall constant for the secondary protonation of $AEEAH^+_p$ and $AEEAH^+_s$. The temperature dependency of the protonation constants is shown in Figure 6-2 and is seen to give a very good fit to a straight line. The parameter values for the reactions in Eqs. (6.5) and (6.6) are given in Table 6-1.

Table 6-1. Temperature dependency of the equilibrium constants for the reactions in Eqs. (6.3) – (6.11) and Henry's law constant for CO_2

Rx. no.	Parameter	c_1	c_2	c_3	c_4	T/°C	Source
6.3	K_{CO_2}	231.465	–12092.1	–36.7816	0.0	0–225	a
6.4	$K_{HCO_3^-}$	216.049	–12431.7	–35.4819	0.0	0–225	a
6.5	K_{AEEAH^+}	–3.0561	–5865.15	0.0	0.0	20–60	This work
6.6	$K_{^+HAEEAH^+}$	0.7568	–5074.99	0.0	0.0	20–60	This work
6.7	$K_{AEEACOO^-_p}$	–32.564	8284.4	0.0	0.0	40–120	This work
6.8	$K_{AEEACOO^-_s}$	–2.5206	–3585.2	0.0	0.0	40–120	This work
6.9	$K_{^+HAEEACOO^-_p}$	–19.951	–292.57	0.0	0.0	40–120	This work
6.10	$K_{^+HAEEACOO^-_s}$	27.08	–16921	0.0	0.0	40–120	This work
6.11	$K_{^-OOCAEEACOO^-}$	–22.992	4014.1	0.0	0.0	40–120	This work
	H_{CO_2}	170.7126	– 8477.711	–21.95743	0.005781	0–100	b

[a]Edwards *et al.* (1978) ; [b]Chen *et al.* (1979)

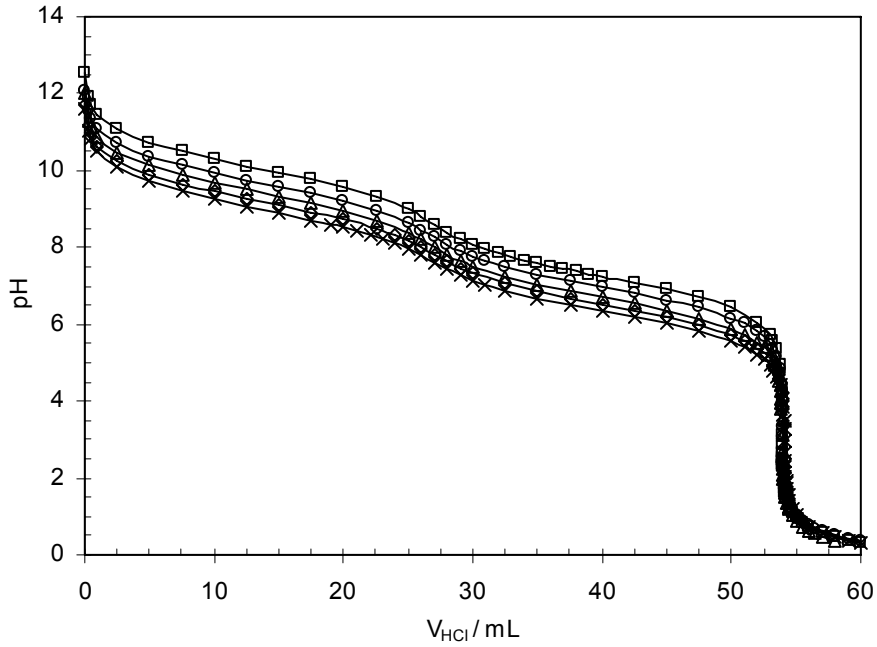

Figure 6-1. pH curves of aqueous solution of 30 mass % AEEA for several temperatures: □, 20 °C; ○, 30 °C; Δ, 40 °C; ◊, 50 °C; ×, 60 °C.

Table 6-2. Protonation constant (pK_a) values of aqueous solution of 30 mass % AEEA for several temperatures

T/°C	pK_{a1}	pK_{a2}
20	10.05	7.21
30	9.70	6.94
40	9.44	6.67
50	9.20	6.49
60	9.00	6.31

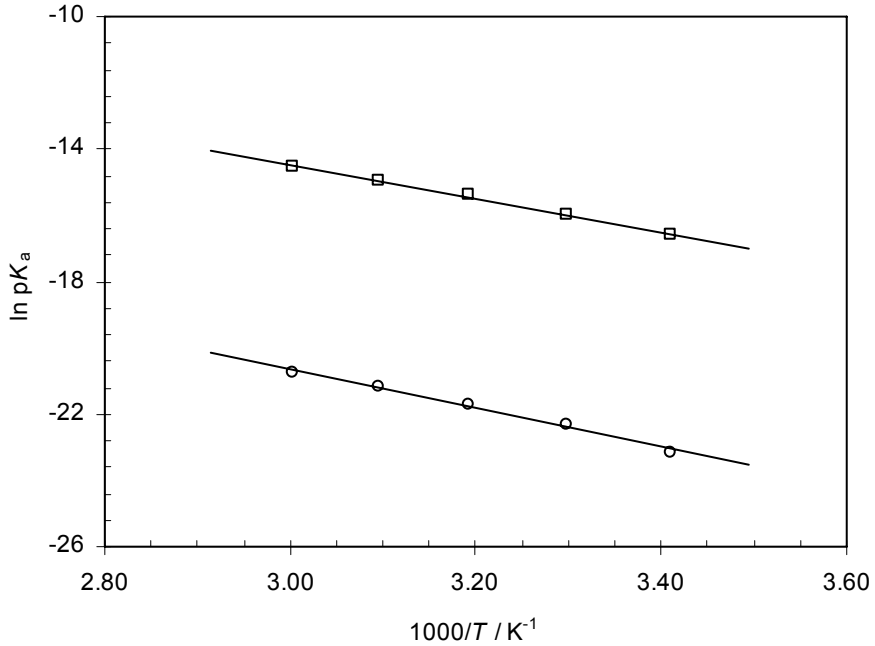

Figure 6-2. Relationship between ln pK_a with 1/T: ○, pK_{a1}; □, pK_{a2}; lines obtained from regression.

6.5.2 VLE–Data Regression

The vapor–liquid equilibrium experiments were performed at temperatures ranging from 40 to 120 °C. The results are given in Figure 6-3 together with the correlations from the initial fit obtained by the model. As shown in Figure 6-3, the model represents the experimental data very well, even without any regression of ionic interaction parameters in the extended Debye–Hückel model. However, this should be taken as a preliminary simulation result. The only parameters initially fitted were the parameters involved in the temperature dependency of the chemical equilibrium constants. It is very unlikely that a model based only on equilibrium constants should be able to describe the complex CO_2–AEEA–H_2O system perfectly.

The short–range terms of the Deshmukh–Mather model were included to test if they could make the model more flexible and if the overall fit could be improved. From the total number of 73 possible binary interaction parameters, only 14 were, by a sensitivity test, found to have significant effect on the correlated CO_2 partial pressure. These parameters are summarized in Table 6-3.

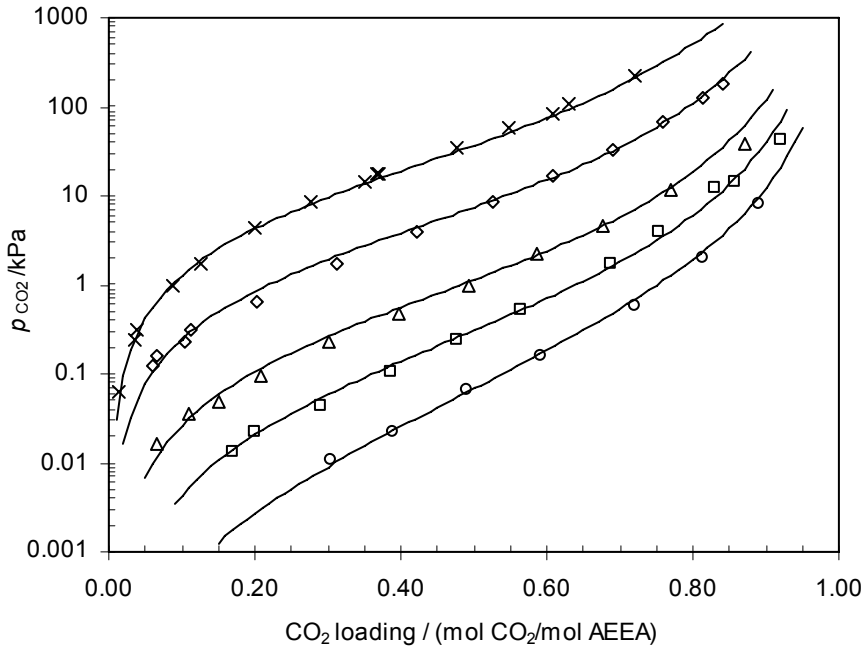

Figure 6-3. Equilibrium solubility of CO_2 in aqueous solution of 30 mass % AEEA. All data points were measured in this work: ○, 40 °C; □, 55 °C; Δ, 70 °C; ◊, 95 °C; ×, 120 °C. Curves were calculated by the initial VLE model.

Table 6-3. Binary interaction parameters (β_{ij})

Binary interaction	β_{ij}
H_2O–CO_2	–10.207
H_2O–AEEA	0.40706
H_2O–HCO_3^-	–26.12
H_2O–$AEEH^+$	0.061122
H_2O–$^+HAEEH^+$	–2.8521
H_2O–$AEECOO^-_p$	0.77294
H_2O–$AEECOO^-_s$	8.9021
H_2O–$^+HAEECOO^-_p$	0.28684
H_2O–$^+HAEECOO^-_s$	–1.1122
H_2O–$^-OOCAEECOO^-$	–1.9413
AEEA–$AEEAH^+$	7.1171
AEEA–$AEECOO^-_p$	62.129
$AEEAH^+$–$AEECOO^-_p$	–31.027
$AEEAH^+$–$^+HAEECOO^-_p$	69.614

A second regression of the VLE data was performed to evaluate the interaction parameters. However, only minor improvements in the overall fit were achieved (see Figures 6-4 and 6-5). The main reason for this was the lack of variation in the experimental information on the system to reliably determine both the equilibrium

constant parameters and the parameters of the activity coefficient model. In addition, the activity coefficients and the mole fractions always appear as products and when using VLE data for the regression, the separation of these two quantities is very difficult. On the other hand, it should be noted that this regression was based on data that are typically used for such a procedure. Very often VLE data of the kind presented in this work are the only data available. The findings here thus highlight the need for a variety of data, not only VLE data, for developing reliable equilibrium models for complex absorption systems.

Indeed, the liquid–phase nonidealities that should be described by the activity coefficient model were lumped into the obtained equilibrium constant parameters during the first regression procedure. The obtained values for the coefficients of the temperature dependency represent only one of several possible sets of coefficients that offer a good fit to the VLE data but do not necessarily have any physical meaning. The coefficients must, therefore, be treated with care. However, some restrictions on the parameters were applied to ensure that the equilibrium constants have somewhat reasonable values. These were based on theoretical considerations about the absolute values as well as the trends in the temperature dependencies, i.e., the slope of the linear functions $\ln K = f(1/T)$. The known coefficients for the MEA carbamate stability constant were utilized and used as starting points for those of the primary and secondary AEEA carbamate constants. The results are shown in Figure 6-6 where the $\ln K$ values are given as functions of $1/T$. The values are within reasonable limits and one would expect them to come together at high temperatures as shown in Figure 6-6. The reason for this is changes in the relative importance of the magnitude of the equilibrium constant and the shift in reaction entropy (see da Silva and Svendsen, 2005). Therefore, as a first estimate, the regressed equilibrium constant parameters given in Table 6-1, used together with the regressed β parameters given in Table 6-3, should be satisfactory.

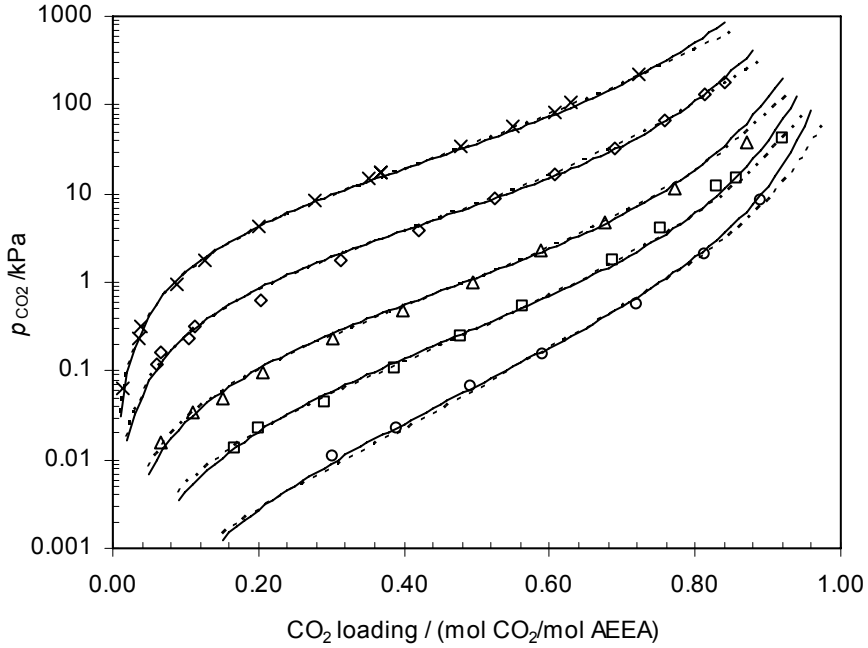

Figure 6-4. Representation of data by model based only on parameters of the equilibrium constants (lines) and by model including the binary interaction parameters (dashed lines). Experimental data: ○, 40 °C; □, 55 °C; Δ, 70 °C; ◊, 95 °C; ×, 120 °C.

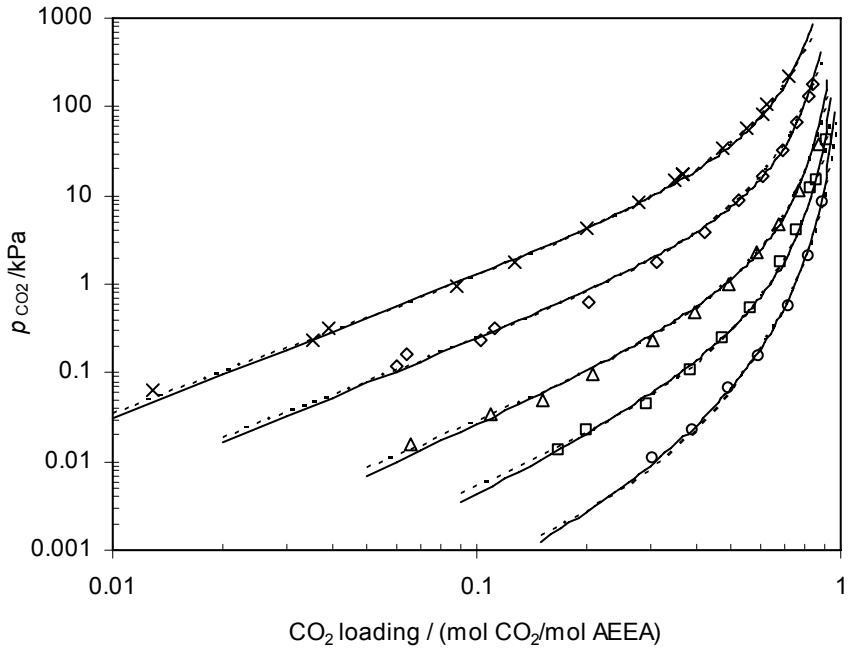

Figure 6-5. Log–log scale of representation of data by model based only on parameters of the equilibrium constants (lines) and by model including the binary interaction parameters (dashed lines). Experimental data: ○, 40 °C; □, 55 °C; Δ, 70 °C; ◊, 95 °C; ×, 120 °C.

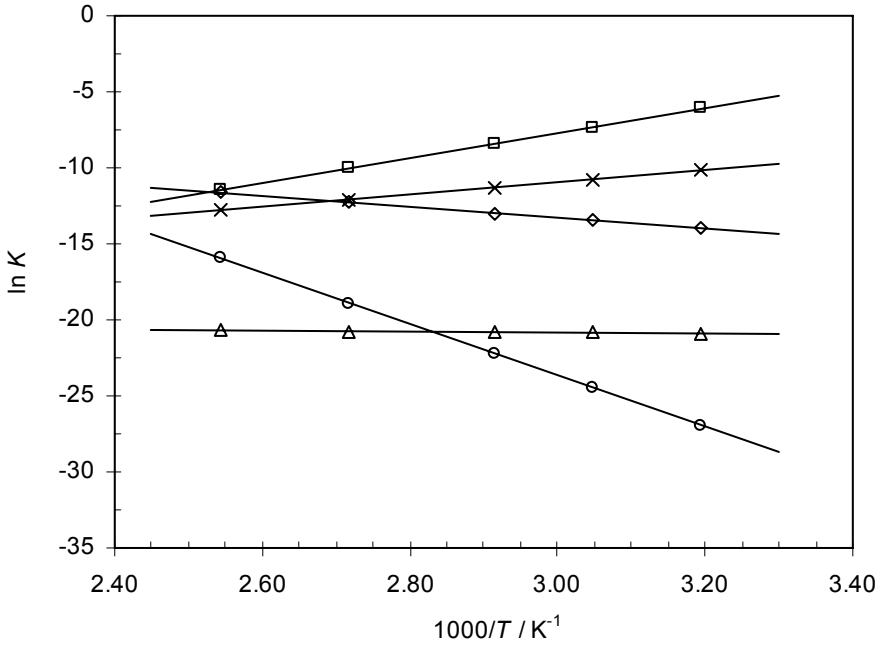

Figure 6-6. Relationship between ln K with $1/T$: □, $K_{AEEACOO_p^-}$; ◊, $K_{AEEACOO_s^-}$; Δ, $K_{^+HAEEACOO_p^-}$; ○, $K_{^+HAEEACOO_s^-}$; ×, $K_{^-OOCAEEACOO^-}$.

6.5.3 Speciation and NMR Analysis Data

Another type of restriction was represented by the NMR speciation data. To ensure reasonable values for the coefficients, it is necessary to require a good representation of the species distribution. To identify the species existing in the liquid phase in the CO_2–AEEA–H_2O system, an NMR study was performed. CO_2-loaded 30 mass % AEEA solutions were investigated at 20 °C and loadings of 0.19, 0.49, and 0.77 (mol CO_2/mol AEEA), respectively. Both ^1H and ^{13}C 1D NMR spectra were acquired. Three types of amine species were identified: amine, primary carbamate, and secondary carbamate. Because of the fast proton exchange with water, the data obtained actually represent the sum of the free and protonated AEEA, the sum of the primary and protonated primary carbamates, and the sum of the secondary and protonated secondary carbamates. The peaks were assigned to particular proton/carbon types with the help of 2D NMR spectra. The different types of proton/carbon atoms are shown for the AEEA molecule in Figure 6-7. An example of a ^{13}C spectrum is given in Figure 6-8. There were observed 4×3 peaks representing the four carbon types for each of the three AEEA species in the spectra. On the spectrum in Figure 6-8, the peaks of highest intensity correspond to primary carbamate, the middle

intensity peaks correspond to AEEA, and the lowest intensity peaks correspond to secondary carbamate. Dicarbamate could not be identified, even at this high loading.

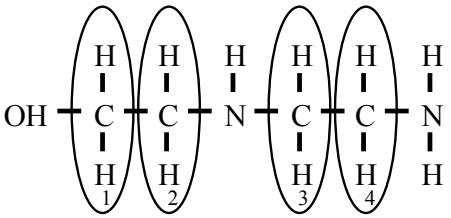

Figure 6-7. The four different carbon atoms in AEEA molecule.

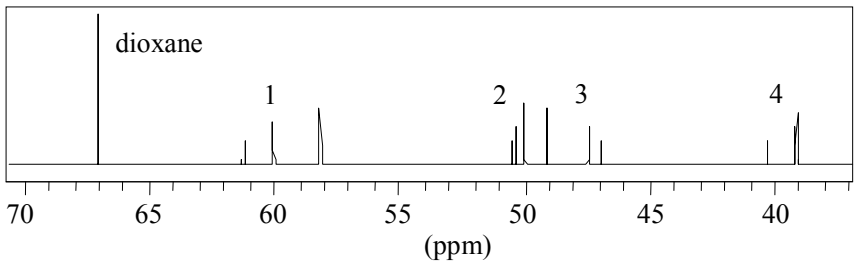

Figure 6-8. ^{13}C spectra of aqueous solution of 30 mass % AEEA and 0.77 (mol CO_2/mol AEEA).

Since the peak intensities correspond to the species concentrations, the NMR spectra were also used for a quantitative investigation of the species distribution as a function of CO_2 loading. The relative species concentrations were evaluated based on the area integrals. The error in the integration is assumed to be ~1%. More details on the integration procedure can be found in Poplsteinova (2004).

The VLE model was fitted to experimental data down to 40 °C, and an extrapolation to 20 °C was calculated. The extrapolated results at 20 °C were then compared to 20 °C data from the NMR experiments, as shown in Figure 6-9. The reason the NMR tests were run at 20 °C was to avoid peak broadening caused by faster amine reaction kinetics at 40 °C. The qualitative agreement between model and experiments is quite good. Quantitatively, the model seems to slightly overpredict the effect of loading. However, the agreement is deemed to be satisfactory. It should be noted that the given loadings are loadings based on the weighed-in concentrations of CO_2 and amine and that these were not in total accordance with the loadings calculated from the NMR data. There is, thus, also a significant uncertainty in the experimental loading values. At the same mole fraction, the total primary carbamate gives the highest deviation of the loading from the model. By

taking an average value of the deviation, the NMR data will, therefore, shift to the left side and is closer to the model prediction (see Figure 6-9).

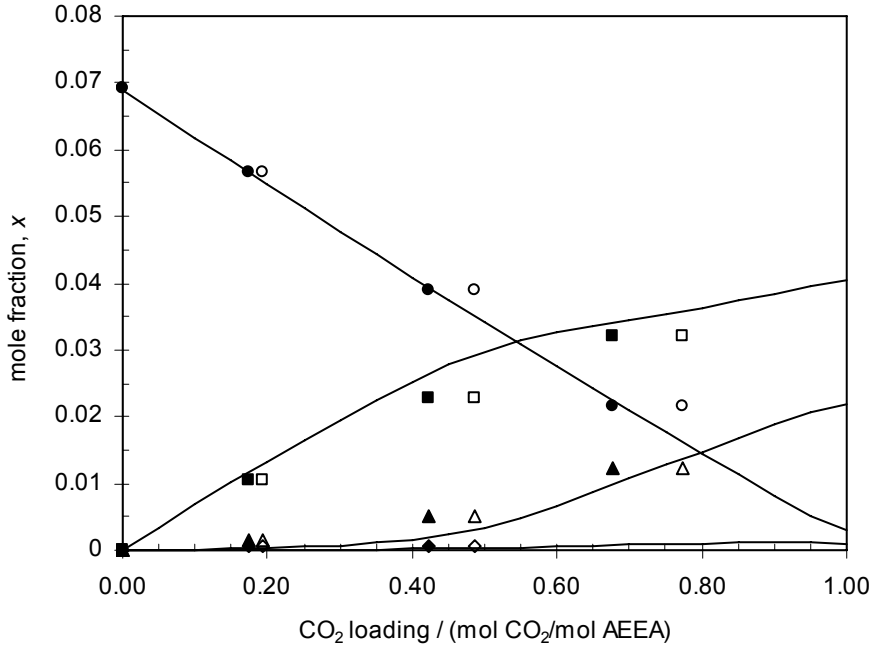

Figure 6-9. Liquid–phase concentrations of a CO_2-loaded 30 mass % AEEA solution at 20 °C in comparison to those analyzed using NMR at 20 °C. Solid lines are calculated by the model and the points are from NMR data: ○, $AEEA_{tot}$ = (AEEA + $AEEAH^+$ + $^+HAEEAH^+$); □, $AEEACOO^-_{p,tot}$ = ($AEEACOO^-_p$ + $^+HAEEACOO^-_p$); Δ, $AEEACOO^-_{s,tot}$ = ($AEEACOO^-_s$ + $^+HAEEACOO^-_s$); ◊, $^-OOCAEEACOO^-$; •, ■, ▲, and ♦: positions at new loadings for $AEEA_{tot}$, $AEEACOO^-_{p,tot}$, $AEEACOO^-_{s,tot}$ and $^-OOCAEEACOO^-$, respectively.

Figure 6-10 shows the distribution of species predicted by the model as a function of loading for 20 °C. As CO_2 is added to a fresh AEEA solution, the dominant product is the carbamate formed by the primary amine group ($AEEACOO^-_p$). At a loading of ~0.5 (mol CO_2/mol AEEA), the primary carbamate is progressively replaced by protonated primary carbamate ($^+HAEEACOO^-_p$). As the loading increases, the pH decreases so that it is low enough to protonate the carbamates. The secondary carbamate ($AEEACOO^-_s$) exists only in small quantities, <0.002% of the primary carbamate for the whole loading range. It is also clear that the dicarbamate only exists in small concentrations in the whole loading range. This was also confirmed by the NMR results. As expected, the formation of bicarbonate increases somewhat at high loadings, but the protonated carbamates are the main constituents in the whole region shown in Figure 6-10.

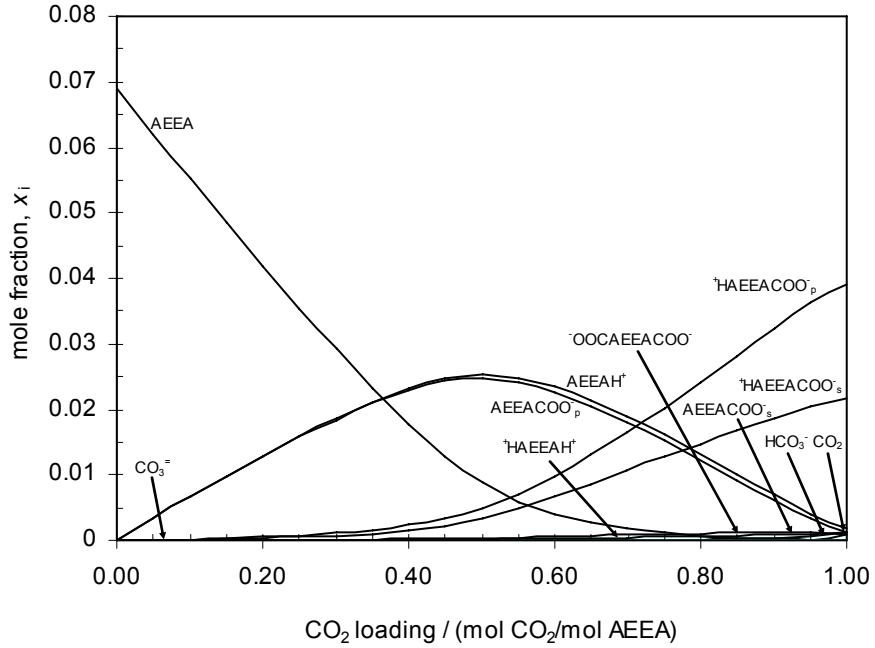

Figure 6-10. Distribution of species in aqueous solution of 30 mass % AEEA at 20 °C.

6.6 Conclusions

Vapor–liquid equilibrium data of CO_2 in aqueous solution of 30 mass % AEEA were measured over a range of temperatures from 40 to 120 °C for partial pressures of CO_2 ranging from 0.01 to 220 kPa. Protonation constant (pK_a) values as functions of temperature were obtained separately by titration analysis. A modified Deshmukh–Mather model was fitted to the data and shown to provide a good representation of the experimental points. ^{1}H and ^{13}C 1D NMR spectra were acquired for the system and used for identification of the system species. In addition, quantitative information on the relative species concentrations was obtained and shown to be in reasonable agreement with model predictions.

PART III

Experimental Kinetic Study

CHAPTER 7

Kinetic Study of CO_2–AEEA–H_2O System

The reaction kinetics between CO_2 and aqueous AEEA solutions have been measured over a range of temperatures from 31 to 50 °C with the concentrations of aqueous AEEA of 1.20, 1.80, 2.40, 2.94, and 3.50, respectively. The reaction mechanism used was the *single step – termolecular mechanism* approach proposed by Crooks and Donnellan (1989) and reviewed by da Silva and Svendsen (2004). The results show that the observed pseudo–first order rate constant is in good agreement with the equation proposed for this mechanism. In addition, physical properties of AEEA, density and viscosity, have been measured over a range of temperatures between 10 and 90 °C. The solubility of N_2O in aqueous AEEA has also been measured to estimate the solubility of CO_2 in aqueous AEEA solution. All these properties were needed to determine the physico–chemical parameters.

7.1 Introduction

Chemical reactions between gases and liquids play an important role in many industrial processes both within gas purification and production. Gas purification is the term used to describe a process to separate a gas mixture from its impurities such as acid gases (e.g., CO_2, H_2S, and SO_2), organic sulfur compounds (e.g., COS, CS_2, mercaptants, and thiophene), and certain other impurities (e.g., H_2O, HCN, NH_3, and hydrocarbons). The gas purification processes include absorption into a liquid, cryogenic separation, adsorption onto a solid (e.g., zeolites, activated carbon, and clays), and chemical conversion to another compound such as chemical oxidation of H_2S, hydrolysis of COS, and methanation (Astarita *et al.*, 1983). In addition, acid gas removal generally refers to removal of CO_2 and H_2S by use of aqueous alkanolamines solutions in which both gases are present in natural gas, synthesis gas, flue gas, and various refinery streams, and CO_2 is also a by–product of ammonia and hydrogen manufacture. The alkanolamines that have proved to be of principal commercial for gas purification are monoethanolamine (MEA), diethanolamine (DEA), and methyldiethanolamine (MDEA) (Kohl and Nielsen, 1997).

The purpose of this chapter is to present the kinetic study of CO_2 absorption in aqueous 30 mass % AEEA solution including a brief review on the kinetic mechanisms proposed for CO_2–alkanolamines–water systems.

7.2 Theory of Chemical Absorption: Enhancement Factor

Absorption into a liquid agent is the most commonly used approach in gas purification process. Gas absorption is a unit operation in which soluble components of a gas mixture dissolve in a liquid agent. This heterogeneous process is carried out in a variety of equipment ranging from a bubbling absorber to a packed tower or plate column.

To improve the overall rate of the process, an intimate gas–liquid contact has to be established and mass transfer has to be improved by increasing turbulence in both gas and liquid phases. However, at the interface boundary layers are always present, in which mass transfer takes place by a combination of chemical and diffusional mechanism, so that, the overall rate of the process is governed by both chemical reaction and mass transfer.

This sub–chapter presents a summary of the important features of the effect of chemical reaction on the absorption process expressed in the terms of enhancement factor.

In the absence of any chemical reaction the mass transfer rate in terms of flux N_A in liquid phase is given by

$$N_A^o = k_L^o \left(C_{A,i} - C_{A,b} \right) \tag{7.1}$$

where subscripts *i* and *b* denote interface and bulk respectively. The actual rate in the presence of chemical reaction can be defined as follows

$$N_A = k_L \left(C_{A,i} - C_{A,b} \right) \tag{7.2}$$

and the value may be larger than that of given by Eq. (7.1).

An enhancement factor E_A is defined as the ratio of the actual rate and the rate that would be observed under the same driving force in the absence of chemical reactions (Astarita *et al*., 1983)

$$E_A = \frac{N_A}{N_A^o} = \frac{k_L}{k_L^o} \tag{7.3}$$

The absorption of a gas by a liquid which is subject to agitation by stirring or by film–flow over solid surface is influenced by two distinct sets of factors (Danckwerts and Kennedy, 1954):

(a). Physico–chemical factors: solubility and diffusivity of a gas in liquid; concentration of reagent (if any); reaction–velocity constant, reaction–equilibrium constant, etc.

(b). Hydrodynamics factors: geometry and scale of equipment; viscosity, density and flowrate of liquid, etc.

There are several physical models for the mass transfer in gas absorption processes: steady–state diffusion through a stagnant film (*two–film theory*), transient absorption into surfaces which are systematically replaced and randomly replaced by fresh liquid (*surface renewal theory*), and combination between two–film theory and surface renewal theory (*film–penetration theory*).

7.2.1 Two–Film Theory

A theory, called two–film theory, was first proposed by Whitman (1923) and by Lewis and Whitman (1924) (Froment and Bischoff, 1990) to describe the phenomenon occurring when a gas phase is brought into contact with a liquid phase. In this theory a stagnant layer is supposed to exist in both phases along the interface as described in Figure 7-1.

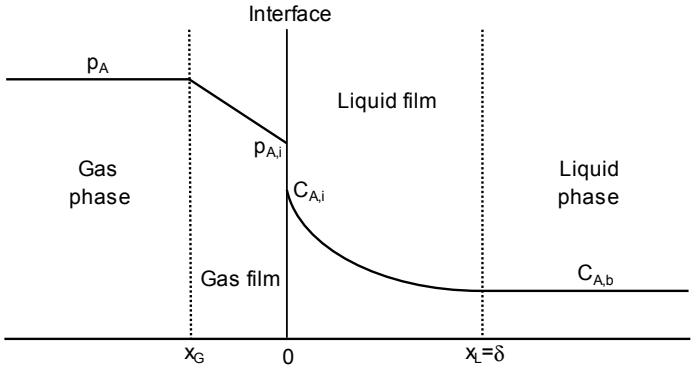

Figure 7-1. Two–film concept for mass transfer between a gas and a liquid

Danckwerts and Kennedy (1954) presented the film theory proposed by Whitman (1923) in which the liquid at the surface is assumed to be in laminar flow parallel to the surface, while liquid below the surface is in turbulent motion. The rate of absorption is determined mainly by molecular diffusion in the surface layers. Although the relative

importance of transport by diffusion and by turbulence will presumably vary continuously with depth below the surface, it is convenient to take as a model a completely stagnant layer of effective thickness δ, overlying liquid of uniform composition. The thickness of the film is assumed to be small enough for the absorption process to be treated as one of steady–state diffusion through the stagnant layer.

In physical absorption, the concentration profile of a volatile component A in the film is linear. The differential equation for mass transfer can be written as

$$D_{\mathrm{A}} \frac{d^2 C_{\mathrm{A}}}{dx^2} = 0 \tag{7.4}$$

with boundary conditions

$$x = 0, \quad C_{\mathrm{A}} = C_{\mathrm{A,i}} \tag{7.5}$$

$$x = \delta, \quad C_{\mathrm{A}} = C_{\mathrm{A,b}} \tag{7.6}$$

Integrating Eq. (7.4) and applying the two boundary conditions yields

$$C_{\mathrm{A}} = C_{\mathrm{A,i}} + \left(C_{\mathrm{A,b}} - C_{\mathrm{A,i}}\right)\frac{x}{\delta} \tag{7.7}$$

Furthermore, the rate of the overall phenomenon, as seen from the interface, follows from the application of Fick's law

$$N_{\mathrm{A}} = -D_{\mathrm{A}} \left.\frac{dC_{\mathrm{A}}}{dx}\right|_{x=0} = \frac{D_{\mathrm{A}}}{\delta}\left(C_{\mathrm{A,i}} - C_{\mathrm{A,b}}\right) = k_{\mathrm{L}}\left(C_{\mathrm{A,i}} - C_{\mathrm{A,b}}\right) \tag{7.8}$$

where $k_{\mathrm{L}} = D_{\mathrm{A}}/\delta$ for the two–film theory.

In chemical absorption, the rate of a reaction cannot be neglected with respect to the mass transfer. Let A be the component of the gas phase reacting with a nonvolatile component B in the liquid phase and let the film be isothermal. In a general form, the reaction can be considered as

$$\mathrm{aA + bB} \rightarrow \mathrm{P} \tag{7.9}$$

and is confined to the liquid phase. Since the chemical reaction is present, for the component A, Eq. (7.4) can then be written as

$$D_{\mathrm{A}} \frac{d^2 C_{\mathrm{A}}}{dx^2} = -r_{\mathrm{A}} \tag{7.10}$$

and for the component B

$$D_{\mathrm{B}} \frac{d^2 C_{\mathrm{B}}}{dx^2} = \frac{b}{a}\left(-r_{\mathrm{A}}\right) \tag{7.11}$$

where $-r_{\mathrm{A}}$ is the rate of disappearance of A defined as

$$-r_{\mathrm{A}} = f\left(C_{\mathrm{A}}, C_{\mathrm{B}}, T\right) \tag{7.12}$$

with the boundary conditions

$$x = 0, \quad C_{\mathrm{A}} = C_{\mathrm{A,i}}, \quad C_{\mathrm{B}} = C_{\mathrm{B,i}} \tag{7.13}$$

$$x = \delta, \quad C_{\mathrm{A}} = C_{\mathrm{A,b}}, \quad C_{\mathrm{B}} = C_{\mathrm{B,b}} \tag{7.14}$$

The influence of a reaction on the absorption rate can be expressed by a dimensionless ratio term ϕ, a ratio between diffusion time, t_{D}, and reaction time, t_{R}, (Astarita *et al.*, 1983).

$$\phi = \frac{t_{\mathrm{D}}}{t_{\mathrm{R}}} \tag{7.15}$$

When $\phi \ll 1$, the reaction is too slow to have any significant influence on the diffusion phenomena, and essentially no absorption rate enhancement will take place. This case is, therefore, called the *slow reaction regime*. Conversely, when $\phi \gg 1$ (*fast reaction regime*), the reaction is fast enough to result in a significant rate enhancement. Finally, when $\phi \to \infty$ (*instantaneous reaction regime*), the reaction is infinitely fast chemical reaction and the rate enhancement reaches its maximum. In this regime, chemical equilibrium is established instantaneously.

The enhancement factors E_{A} for those regimes can, according to Astarita *et al.* (1983), be defined as the following and can be seen in Figure 7-2.

Slow reaction regime:

$$E_{\mathrm{A}} = 1 \tag{7.16}$$

Fast reaction regime:

$$E_{\mathrm{A}} = \sqrt{\phi} \tag{7.17}$$

Instantaneous reaction regime:

$$E_{\mathrm{A}} = E_{\mathrm{A}\infty} = \frac{\left(C_{\mathrm{A,i}} - C_{\mathrm{A,b}}\right)_{\mathrm{eq.}}}{\left(C_{\mathrm{A,i}} - C_{\mathrm{A,b}}\right)} \tag{7.18}$$

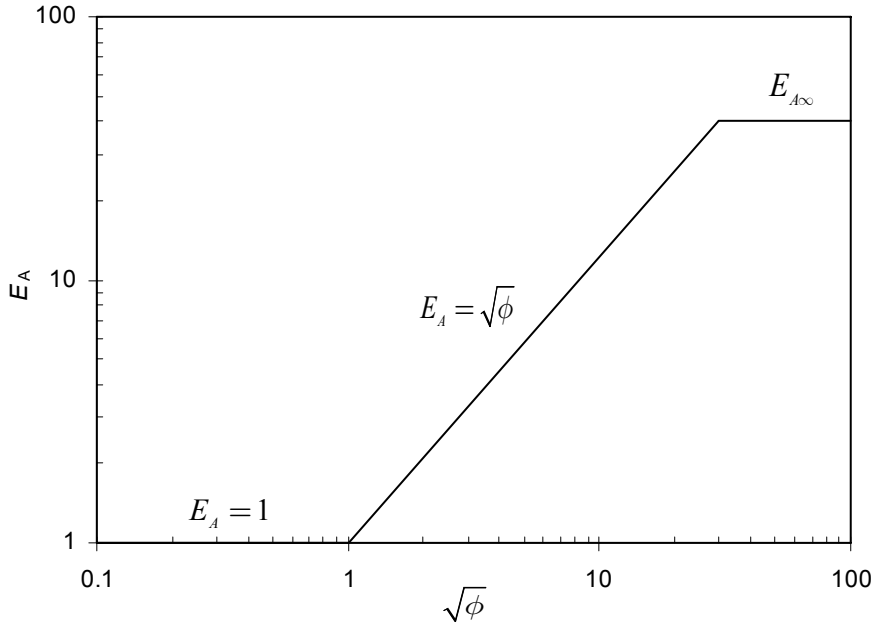

Figure 7-2. Asymptotic behavior for enhancement factor $E_A = f(\phi)$

Expressions for the enhancement factor have been developed by many authors as a selection is given in Table 7-1.

Table 7-1. Enhancement factors for several types of reactions

No	Type of reaction	Enhancement factor E_A	Source
1.	First–order and pseudo–first–order irreversible $A \rightarrow P$	$E_A = \frac{Ha}{\tanh(Ha)}\left(1 - \frac{C_{A,b}}{C_{A,i}}\frac{1}{\cosh(Ha)}\right)$ where Hatta number $= Ha = \delta\sqrt{\frac{k}{D_A}} = \frac{\sqrt{kD_A}}{k_L}$ In the presence of liquid reagent B as an absorbent (very fast irreversible reaction): $E_A = \left(1 + \frac{D_A}{D_B}\frac{C_{B,b}}{C_{A,i}}\right)$	van Krevelen and Hoftijzer (1948); Danckwerts and Kennedy (1954)
2.	Second–order irreversible $aA+bB \rightarrow P$	$E_A = \frac{R + 1/Da}{1 + R + 1/Da}$ where $R = \frac{k'C_{B,b}\varepsilon_L}{k_L a} = \frac{k'C_{B,b}}{k_L a'}, \quad Da = k_L a\tau = k_L a\frac{V_R}{Q}$ For instantaneous reaction: $E_A = \left(1 + \frac{a}{b}\frac{D_B}{D_A}\frac{C_{B,b}}{C_{A,i}}\right)$	Roizard and Wild (2002); Versteeg *et al.* (1989)

Table 7-1. (continued)

No	Type of reaction	Enhancement factor E_A	Source
3.	m^{th}–order irreversible $\gamma_A A \rightarrow P$ $(m,n)^{th}$–order irreversible $\gamma_A A+\gamma_B B \rightarrow P$	$E_A = \frac{Ha}{\tanh(Ha)}\left(1-\frac{C_{A,b}}{C_{A,i}}\frac{1}{\cosh(Ha)}\right)$ $Ha = \frac{2}{m+1}\frac{\gamma_A k C_{A,i}^{m-1}}{D_A}\delta^2$ for m^{th}–order and $Ha = \frac{2}{m+1}\frac{\gamma_A k' C_{A,i}^{m-1} C_{B,i}^{n}}{D_A}\delta^2$ for $(m,n)^{th}$–order	Hikita and Asai (1963) quoted by Onda *et al.* (1970)
4.	First–order reversible $A \underset{k_{-1}}{\overset{k_1}{\rightleftharpoons}} E$	Equilibrium concentration of A on the reacting phase side of the interface: $E_A = 1+\frac{D_E}{D_A}K$ For instantaneous reaction: $E_A = \left(1-\frac{C_{A,b}}{C_{A,i}}\right)\left(1+\frac{D_E}{D_A}K\right)$ Equilibrium in bulk of solution: $E_A = \frac{1+K}{1+\frac{K\tanh\beta}{\beta}}$ where $\beta = \frac{\sqrt{D_A k_1 (K+1)/K}}{k_L}$ Mass transfer by convection within the film layers is insignificant: $E_A = \frac{\mu_1^2}{\frac{K_1}{D_{EA}}+\frac{\tanh(\mu_1 Ha)}{\mu_1 Ha}}$ where $K_1 = k_{-1}/k_1, \quad D_{EA} = D_E/D_A,$ $\mu_1 = \left[1+(K_1/D_{EA})\right]^{1/2}, \quad Ha = \sqrt{k_1 D_A}/k_L$	Olander (1960); Danckwerts and Kennedy (1954); Huang and Kuo (1965)
5.	First–order reversible $A \underset{k_{-1}}{\overset{k_1}{\rightleftharpoons}} 2E$	$E_A = 1+\frac{D_E}{2D_A}\frac{\sqrt{K}}{\sqrt{C_{A,i}}+\sqrt{C_{A,b}}}$ For instantaneous reaction: $E_A = \left(1-\frac{C_{A,b}}{C_{A,i}}\right)\left(1+\frac{D_E}{2D_A}\frac{\sqrt{K}}{\sqrt{C_{A,i}}+\sqrt{C_{A,b}}}\right)$	Olander (1960)

Table 7-1. (continued)

No	Type of reaction	Enhancement factor E_A	Source
6.	Second–order reversible $A+B \underset{k_{-1}}{\overset{k_1}{\rightleftharpoons}} E$	$E_A = 1+\left(\frac{D_B}{D_A}\right)\frac{C_{B,b}}{C_{A,i}+\frac{D_B/D_E}{K}}$ For instantaneous reaction: $E_A = \left(1-\frac{C_{A,b}}{C_{A,i}}\right)\left(1+\left(\frac{D_B}{D_A}\right)\frac{C_{B,b}}{C_{A,i}+\frac{D_B/D_E}{K}}\right)$	Olander (1960); Onda *et al.* (1970)
7.	Second–order reversible $A+B \underset{k_{-1}}{\overset{k_1}{\rightleftharpoons}} E+F$	$E_A = 1+\frac{D_E}{D_A}\frac{\phi}{C_{A,i}-C_{A,b}}$ where $\phi = 1/2\left\{\left[\left(\frac{D_F}{D_E}-1\right)\sqrt{KC_{A,b}C_{B,b}}+\frac{D_F}{D_B}KC_{A,i}\right]^2+4\left[\frac{D_B}{D_E}C_{B,b}+\sqrt{KC_{A,b}C_{B,b}}\right]\left(\frac{D_F}{D_B}\right)KC_{A,i}\right\}^{1/2}$ $-1/2\left[\frac{D_F}{D_E}\sqrt{KC_{A,b}C_{B,b}}+\frac{D_F}{D_B}KC_{A,i}\right]$	Olander (1960)
8.	Generalized reversible chemical reactions $\gamma_A A_{(g)}+\gamma_B B_{(l)} \underset{k_{-1}}{\overset{k_1}{\rightleftharpoons}} \gamma_E E_{(l)}+\gamma_F F_{(l)}$	$E_A = \frac{\left(1-\frac{C_{A,b}}{C_{A,i}}\right)\left(1+\frac{p+1}{m+1}\frac{D_E/D_A}{\gamma_E/\gamma_A T}\right)+\frac{D_E/D_A}{\gamma_E/\gamma_A}\left(\frac{p+1}{m+1}\frac{C_{A,b}/C_{A,i}}{T}-\frac{C_{E,b}}{C_{A,i}}\right)\left(1-\frac{1}{\cosh\sqrt{M}}\right)}{1+\frac{p+1}{m+1}\frac{D_E/D_A}{\gamma_E/\gamma_A T}\frac{\tanh\sqrt{M}}{\sqrt{M}}}$ where $M = M'\left(\frac{C_{B,i}}{C_{B,b}}\right)^n\left(1+\frac{m+1}{p+1}\frac{\gamma_E/\gamma_A}{D_E/D_A}T\right)$ $M' = \frac{2}{m+1}\frac{\gamma_A k_1 C_{A,i}^{m-1} C_{B,b}^n}{D_A}\delta^2$ $T = \frac{\left(C_{A,i}^{p+q-m-n}/K\right)\left(C_{E,i}/C_{A,i}\right)^{p-1}\left(C_{F,i}/C_{A,i}\right)^q}{\left(C_{B,i}/C_{A,i}\right)^n}$ m, n, p, and q are the reaction orders with respect to A, B, E, and F, respectively	Onda *et al.* (1970)
9.	High order reversible $A+nB \underset{k_{-1}}{\overset{k_1}{\rightleftharpoons}} E$	$E_A = 1-\frac{1}{n}\frac{D_B}{D_A}\frac{C_{B,b}}{C_{A,i}}\frac{\frac{C_{B,i}}{C_{B,b}}-1}{1-\frac{C_{A,b}}{C_{A,i}}}$	Huang and Kuo (1965)

7.2.2 Penetration Theory

In the penetration theory, it is assumed that small liquid elements are continuously brought from the bulk of the liquid phase to the interface, where they stay for some time t^*; after which the elements are brought back to the bulk of the liquid where they get mixed with it. During the time, an element stays at the interface and the diffusion phenomenon is, therefore, unsteady. Rearranging Eq. (7.4) for pure physical absorption in a plane film into an unsteady–state form leads to

$$D_{\mathrm{A}} \frac{\partial^2 C_{\mathrm{A}}}{\partial x^2} = \frac{\partial C_{\mathrm{A}}}{\partial t} \tag{7.19}$$

with the boundary conditions

$$C_{\mathrm{A}}(x,0) = C_{\mathrm{A,b}} \tag{7.20}$$

$$C_{\mathrm{A}}(0,t) = C_{\mathrm{A,i}} \tag{7.21}$$

$$C_{\mathrm{A}}(\infty,t) = C_{\mathrm{A,b}} \tag{7.22}$$

The solution to the system of Eqs. (7.19) to (7.22) gives the concentration distribution expressed as follows

$$\frac{C_{\mathrm{A}} - C_{\mathrm{A,b}}}{C_{\mathrm{A,i}} - C_{\mathrm{A,b}}} = \mathrm{erfc}\left(\frac{x}{2\sqrt{D_{\mathrm{A}} t}}\right) \tag{7.23}$$

where

$$\mathrm{erfc}\, u = 1 - \mathrm{erf}\, u = 1 - \frac{2}{\sqrt{\pi}} \int_0^u e^{-u^2} du \tag{7.24}$$

Note that the instantaneous rate of mass transfer into the surface element is time dependent:

$$N_{\mathrm{A,inst}}(t) = -D_{\mathrm{A}} \left(\frac{\partial C_{\mathrm{A}}}{\partial x}\right)_{x=0} = \sqrt{\frac{D_{\mathrm{A}}}{\pi t}} \left(C_{\mathrm{A,i}} - C_{\mathrm{A,b}}\right) \tag{7.25}$$

The average rate of mass transfer over the time interval 0 to t^* is

$$N_{\mathrm{A}} = \frac{1}{t^*} \int_0^{t^*} N_{\mathrm{A,inst}}(t)\, dt = 2\sqrt{\frac{D_{\mathrm{A}}}{\pi t^*}} \left(C_{\mathrm{A,i}} - C_{\mathrm{A,b}}\right) = k_{\mathrm{L}} \left(C_{\mathrm{A,i}} - C_{\mathrm{A,b}}\right) \tag{7.26}$$

where $k_L = 2\sqrt{D_A/\pi t^*}$ for the penetration theory.

7.2.3 Surface Renewal Model

A more complex model of the fluid mechanics involved is the surface renewal model. This model considers a transient absorption into surfaces both systematically replaced and randomly replaced by a fresh liquid.

In this model, the interface is regarded as being formed by a variety of elements, each one of which has been brought to the surface some time *t* before the instant of observation. The distribution of the surface element contact times is described by a distribution function $\psi(t) = se^{-st}$, where

$$\psi(t) = \frac{1}{t^*} \text{ for } t < t^* \quad \text{and} \quad \psi(t) = 0 \text{ for } t > t^* \tag{7.27}$$

The rate of absorption at the surface is then an average of the rates of absorption in each element defined as

$$N_A = \int_0^\infty N_{A,inst}(t)\psi(t)dt = \sqrt{\frac{D_A}{\pi}}\left(C_{A,i} - C_{A,b}\right)\int_0^\infty \frac{se^{-st}}{\sqrt{t}}dt = k_L\left(C_{A,i} - C_{A,b}\right) \tag{7.28}$$

where

$$k_L = \sqrt{D_A s} \tag{7.29}$$

For a first–order irreversible reaction, the equation governing diffusion, reaction, and accumulation of A may be written as

$$D_A\frac{\partial^2 C_A}{\partial x^2} - kC_A = \frac{\partial C_A}{\partial t} \tag{7.30}$$

with the boundary conditions

$$C_A(x,0) = 0 \tag{7.31}$$

$$C_A(0,t) = C_{A,i} \tag{7.32}$$

$$C_A(\infty,t) = 0 \tag{7.33}$$

In the case of a pseudo–first order reaction (e.g., the reaction between CO_2 and alkanolamines), $k = k'C_{B,b}$. Equation (7.30) is conveniently integrated by means of the

Laplace transform. Transforming with respect to time leads to (Froment and Bischoff, 1990)

$$\frac{d^2\overline{C_A}}{dx^2}-\left(\frac{k+s}{D_A}\right)\overline{C_A}=0 \tag{7.34}$$

Accounting for the boundary conditions, the solution of Eq. (7.34) yields

$$\overline{C_A}=\frac{C_{A,i}}{s}\exp\left[-\sqrt{\frac{k+s}{D_A}}x\right] \tag{7.35}$$

Finally, $C_A(x,t)$ is obtained by an inverse transformation of Eq. (7.35).

$$\frac{C_A}{C_{A,i}}=\frac{1}{2}\exp\left(-x\sqrt{\frac{k}{D_A}}\right)\operatorname{erfc}\left(\frac{x}{2\sqrt{D_A t}}-\sqrt{kt}\right)+\frac{1}{2}\exp\left(x\sqrt{\frac{k}{D_A}}\right)\operatorname{erfc}\left(\frac{x}{2\sqrt{D_A t}}+\sqrt{kt}\right) \tag{7.36}$$

For large values of kt, Eq. (7.36) reduces to

$$\frac{C_A}{C_{A,i}}=\exp\left(-x\sqrt{\frac{k}{D_A}}\right) \tag{7.37}$$

At time t, the instantaneous rate of absorption in an element having a surface age t is given by

$$N_A(t)=\sqrt{kD_A}C_{A,i}\left[\operatorname{erf}\left(\sqrt{kt}\right)+\frac{e^{-kt}}{\sqrt{\pi kt}}\right] \tag{7.38}$$

With Danckwerts' age distribution function, the average rate of absorption at the surface is given by

$$N_A=\sqrt{D_A(k+s)}C_{A,i}=\sqrt{D_A\left(k+\frac{k_L^2}{D_A}\right)}C_{A,i}=k_L C_{A,i}\sqrt{1+\frac{kD_A}{k_L^2}} \tag{7.39}$$

Hence, the enhancement factor E_A can be expressed by

$$E_A=\sqrt{1+\frac{kD_A}{k_L^2}}=\sqrt{1+Ha^2} \tag{7.40}$$

The correlations of the enhancement factor (E_A) for other types of reactions using both the penetration theory and the surface renewal model can be found in the literature such as Danckwerts and Kennedy (1954), Porter (1966), DeCoursey (1974, 1982), Olander (1960),

Huang and Kuo (1965), Perry and Pigford (1953), Brian (1964), Secor and Beutler (1967), and Onda *et al*. (1970).

7.2.4 Film–Penetration Theory

Similar to the surface renewal theory, the *film–penetration theory* adopts the unsteady–state molecular diffusion mechanism as the means of mass transport through the film or the liquid element. An example for the derivation of the enhancement factor for the gas absorption with a simple first–order or pseudo first–order reversible reaction using this theory can be found in Huang and Kuo (1965).

7.3 Review on the Kinetics between CO_2 and Alkanolamine Solutions

A large number of publications on kinetic experimental data and kinetic mechanisms between CO_2 and alkanolamines can be found in the literature. This sub-chapter provides a brief review on the reaction mechanisms between CO_2 and alkanolamine solutions. An overview on the reaction mechanisms between CO_2 and alkanolamines both in aqueous and non–aqueous solutions can be found in Versteeg *et al.* (1996).

7.3.1 The Reaction Mechanism for Primary and Secondary Alkanolamines

Danckwerts and McNeil (1967) proposed a reaction mechanism between CO_2 and primary and secondary alkanolamines in a two–step reaction

step 1: carbamate formation; rate determining

$$CO_2 + R_1R_2NH \rightleftharpoons R_1R_2NCOO^- + H^+ \tag{7.41}$$

step 2: protonated alkanolamine formation; instantaneous reaction

$$R_1R_2NH + H^+ \rightleftharpoons R_1R_2NH_2^+ \tag{7.42}$$

with a second–order overall reaction as follows

$$CO_2 + 2R_1R_2NH \rightleftharpoons R_1R_2NCOO^- + R_1R_2NH_2^+ \tag{7.43}$$

Experiments on the reaction between CO_2 and primary and secondary alkanolamines in aqueous solutions have been studied by many authors (see Blauwhoff *et al.*, 1983 and Versteeg *et al.*, 1996). However, only for MEA, as a primary amine, the overall reaction

order and the value of the kinetic constant are in accordance with the mechanism of reaction (7.43). For other primary and secondary alkanolamines, the overall reaction orders were found to be varying between two and three, both for aqueous and non–aqueous solutions. For example, the overall reaction order for DEA, as a secondary alkanolamine, was found to be three and by some authors between two and three. Therefore, the reaction mechanism between CO_2 and alkanolamines needs to be modified.

The *zwitterion–mechanism*. This reaction mechanism was first proposed by Caplow (1968) and reintroduced by Danckwerts (1979) in which the reaction between CO_2 and alkanolamines results in the formation of a zwitterion intermediate followed by the removal of a proton by a base B:

$$CO_2 + R_1R_2NH \underset{k_{-1}}{\overset{k_2}{\rightleftharpoons}} R_1R_2NH^+COO^- \tag{7.44}$$

$$R_1R_2NH^+COO^- + B \underset{k_{-b}}{\overset{k_b}{\rightleftharpoons}} R_1R_2NCOO^- + BH^+ \tag{7.45}$$

By using the pseudo steady–state assumption for the zwitterion concentration, the overall forward reaction rate can be expressed as (Versteeg *et al.*, 1996)

$$r_{CO_2} = -\frac{k_2[CO_2][R_1R_2NH]}{1+\frac{k_{-1}}{\sum k_b[B]}} \tag{7.46}$$

where k_2 and k_{-1} are the forward and reverse rate constants of reaction (7.44) and $\sum k_b[B]$ is the contribution to the zwitterion deprotonation by all bases present in the solution (e.g., H_2O, OH^-, and free alkanolamine).

Simplification of the reaction rate expression above for the two asymptotic situations can be evaluated from its denominators (Versteeg *et al.*, 1996)

1). $\frac{k_{-1}}{\sum k_b[B]} \ll 1$; resulting in a simple second–order reaction and the zwitterion formation being the rate limiting step (e.g., MEA in aqueous solutions).

$$r_{CO_2} = -k_2[CO_2][R_1R_2NH] \tag{7.47}$$

2). $\frac{k_{-1}}{\sum k_b[B]} \gg 1$; resulting in a more complex reaction rate expression with the possibility to have an overall reaction order of three.

$$r_{CO_2} = -\frac{k_2 \sum k_b [B]}{k_{-1}} [CO_2][R_1R_2NH] \tag{7.48}$$

The overall reaction order for the transition region between the two asymptotic cases changes from two to three. Therefore, the reaction rate expression in Eq. (7.46) can cover the shifting reaction orders for the reaction system as previously noted.

The *single step, termolecular mechanism*. This mechanism was proposed by Crooks and Donnellan (1989) and has been reviewed by da Silva and Svendsen (2004). The reaction mechanism uses the generally accepted mechanism proposed by Danckwerts (1979) in which the zwitterion intermediate is formed by making the assumption that the reaction proceeds through a loosely–bound encounter complex as the initial product. The forward reaction rate for this mechanism is

$$r_{CO_2} = -k_{obs}[CO_2] \tag{7.49}$$

where

$$k_{obs} = k_{AM}[R_1R_2NH]^2 + k_w[R_1R_2NH][H_2O] \tag{7.50}$$

However, Eq. (7.49) is equivalent to the asymptotic limit of the zwitterion mechanism described by Eq. (7.48) in which the zwitterion deprotonation mainly by water and the alkanolamine in aqueous solutions. This reaction mechanism can also explain the broken order and higher order kinetics observed as shown by da Silva and Svendsen (2004).

7.3.2 The Reaction Mechanism for Tertiary Alkanolamines

Tertiary alkanolamines cannot react with CO_2 directly. The tertiary alkanolamine acts as a base for CO_2 to react with hydroxide in solution according to the following reaction mechanism (Barth *et al.,* 1981)

$$R_1R_2R_3N + H_2O \rightleftharpoons R_1R_2R_2NH^+ + OH^- \tag{7.51}$$

$$CO_2 + OH^- \rightleftharpoons HCO_3^- \tag{7.52}$$

with the overall reaction:

$$CO_2 + R_1R_2R_3N + H_2O \rightleftharpoons R_1R_2R_2NH^+ + HCO_3^- \tag{7.53}$$

Reaction (7.53) was first proposed by Donaldson and Nguyen (1980) in what is called the base–catalyzed hydration of CO_2.

Jørgensen and Faurholt (1954) studied the reaction for TEA at high pH–values of ~13 and concluded that a monoalkylcarbonate was formed with the overall reaction

$$CO_2 + R_2NCH_2CH_2OH + OH^- \rightleftharpoons R_2NCH_2CH_2OCOO^- + H_2O \quad (7.54)$$

The reaction is found to be strongly pH–dependent and can be neglected at low pH–values (pH < 11) (Versteeg *et al.*, 1996).

7.3.3 Reactions in Aqueous Solution

In aqueous solutions when CO_2 is dissolved in water the following reactions also occur to form carbonic acid and bicarbonate ion

$$CO_2 + H_2O \rightleftharpoons H_2CO_3 \quad (7.55)$$

$$CO_2 + OH^- \rightleftharpoons HCO_3^- \quad (7.56)$$

The contribution of reaction (7.55) to the overall reaction rate is negligible, but the influence of reaction (7.56) on the absorption rate is found to be more complicated (see Versteeg *et al.*, 1996). This reaction is fast and can enhance mass transfer even for low concentration of hydroxyl ion.

7.4 Materials and Methods

7.4.1 Materials

Sample solutions of AEEA (purity >99 mass %) were prepared from the received chemical from Acros Organics in mixtures with deionized water with concentrations of 1.20, 1.80, 2.40, 2.94, and 3.50 M respectively. The AEEA as received does not seem to contain any active amine impurities that significantly affect the overall reaction rate. The CO_2 (purity >99.9992 mol %), N_2 (purity >99.6 mol %), and nitrous oxide (N_2O, purity >99.998 mol %) gases used were obtained from AGA Gas GmbH and used as source of CO_2, N_2, and N_2O, respectively.

7.4.2 Methods

Density and viscosity measurements. Density measurements of aqueous AEEA solutions were performed using pycnometer for variation of temperatures and mass fraction of AEEA. In addition, the densities of 30 mass % AEEA at different CO_2 loadings

were also measured. Viscosity measurements for different concentrations of AEEA were performed using Modular Compact Rheometer (PHYSICA MCR 100) from 20 to 50 °C.

N_2O solubility measurements. Solubility and diffusivity data are needed for the determination of the reaction kinetics. When CO_2 is absorbed into the alkanolamine solutions, CO_2 reacts with the alkanolamines and, therefore, it is not possible to determine the solubility and diffusivity directly. So the properties must be estimated from the corresponding data of similar non–reacting gases. N_2O is a non–reacting gas which can be used to estimate the properties of CO_2. The "N_2O analogy" may, therefore, be applied to estimate the solubility of CO_2 in aqueous alkanolamine solutions according to:

$$\left(\text{solubility of } CO_2\right)_{\text{Amine}} = \left(\frac{\text{solubility of } CO_2}{\text{solubility of } N_2O}\right)_{\text{water}} \times \left(\text{solubility of } N_2O\right)_{\text{Amine}} \qquad (7.57)$$

The N_2O solubility experiments were performed using an apparatus as shown in Figure 7-3. The apparatus consists of a 1130–mL gas steel vessel and a 750–mL absorption flask and is equipped by a ProMinent gear pump, Druck PTX 610 (max. 800 kPa) and PTX7517–1 (max. 200 kPa) pressure transmitters with an accuracy of ±0.3% of full scale each, a motor and stirrer, a water bath, and a K–type thermocouple.

Before starting the experiment, the absorption flask was first flushed by N_2. A ~370–mL of a fresh AEEA solution with certain concentration was passed into the absorption flask. N_2O gas was then passed from the gas vessel. The solution was stirred and heated to a desired temperature. Equilibrium was obtained when the total pressure in the system showed a constant value. This took ~60 min including the heating period.

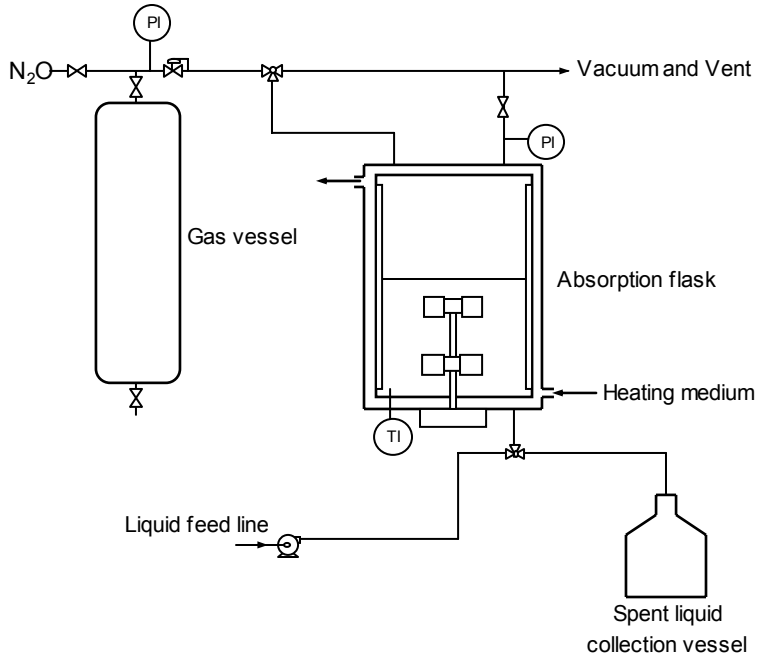

Figure 7-3. Experimental set–up of N_2O solubility

Kinetic measurements. The kinetic experiments for the CO_2–AEEA–H_2O system were performed using the string of disc contactor, as shown in Figure 7-4. The apparatus mainly contains a disc contactor equipped by a Fisher–Rosemount BINOS® 100 NDIR CO_2 analyzer (2 channels: 2000 ppm and 1 vol% CO_2), a BRONKHORST HI–TEC mass flow controller, a peristaltic liquid pump (EH PROMASS 83), a gas blower, and five K–type thermocouples. The disc contactor contains 43 discs with diameter of 1.5 cm and thickness of 0.4 cm, as shown in Figure 7-5. The active mass transfer area for this arrangement is ~226.15 cm^2. The characteristic active length of the column is ~64.5 cm. The disc absorption column is operated in counter–current mode with liquid flow from top to bottom and gas flow in the opposite direction. The set–up is equipped with thermocouples at the inlet and outlet of both phases and inside the chamber. The liquid and gas flows can be independently adjusted using a liquid pump and gas blower respectively. The flow of the blower is controlled by a Siemens Micro Master Frequency Transmitter and has a maximum flowrate of 1.75 Nm^3/hr.

A CO_2-unloaded AEEA solution with a certain concentration was passed to the column with a flowrate of ~46 mL min^{-1} which is the minimum flowrate where the absorption flux is independent of the liquid flowrate. A CO_2–N_2 gas mixture containing 10

vol % CO_2 was then lead into the column with a flowrate of 1.12 NL min^{-1}. The process was terminated as the temperature reached the desired level and the analyzer showed a constant value for the CO_2 volume percent. The data acquisition was performed using FieldPoint and LabVIEW.

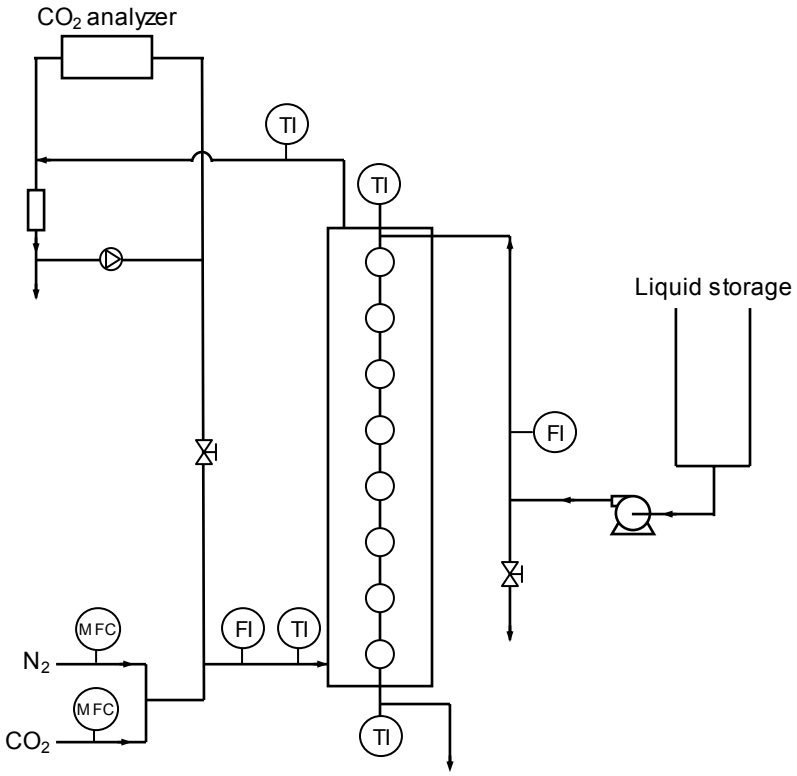

Figure 7-4. Experimental set–up of disc absorption column

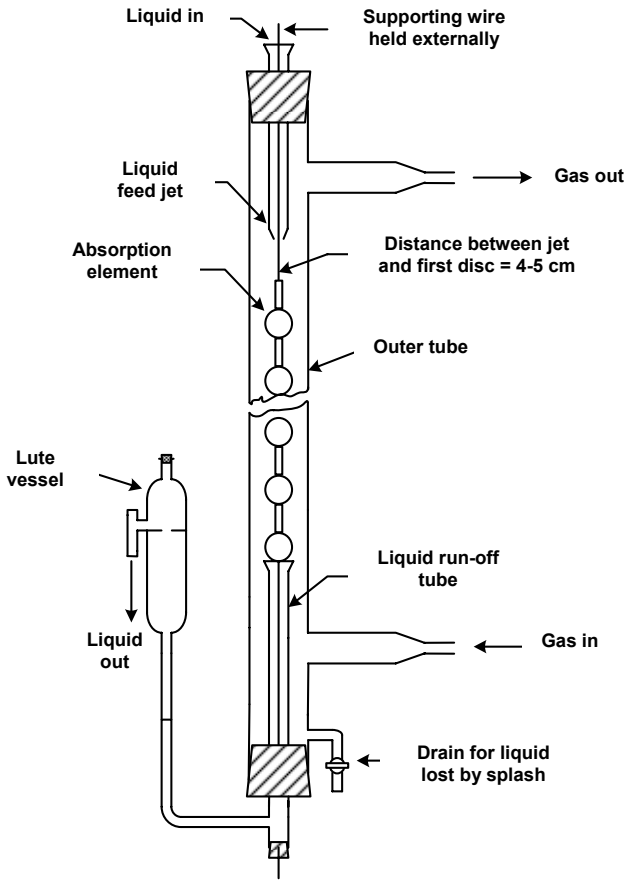

Figure 7-5. Arrangement of disc absorption column

7.5 Absorption Rate and Mass Transfer Coefficient Determinations

The disc contactor used in this kinetic study has been characterized by Dindore (2004) to evaluate hydrodynamics of both gas and liquid flow. Determination of physico–chemical parameters of new systems, e.g., disc contactor, as well as for simulating the industrial equipment with the disc column is necessary to establish the mass transfer and pressure drop characteristics of the disc column.

The total absorption flux of the solute was calculated by taking the solute balance over the entire system, i.e., the difference between the flow of the solute into the system and that going out of the system to the gas analyzer. This flux calculation method gives higher accuracy compared to that based on the balance just over the disc contactor. The overall absorption rate in the disc contactor is then given by

$$r_{\text{solute}} = \frac{Q_{\text{solute}}^{\text{in}} - Q_{\text{solute}}^{\text{out}}}{v_{\text{m}}^{0}} \tag{7.58}$$

where, r_{solute} is the molar absorption rate (mol s^{-1}) and v_m^0 is the molar volume at normal condition. The amount of the solute entering into the system can be obtained from the mass flow controller reading. The amount of the solute going out of the system through the gas analyzer is obtained from the following equation

$$Q_{\text{solute}}^{\text{out}} = Q_{\text{N}_2}^{\text{in}} \frac{y_{\text{solute}}^{\text{out}}}{1 - \left(\frac{p_{\text{solution}}}{P}\right) - y_{\text{solute}}^{\text{out}}} \tag{7.59}$$

The liquid–side mass transfer coefficient can be calculated from the absorption rate as follows

$$k_{\text{L}} = \frac{r_{\text{solute}}}{a\Delta C_{\text{LM}}} \tag{7.60}$$

where a is total mass transfer area in the disc contactor and ΔC_{LM} is the logarithmic mean driving force over the disc contactor defined as

$$\Delta C_{\text{LM}} = \frac{\left(mC_{\text{G,in}} - C_{\text{L,out}}\right) - \left(mC_{\text{G,out}} - C_{\text{L,in}}\right)}{\ln\left(\frac{mC_{\text{G,in}} - C_{\text{L,out}}}{mC_{\text{G,out}} - C_{\text{L,in}}}\right)} \tag{7.61}$$

Absorption of CO_2 into deionized water is an ideal system for characterization of the liquid–side mass transfer coefficient k_{L} in the disc contactor. Using the correlation given by Stephens and Morris (1951), the liquid–side mass transfer coefficient in the disc contactor is (Dindore, 2004)

$$\frac{k_{\text{L}}}{D} = \alpha\left(\frac{4\Gamma}{\mu}\right)^n \left(\frac{\mu}{\rho D}\right)^{0.5} \tag{7.62}$$

with $\alpha = 308.5$ and $n = 1.1$, μ and ρ are the viscosity and density of the liquid and D is the diffusivity of the solute in the liquid phase. Γ is the wetting rate in the apparatus defined as

$$\Gamma = \frac{\left(\text{Liquid flow rate}\right) \times \left(\text{Length of string}\right)}{\text{Surface area of string}} \tag{7.63}$$

The Stephens–Morris correlation has been used by some authors to correlate the liquid–side mass transfer coefficient with operating and physical parameters for this system as shown in Table 7-2. There is no agreement on the values of α and n obtained

among the authors. The difference in correlation of the parameter values is caused by variations in factors such as disc–type, disc morphology etc.

Table 7-2. Constants for the Stephens–Morris correlation

Author	α	*n*	Comment
Stephens and Morris (1951)	6.53	0.7	–
Taylor and Roberts (1956)	18.03	0.4	$\Gamma < 0.0641$ kg m^{-1} s^{-1}
Taylor and Roberts (1956)	0.60	1.0	$\Gamma > 0.0641$ kg m^{-1} s^{-1}
Xu *et al.* (1992)	14.13	0.918	–
Dindore (2004)	308.5	1.1	$\Gamma < 7.35\times10^{-4}$ kg m^{-1} s^{-1}

Stephens and Morris (1951) also correlated the gas–side mass transfer coefficient k_G using ammonia absorption into water from dilute mixtures with air as follows

$$\frac{k_G P}{v\rho_d} = 0.328\Gamma^{0.13}\left(\frac{vd\rho}{\mu}\right)^{-0.33}\left(\frac{\mu}{\rho D}\right)^{-0.56}\left(\frac{P}{p_i}\right) \tag{7.64}$$

where ρ_d is density of solute gas, v is gas velocity, d is equivalent diameter for gas flow, P is total pressure of the system, and p_i is partial pressure of solute gas.

Dindore (2004) used SO_2 absorption into aqueous NaOH solution to determine the gas–side mass transfer coefficient for the disc contactor defined as

$$Sh=0.11Re^{0.73}Sc^{-0.56} \tag{7.65}$$

where m is the distribution coefficient of the solute; ratio of concentration of the solute in the solvent to that of the solute in the gas phase at equilibrium conditions.

7.6 Kinetic Study using the String of Disc Contactor

In chemical absorption, the rate of a reaction cannot be neglected with respect to the mass transfer. The absorption flux is, therefore, enhanced due to the chemical reaction. Rewriting Eq. (7.2) gives the average absorption flux enhanced by the chemical reaction.

$$N_A = E_A k_L^{\circ}\left(C_{A,i} - C_{A,b}\right) \tag{7.66}$$

The correlations of the enhancement factor (E_A) based on the different mass transfer and chemical reaction models have been described in Section 7.2.

As a first approximation, let the reaction between CO_2 and all bases B present in the solution (i.e., AEEA, H_2O, and other bases) be the second–order irreversible reaction according to the reaction rate:

$$r_{CO_2} = -k_2 C_{CO_2} C_B \tag{7.67}$$

The concentration of B is reasonably high, and it can be assumed that the concentration of B is approximately constant during the reaction ($C_B \approx C_{B0}$). This is also the case in the film, and the reaction can, therefore, be assumed to be a pseudo–first order irreversible reaction defined as

$$r_{CO_2} = -k_2^{'} C_{CO_2} \tag{7.68}$$

where

$$k_2^{'} = k_2 C_{B0} \tag{7.69}$$

In the case of pseudo–first order irreversible reaction, the enhancement factor due to chemical reaction based on the surface renewal theory is given by Eq. (7.40) where

$$Ha = \frac{\sqrt{k_2 D_A C_{B0}}}{k_L} \tag{7.70}$$

For the slow reaction regime ($Ha < 0.3$), there is no enhancement due to chemical reaction. In this regime the absorption flux depends on the mass transfer coefficient and hence on the liquid velocity (Dindore *et al.*, 2005). The enhancement due to chemical reaction occurs in the fast reaction regime ($2 < Ha \ll E_{A\infty}$) where the absorption flux is independent of the mass transfer coefficient and hence independent of the liquid velocity. Thus, in this regime the measurement of the absorption flux must be performed to determine the mechanism and reaction kinetics of the CO_2 absorption.

The reaction mechanism of the CO_2–AEEA–H_2O system can be evaluated by the *single step, termolecular mechanism* proposed by Crooks and Donnellan (1989). This mechanism has been reviewed by da Silva and Svendsen (2004) using ab initio methods. It was concluded that the single–step mechanism is the most likely compared to the zwitterion mechanism. The base species present in the solution are AEEA, H_2O, and other bases. If AEEA and H_2O are the dominating bases, the forward reaction rate for this

mechanism is, according to Crooks and Donnellan (1989), written in Eqs. (7.49) and (7.50). Rewriting these equations leads to

$$r_{CO_2} = -\left[k_{AEEA}[AEEA] + k_{H_2O}[H_2O]\right][AEEA][CO_2] \tag{7.71}$$

Using the approach mentioned above, the reaction rate constants and the order of the reaction can then be obtained.

The enhancement factor for the system is then given by

$$E_A = \sqrt{1 + \frac{k_{obs} D_{CO_2}}{k_L^2}} \tag{7.72}$$

where

$$k_{obs} = k_{AEEA}[AEEA]^2 + k_{H_2O}[AEEA][H_2O] \tag{7.73}$$

Substituting Eq. (7.72) into Eq. (7.66) yields the average absorption flux as follows

$$N_A = k_L \sqrt{1 + \frac{k_{obs} D_{CO_2}}{k_L^2}} \left(C_{CO_2,i} - C_{CO_2,b}\right) \tag{7.74}$$

where $C_{CO_2,i}$ is the interfacial concentration of CO_2. Since the reaction occurs in the fast reaction regime and at very low CO_2 loadings, the concentration of CO_2 in the bulk will practically approach zero. The Eq. (7.74) can, therefore, be simplified to

$$N_A = k_L \sqrt{1 + \frac{k_{obs} D_{CO_2}}{k_L^2}} C_{CO_2,i} \tag{7.75}$$

7.7 Results and Discussion

7.7.1 Density and Viscosity Measurements

The densities of aqueous solutions of AEEA were measured for different mass fractions of AEEA over a range of temperatures from 10 to 90 °C and for solutions partially loaded with CO_2. The results can be seen in Figures 7-6 – 7-8.

Figure 7-6 shows the densities of aqueous AEEA solution for different mass fractions in comparison to those of other alkanolamines obtained from Cheng *et al.* (1996) at 25 °C. The density of aqueous AEEA solution can be approximated by use of a third–order polynomial as follows

$$\rho_{\mathrm{AEEA}} = 997.05 + 46.613x + 177.12x^2 - 195.76x^3 \qquad (7.76)$$

where x is the mass fraction of AEEA in the aqueous solution. The correlation coefficient is 0.999.

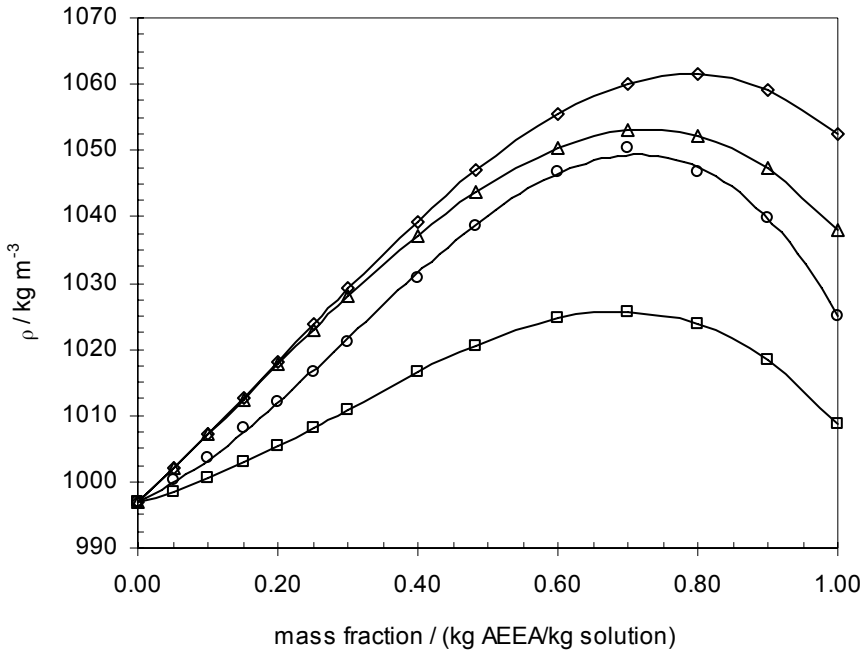

Figure 7-6. Densities of aqueous AEEA solutions and those of other alkanolamines from Cheng *et al.* (1996) for different mass fractions at 25 °C: ○, AEEA; □, MEA; Δ, MDEA; ◊, DGA.

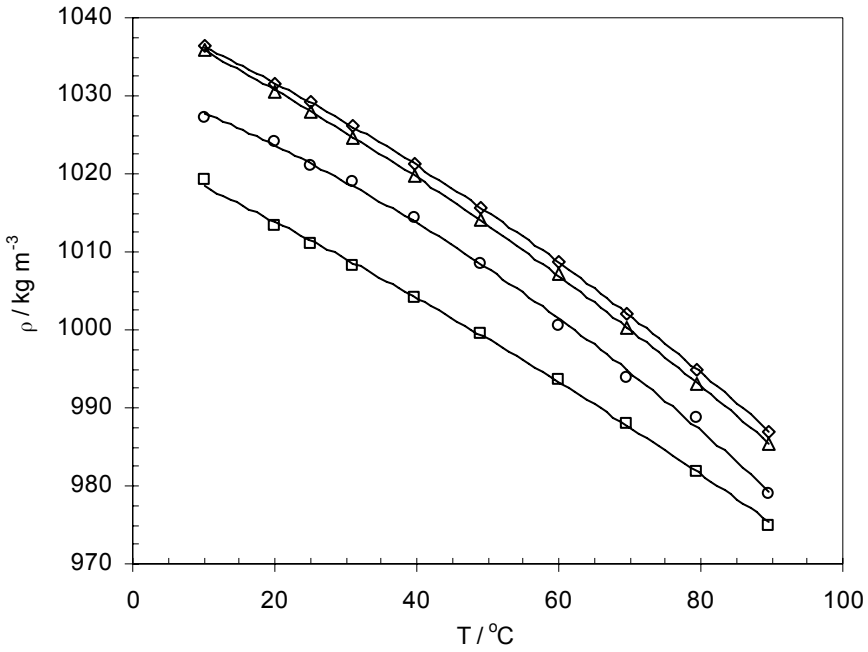

Figure 7-7. Densities of aqueous 30 mass % AEEA solutions and those of 30 mass % other alkanolamines from Cheng *et al.* (1996) at different temperatures: ○, AEEA; □, MEA; Δ, MDEA; ◊, DGA.

Figure 7-7 shows the densities of aqueous 30 mass % AEEA solution for different temperatures which can be approximated by use of a second–order polynomial as the following

$$\rho_{\text{AEEA}} = 1031.4 - 0.3329T - 0.0028T^2 \tag{7.77}$$

where T is the temperature in °C with the correlation coefficient of 0.998.

Figure 7-8 shows the densities of aqueous 30 mass% AEEA solution partially loaded with CO_2 at 25 °C. It can be seen from the figure that as CO_2 added into the solution the volume of the solution increases. Thus, the actual density is found to be lower than what would be expected if CO_2 just came as an addition to the weight. The density correlation can then be approximated as

$$\begin{aligned} \rho_{\text{AEEA sol}} &= \rho_{\text{CO}_2\text{-unloaded AEEA}} + W_{\text{CO}_2\text{ added}} - \Delta\rho \\ &= 1021.1 + W_{\text{CO}_2\text{ added}} - \Delta\rho \end{aligned} \tag{7.78}$$

where $W_{\text{CO}_2\text{ added}}$ is the amount of CO_2 added into the solution in kg m^{-3} and the volume expansion is correlated in terms of density as

$$\Delta\rho = 0.1518 W_{\text{CO}_2\text{ added}} \tag{7.79}$$

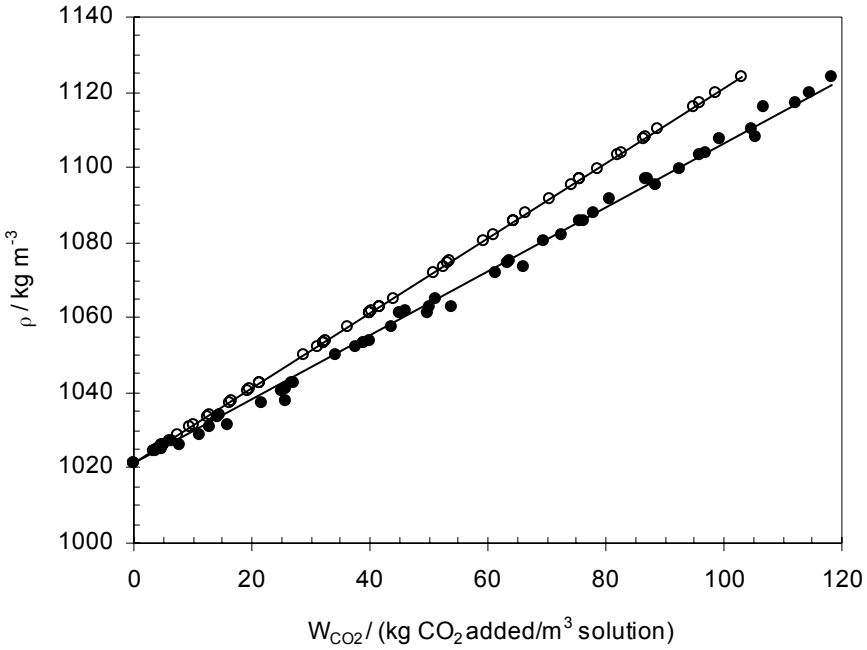

Figure 7-8. Densities of aqueous 30 mass% AEEA solution partially loaded with CO_2 at 25 °C: •, experiment; ○, calculated value without volume expansion.

The viscosity measurements of aqueous solutions of AEEA for different concentrations were performed using a Modular Compact Rheometer (PHYSICA MCR 100) over a range of temperatures from 20 to 50 °C. The experimental results can be seen in Figure 7-9.

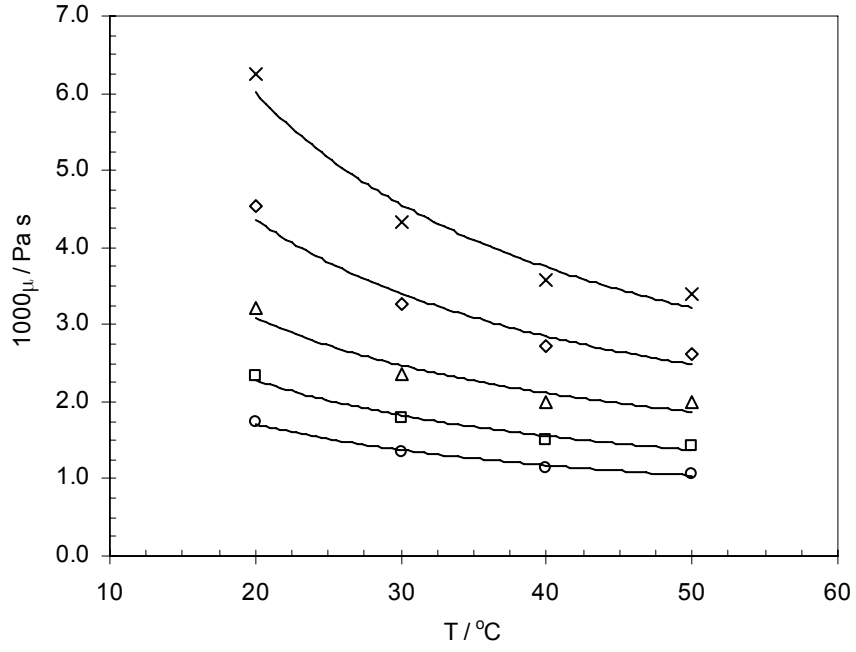

Figure 7-9. Viscosities of aqueous AEEA solution over a range of temperatures from 20 to 50 °C: ○, 1.20 M; □, 1.80 M; Δ, 2.40 M; ◊, 2.94 M; ×; 3.50 M.

It can be seen from Figure 7-9 that the viscosities of aqueous AEEA solutions decrease as the temperature increases. In addition, as the concentration of the solution increases the solution is more viscous at the same temperature.

7.7.2 N_2O Solubility Measurements

The solubility of N_2O in aqueous solutions of AEEA was measured for various concentration of AEEA over a range of temperatures from 25 to 55 °C. The results can be seen in Figure 7-10.

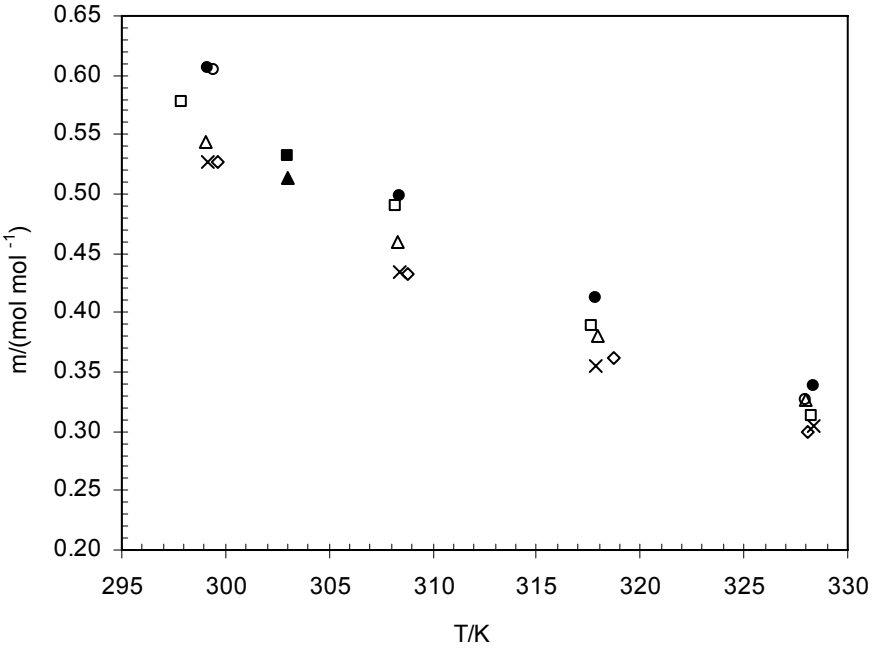

Figure 7-10. Solubility of N_2O in aqueous solutions of AEEA over a range of temperatures from 25 to 55 °C: ○, 1.20 M; □, 1.80 M; Δ, 2.40 M; ◊, 2.94 M; ×; 3.50 M; •, (H_2O; Versteeg and van Swaaij, 1988); ■, (MEA 1.20 M; Littel *et al.*, 1992); ▲, (MEA 3.50 M; Littel *et al.*, 1992).

Figure 7-10 shows the solubility of N_2O in aqueous solutions of AEEA in comparison to that of N_2O in water and aqueous MEA. The solubility of a gas in an electrolyte as well as in a weak electrolyte solution, is usually less than that in salt–free water; this solubility decrease is called *salting–out*. According to Prausnitz *et al.* (1999), the salting–out effect follows from a consideration of hydration forces in which the ions (especially cations) of the electrolyte solution like to form complexes with water (hydration), thereby leaving less "free" water available to dissolve the gas. The salting–out effect of an ion usually rises with increasing ionic charge and decreasing ionic radius. Based on this reason, since

AEEA has two amine groups (i.e., primary and secondary), it will produce more heavily charged cations, in the forms of monoprotonated and diprotonated, compared to MEA, and the salting–out effect can be envisaged to be stronger than that in MEA. Consequently, the gas solubility decrease is higher compared to MEA at a fixed temperature as shown in Figure 7-10. From the figure, it can also be seen that the solubility of N_2O in water is the highest at a fixed temperature.

To estimate the solubility of CO_2 in aqueous solutions of AEEA, Eq. (7.57) can be applied where the solubility of CO_2 and that of N_2O in water can be estimated by use of the correlations given by Versteeg and van Swaaij (1988) as a function of temperature according to

$$H_{CO_2\text{-}H_2O} = 2.82\times10^6 \exp(-2044/T) \quad \text{Pa m}^3\ \text{mol}^{-1} \tag{7.80}$$

$$H_{N_2O\text{-}H_2O} = 8.55\times10^6 \exp(-2284/T) \quad \text{Pa m}^3\ \text{mol}^{-1} \tag{7.81}$$

From Eqs. (7.80) and (7.81) the ratio of the solubility of CO_2 and that of N_2O in water can be defined as

$$C_1 = \left(\frac{\text{solubility of CO}_2}{\text{solubility of N}_2\text{O}}\right)_{\text{water}} = 3.04\exp(-240/T) \tag{7.82}$$

7.7.3 Kinetic Study of the CO_2–AEEA–H_2O System

The reaction kinetics of the CO_2–AEEA–H_2O system have been studied using the string of disc contactor over a range of temperatures from 31 to 50 °C at various concentrations of aqueous CO_2–unloaded AEEA solutions. In Section 6.1, the series of physical and chemical reaction equilibria for the CO_2–AEEA–H_2O system were described. The reactions between CO_2 and AEEA consist of the formation of carbamates and that of dicarbamate of AEEA according to the reactions as follows

(i) formation of carbamates:

$$\text{AEEA}+\text{CO}_{2\,(l)} \rightleftarrows \text{AEEACOO}^-_{\text{p}} \tag{7.83}$$

$$\text{AEEA}+\text{CO}_{2\,(l)} \rightleftarrows \text{AEEACOO}^-_{\text{s}} \tag{7.84}$$

(ii) formation of dicarbamate:

$$\text{AEEACOO}^-_{\text{p}}+\text{CO}_{2\,(l)} \rightleftarrows {}^-\text{OOCAEEACOO}^- \tag{7.85}$$

$$AEEACOO_p^- + CO_{2(l)} \rightleftarrows {}^-OOCAEEACOO^- \quad (7.86)$$

where the proton transfers between H_2O and H_3O^+ have been taken out of the above reactions.

According to the speciation result in Figure 6-10, it was known that at low CO_2 loadings, at which the experiments were performed (~zero CO_2 loading), the species present are mainly the primary carbamate of AEEA as a product, the monoprotonated AEEA, and the remaining free AEEA. The other products (e.g. the secondary carbamate and dicarbamate of AEEA) are just present in very small amounts and the formation of them can, therefore, be disregarded. Thus, the main reaction is the formation of the primary carbamate of AEEA according to Eq. (7.83). In addition, to evaluate the reaction mechanisms of the formation of the secondary carbamate and that of dicarbamate of AEEA, more experimental work needs to be conducted and it might be for future work.

Since the experiments were conducted at high enough concentrations of AEEA, the reaction between CO_2 and AEEA can then be expressed by a pseudo–first order irreversible reaction approach defined in Eq. (7.68). The observed pseudo–first order reaction rate constants, k_{obs}, were determined using the string of disc contactor at various concentration of AEEA ranging from 1.20 to 3.50 mol L^{-1} over a range of temperatures between 31 and 50 °C. The results can be seen in Appendix A.

By assuming the pseudo–first order reaction, the second–order rate constant was extracted by taking the best–fit straight line between k_{obs}/[AEEA] and $1/T$. An Arrhenius expression for values of the rate constant obtained in this work is defined as follows

$$k_2 = k_{2,25^\circ C} \exp\left[-\frac{\Delta E}{R}\left(\frac{1}{T} - \frac{1}{298.15}\right)\right] \quad (7.87)$$

where $k_{2,25^\circ C} = 1.18\times10^4$ L mol^{-1} s^{-1}, $\Delta E = 3.63\times10^4$ J mol^{-1}, and $R = 8.314$ J mol^{-1} K^{-1}.

Using Eq. (7.87), the predicted value of the second–order rate constant k_2 at 25 °C for AEEA is found to be higher than those of MEA and DEA, but it is much lower compared to Piperazine (PZ), as shown in Table 7-3. From the table, it is known that the activation energy obtained in this work is also comparable to those of MEA and DEA.

Table 7-3. The comparison of AEEA kinetics at 25 °C.

Amine	$k_{2,25°C}$ /(L mol^{-1} s^{-1})	ΔE/ J mol^{-1}	Source
AEEA	11800	36300	This work
PZ	53700	33600	Bishnoi and Rochelle (2000)
MEA	7000	17900	Hikita *et al.* (1979)
DEA	1200	41800	Sada *et al.* (1976), Danckwerts and Sharma (1966)

Furthermore, the reaction mechanism of the CO_2–AEEA–H_2O system can be approached by the *single step–termolecular mechanism* as proposed by Crooks and Donnellan (1989). The values of k_{obs} divided by the concentration of AEEA result in a linear equation expressed in Eq. (7.88). Plots of this equation in Figure 7-11 gave good straight lines.

$$\frac{k_{obs}}{[\mathrm{AEEA}]} = k_{\mathrm{AEEA}}[\mathrm{AEE}A] + k_{\mathrm{H_2O}}[\mathrm{H_2O}] \tag{7.88}$$

By taking an average value of water concentration (42.71 mol L^{-1}), the reaction rate constants of AEEA, k_{AEEA}, and those of water, $k_{\mathrm{H_2O}}$, were calculated from the plots and the result can be seen in Table 7-4.

Table 7-4. The reaction rate constants of AEEA and those of water

T / °C	k_{AEEA}	$k_{\mathrm{H_2O}}$
32.1	3012	221.4
34.9	3356	257.0
39.6	3967	324.3
44.2	4664	407.2
48.8	5440	506.9

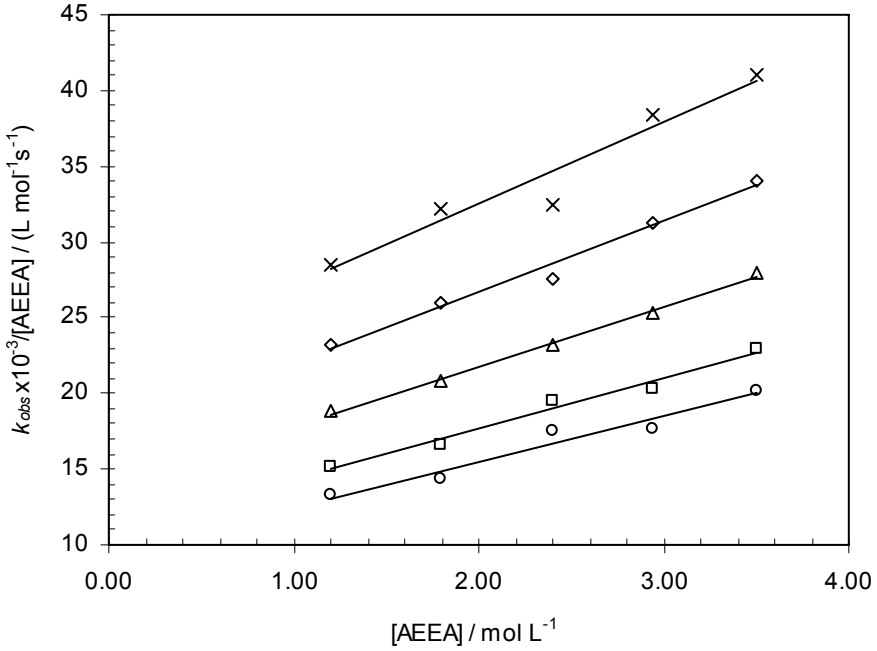

Figure 7-11. Variation of k_{obs}/[AEEA] with [AEEA] over a range of temperatures from 31 to 50 °C: ○, 1.20 M; □, 1.80 M; Δ, 2.40 M; ◊, 2.94 M; ×; 3.50 M.

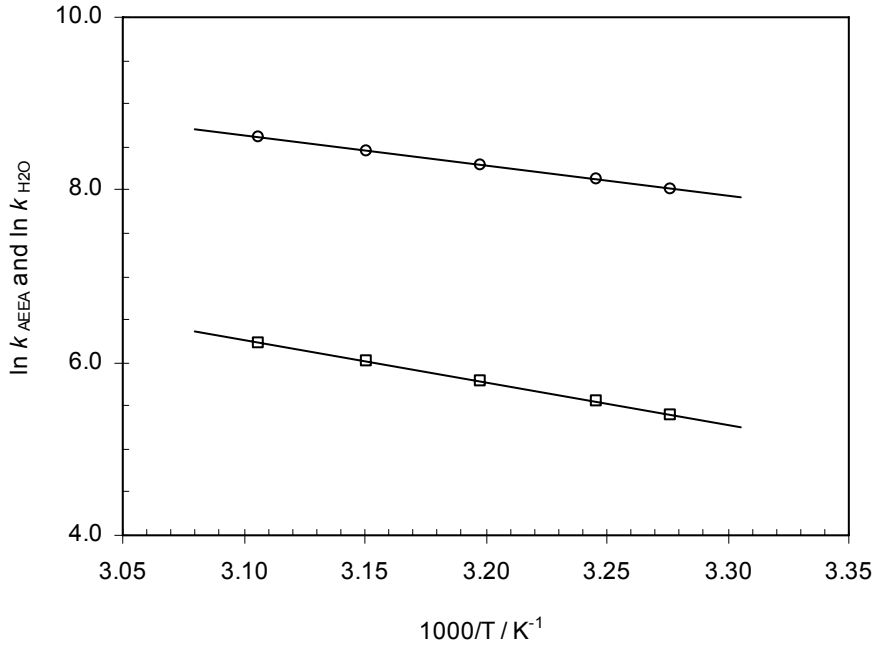

Figure 7-12. Relationship between ln k with 1/T: ○, AEEA; □, H_2O.

In Figure 7-12 an Arrhenius–plot is given. From this figure, the reaction rate constant of AEEA k_{AEEA} and that of water k_{H_2O} can be expressed as follows

$$k_{\mathrm{AEEA}} = 2.60\times10^{8}\exp\left(\frac{-3470}{T}\right) \tag{7.89}$$

$$k_{\mathrm{H_2O}} = 1.82\times10^{9}\exp\left(\frac{-4860}{T}\right) \tag{7.90}$$

Applying Eqs. (7.89) and (7.90) at a temperature of 25 °C, the predicted values for both the reaction rate constant of AEEA and that of water obtained in this work were found to be comparable to those of the Potassium glycinate (PG) system (Kumar *et al.,* 2003) and those of MEA system (Aboudheir *et al.,* 2003), as seen in Table 7-5.

Table 7-5. Reaction rate constant of AEEA and that of water for the CO_2–AEEA–H_2O system in comparison to those of PG and MEA systems at 25 °C.

Absorbent	$k\times10^{-3}$ /L^2 mol^{-2} s^{-1}	$k_{\mathrm{H_2O}}$ /L^2 mol^{-2} s^{-1}	C / mol L^{-1}	Source
AEEA	2.31	152	1.20 – 3.50	This work
PG	2.09	118	0.10 – 4.00	a
MEA	1.71	73.7	0.19 – 5.50	b

[a]Kumar *et al.* (2003)

[b]Aboudheir *et al.* (2003)

The kinetic data of the CO_2–AEEA–H_2O system available in the literature are very limited. The only reference found to be compared to this work was that of Bouhamra and Alper (2000). Figure 7-13 shows a comparison between the predicted k_{obs} in this work and those of Bouhamra and Alper (2000) at 25 °C. It can be seen that the correlation of k_{obs} obtained from this work represents the data very well at higher concentrations of AEEA but seem to overpredicts them at lower concentrations of AEEA. As shown by Bouhamra and Alper (2000), a first-order reaction with respect to the AEEA concentration was obtained within the concentration range of 0.015 to 0.05 mol L^{-1}. This indicates that at low concentrations of AEEA a shift on the reaction order occurs. They used the zwitterion intermediate mechanism to interpret and explain the data. However, the termolecular mechanism as given in Eq. (7.88) can explain this behavior equally well as at low amine concentrations, the water term in Eq. (7.88) will dominate.

Based on the results obtained, it was shown that the termolecular mechanism provides a good representation of the experimental data in the whole concentration range.

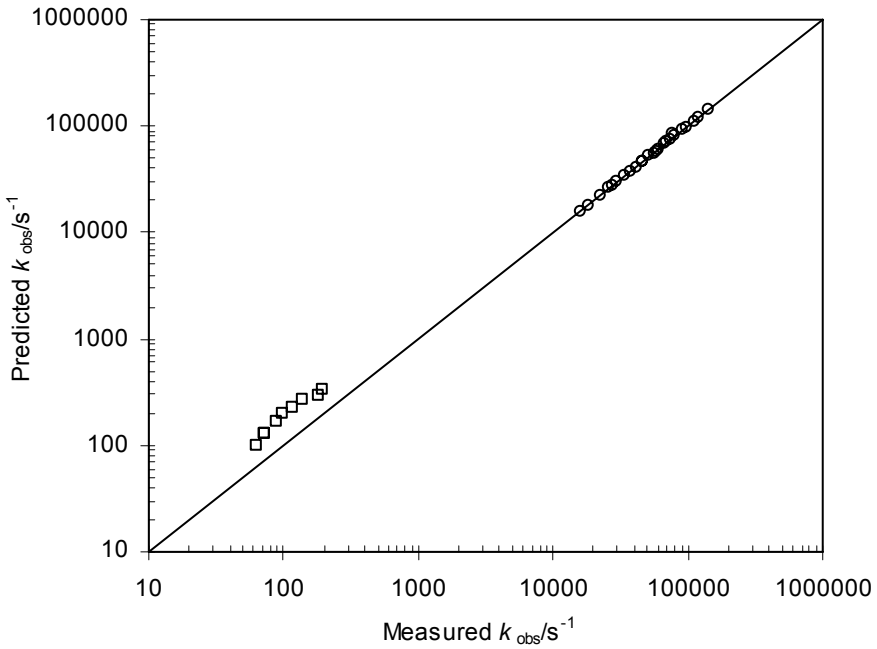

Figure 7-13. Comparison of measured and predicted k_{obs} obtained by the termolecular mechanism of CO_2–AEEA–H_2O system: ○, this work; □, Bouhamra and Alper (2000).

It was also found from this study that the activation energy of AEEA in Eq. (7.89) was indirectly affected by the diffusivity and solubility of CO_2. The enhancement factor calculated using the diffusivity and solubility values of CO_2 in the amine solution was found to be higher compared to the use of the diffusivity and solubility values of CO_2 in water. A small change in those values significantly affected the enhancement factor from which the observed reaction rate constants were obtained. The change in the observed reaction rate constants, therefore, affected the activation energy observed in this work. It is thus very important to measure the CO_2 solubility in the real system, and to have real system viscosities for estimation of diffusivities. The activation energies obtained based on solubilities and diffusivities in water as many studies have done should, therefore, be treated with care.

7.8 Conclusions

The kinetic mechanism of the CO_2–AEEA–H_2O system has been studied using the string of disc contactor by the *single step – termolecular mechanism* approach proposed by Crooks and Donnellan (1989). The results show that this mechanism can be applied to determine the reaction mechanism of the CO_2–AEEA–H_2O system. In addition, some physical properties, density and viscosity, have been measured to determine the physico–chemical parameters. The solubility of N_2O in AEEA was also measured to estimate the solubility of CO_2 in AEEA solution.

CHAPTER 8

Summary and Suggestions for Future Work

8.1 Summary

The development and characterization of new absorbents for CO_2 capture have been studied. The work includes selection of new absorbents (screening tests), vapor–liquid equilibrium experiments, and kinetic study using the string of disc contactor for the selected absorbent.

The work on selection of new absorbents for CO_2 capture was performed by absorption study of CO_2 into both single absorbents and absorbent mixtures for amine–based and non–amine–based systems. It has been found that the aqueous 30 mass % AEEA solution seems to be a potentially good absorbent for capturing CO_2. It offers high absorption rate combined with high absorption capacity. In addition to AEEA, MMEA also needs to be considered. It could have a greater potential than indicated from the study when used in contactors where the two phases are separated, like in membrane contactors.

AEEA as the selected absorbent obtained from the screening tests was further investigated to determine its vapor–liquid equilibrium characteristics. From the VLE data, it was known that AEEA also offers higher cyclic capacity and lower the regeneration energy requirement for some cases studied compared to MEA. Moreover, a VLE thermodynamic modeling of the aqueous AEEA solution was performed by use of a modified Deshmukh–Mather model (Deshmukh and Mather, 1981) as well as NMR analyses to determine the species distribution in the liquid phase as function of CO_2 loading.

The kinetic mechanism of the CO_2–AEEA–H_2O system has also been studied using the string of disc contactor by the *single step – termolecular mechanism* approach (Crooks and Donnellan, 1989). It was shown that this mechanism can be applied to determine the reaction mechanism of the CO_2–AEEA–H_2O system. In addition, the physical properties, density and viscosity, have been measured to determine the physico–chemical parameters.

The solubility of N_2O in AEEA was also measured to estimate the solubility of CO_2 in AEEA solution.

8.2 Suggestions for Future Work

- In the VLE modeling as well as in the design of the columns, the need of the physical property data is a must. The physical property data of AEEA are very limited found in the literature; its physical properties, therefore, need to be measured such as heat of absorption measured by calorimetry, dielectric constant, heat capacity, conductivity, etc.
- A VLE model was implemented for the CO_2–AEEA–H_2O system with very complex chemical equilibrium reactions. Parameter regression was performed and reasonable representation of experimental data was obtained. However, more experimental data on the binary VLE are needed to reduce the number of regressed parameters. Thus, more reliable parameters and the predictive properties of the model can be obtained.
- From the screening test results, it was known that MMEA also needs to be considered as a potential absorbent to capture CO_2. It could have a greater potential than indicated from the study when used in contactors where the two phases are separated, like in membrane contactors.
- The number of absorbents investigated in the screening test experiments were limited to ~30 systems. A larger number of absorbents than 30 systems will, of course, be needed to give the possibility to obtain more than one absorbent candidates offering better performances compared to MEA.
- In addition to the constant mass % used for the concentration expressions to compare the absorbent performances, the constant molar concentrations should also be used in the future work.

References

Aboudheir, A.; Tontiwachwuthikul, P.; Chakma, A.; Idem, R. Kinetics of the Reactive Absorption of Carbon Dioxide in High CO_2-lodeded, Concentrated Aqueous Monoethanolamine Solutions. *Chem. Eng. Sci.* **2003**, *58*, 5195–5210.

Astarita, G.; Savage, D. W.; Bisio, A. *Gas Treating with Chemical Solvents;* John Wiley & Sons: New York, 1983.

Atwood, K.; Arnold, M. R.; Kindrick, R. C. Equilibria for the System, Ethanolamines–Hydrogen Sulfide–Water. *Ind. Eng. Chem.* **1957,** *49,* 1439–444.

Austgen, D. M. *A Model of Vapor–Liquid Equilibria for Acid Gas–Alkanolamine–Water Systems;* University of Texas: Austin, TX, 1989.

Austgen, D. M.; Rochelle, G. T.; Chen, C. –C. Model of Vapor–Liquid Equilibria for Aqueous Acid Gas–Alkanolamine Systems. 2. Representation of H_2S and CO_2 Solubility in Aqueous MDEA and CO_2 Solubility in Aqueous Mixtures of MDEA with MEA or DEA. *Ind. Eng. Chem. Res.* **1991,** *30,* 543–555.

Austgen, D. M.; Rochelle, G. T.; Peng, X.; Chen, C. –C. Model of Vapor–Liquid Equilibria for Aqueous Acid Gas–Alkanolamine Systems Using the Electrolyte–NRTL Equation. *Ind. Eng. Chem. Res.* **1989,** *28,* 1060–1073.

Barth, D.; Tondre, C.; Lappai, G.; Delpuech, J. J. Kinetic Study of Carbon Dioxide Reaction with Tertiary Amines in Aqueous Solutions. *J. Phys. Chem.* **1981,** *85,* 3660–3667.

Bishnoi, S. *Carbon Dioxide Absorption and Solution Equilibrium in Piperazine Activated Methyldiethanolamine;* University of Texas: Austin, TX, 2000

Bishnoi, S.; Rochelle, G. T. Absorption of Carbon Dioxide into Aqueous Piperazine: Reaction Kinetics, Mass Transfer and Solubility. *Chem. Eng. Sci.* **2000,** *55,* 5531–5543.

Blauwhoff, P. M. M.; Versteeg, G. F.; van Swaaij, W. P. M. A Study on the Reaction between CO_2 and Alkanolamines in Aqueous Solutions. *Chem. Eng. Sci.* **1983,** *38,* 1411–1429.

Bouhamra, W.; Alper, E. Reaction Kinetics of Carbon Dioxide, Carbonyl Sulfide and Carbon Disulfide with Aqueous 2-(2-Aminoethylamino) Ethanol. *Chem. Eng. Technol.* **2000,** *23,* 421–423.

Brelvi, S. W.; O'Connell, J. P. Corresponding State Correlation for Liquid Compressibility and Partial Molal Volumes of Gases at Infinite Dilution in Liquids. *AIChE J.* **1972,** *18,* 1239–1243.

Brian, P. L. T. Gas Absorption Accompanied by an Irreversible Reaction of General Order. *AIChE J.* **1964,** *10*, 5–10.

Bromley, L. A. Approximate Individual Ion Values of β (or B) in extended Debye–Hückel Theory for Uni–univalent Aqueous Solutions at 298.15 K. *J. Chem. Thermo.* **1972,** 4, 669–673.

Bromley, L. A. Thermodynamic Properties of Strong Electrolytes in Aqueous Solutions. *AIChE J.* **1973,** *19,* 313–320.

Buckingham, P. A. Fluor Solvent Process Plants: How They are Working. *Hydrocarbon Process*. **1964,** *43(4),* 113–116.

Bucklin, R. W. DGA – A Workhorse for Gas Sweetening. *Oil Gas J.* **1982,** *11,* 204–210.

Button, J. K.; Gubbins, K. E. SAFT Prediction of Vapour–Liquid Equilibria of Mixtures Containing Carbon Dioxide and Aqueous Monoethanolamine or Diethanolamine *Fluid Phase Equilib.* **1999,** *158–160,* 175–181.

Caplow, M. Kinetics of Carbamate Formation and Breakdown. *J. Am. Chem. Soc.,* **1968,** *90,* 6795–6803.

Carson, J. K.; Marsh, K. N.; Mather, A. E. Enthalpy of Solution of Carbon Dioxide in (Water + Monoethanolamine, or Diethanolamine, or *N*-Methyldiethanolamine) and (Water + Monoethanolamine + *N*-Methyldiethanolamine) at T = 298.15 K. *J. Chem. Thermodynamics* **2000,** *32,* 1285–1296.

Chakma, A.; Meisen, A. Solubility of CO_2 in Aqueous Methyldiethanolamine and *N,N*–Bis(hydroxyethyl)piperazine Solutions. *Ind. Eng. Chem. Res.* **1987,** *26,* 2461–2466.

Chen, C. –C.; Britt, H. I.; Boston, J. F.; Evans, L. B. Local Composition Model for Excess Gibbs Energy of Electrolyte Systems. *AIChE J.* **1982,** *28,* 588–596.

Chen, C. –C.; Britt, H. I.; Boston, J. F.; Evans, L. B. Extension and Application of the Pitzer Equation for Vapor–Liquid Equilibrium of Aqueous Electrolyte Systems with Molecular Solutes. *AIChE J.* **1979,** *25,* 820–831.

Chen, C. –C.; Evans, L. B. A Local Composition Model for the Excess Gibbs Energy of Aqueous Electrolyte Systems. *AIChE J.* **1986,** *32,* 444–454.

Cheng, S.; Meisen, A.; Chakma, A. Predict Amine Solution Properties Accurately. *Hydrocarbon Process.* **1996,** *2,* 81–84.

Chirico, R. D.; Frenkel, M.; Diky, V. V.; Marsh, K. N.; Wilhoit, R. C. ThermoML–An XML–Based Approach for Storage and Exchange of Experimental and Critically Evaluated Thermophysical and Thermochemical Property Data. 2. Uncertainties. *J. Chem. Eng. Data* **2003,** *48,* 1344–1359.

Chiu, L. –F.; Liu, H. –F.; Li, M. –H. Heat Capacity of Alkanolamines by Differential Scanning Calorimetry. *J. Chem. Eng. Data* **1999,** *44,* 631–636.

Clegg, S. L.; Pitzer, K. S. Thermodynamics of Mutlicomponent, Miscible, Ionic Solutions: Generalized Equations for Symmetrical Electrolytes. *J. Phys. Chem.* **1992,** *96,* 3513–3520.

Crooks, J. E. ; Donnellan, J. P. Kinetics and Mechanism of the Reaction between Carbon Dioxide and Amines in Aqueous Solution. *J. Chem. Soc. Perkin. Trans.* **1989,** II, 331–333

da Silva, E. F.; Svendsen, H. F. Ab Initio Study of the Reaction of Carbamate Formation from CO_2 and Alkanolamines. *Ind. Eng. Chem. Res.* **2004,** *43,* 3413–3418.

da Silva, E. F.; Svendsen, H. F. Study of the Carbamate Stability of Amines Using ab Initio Methods and Free–Energy Perturbations. Accepted *Ind. Eng. Chem. Res.* **2005.**

Danckwerts, P. V. The Reaction of CO_2 with Ethanolamines. *Chem, Eng. Sci.* **1979,** *34,* 443–446.

Danckwerts, P. V.; Kennedy, A. M. Kinetics of Liquid–Film Process in Gas Absorption. Part I: Models of the Absorption Process. *Trans. Inst. Chem. Eng.* **1954,** *32*, S49–S52.

Danckwerts, P. V.; McNeil, K. M. The Absorption of Carbon Dioxide into Aqueous Amine Solutions and the Effects of Catalysis. *Trans. Inst. Chem. Eng.* **1967,** *45,* T32–T49.

Danckwerts, P.V.; Sharma, M. M. The Absorption of Carbon Dioxide into Solutions of Alkalis and Amine (with some Notes on Hydrogen Sulphide and Carbonyl Sulphide). *Chem. Eng.* **1966,** *10,* CE244–CE280.

Debye, V. P.; Hückel, E. The Theory of Electrolyte. *Physikalische Zeitschrift* **1923,** *24,* 185–206.

DeCoursey, W. J. Absorption with Chemical Reaction: Development of a New Relation for the Danckwerts Model. *Chem. Eng. Sci.* **1974,** *29*, 1867–1872.

DeCoursey, W. J. Enhancement Factor for Gas Absorption with Reversible Reaction. *Chem. Eng. Sci.* **1982,** *37*, 1483–1489.

Deshmukh, R. D.; Mather, A. E. A Mathematical Model for Equilibrium Solubility of Hydrogen Sulfide and Carbon Dioxide in Aqueous Alkanolamine Solutions. *Chem. Eng. Sci.* **1981,** *36,* 355–362.

Desideri, U.; Corbelli, R. CO_2 Capture in Small Size Cogeneration Plants: Technical and Economical Considerations. *Energy Convers. Mgmt.* **1998,** *39,* 857–867.

Dindore, V. Y. *String of Disc Contactor: Process Details and Experimental Set Up;* SINTEF Report; Trondheim, 2004.

Dindore, V. Y.; Brilman, D. W. F.; Versteeg, G. F. Hollow Fiber Membrane Contactor as a Gas–Liquid Model Contactor. *Chem. Eng. Sci.* **2005,** *60*, 467–479.

Donaldson, T. L.; Nguyen, Y. N. Carbon Dioxide Reaction Kinetics and Transport in Aqueous Amine Membranes. *Ind. Eng. Chem. Fundam.* **1980,** *19,* 260–266.

Edwards, T. J.; Maurer, G.; Newman, J.; Prausnitz, J. M. Vapor–Liquid Equilibria in Multicomponent Aqueous Solutions of Volatile Weak Electrolytes. *AIChE J.* **1978,** *24,* 966–976.

Edwards, T: J.; Newman, J.; Prausnitz, J. M. Thermodynamics of Aqueous Solutions Containing Volatile Weak Electrolytes. *AIChE J.* **1975,** *21,* 248–259.

Elliot, J. R.; Lira, C. T. *Introductory Chemical Engineering Thermodynamics;* Prentice Hall PTR: New Jersey, 1999.

Feron, P. H. M.; Jansen, A. E. Capture of Carbon Dioxide using Membrane Gas Absorption and Reuse in the Horticultural Industry. *Energy Convers. Mgmt.* **1995,** *36,* 411–414.

Feron, P. H. M.; Jansen, A. E. The Production of Carbon Dioxide from Flue Gas by Membrane Gas Absorption. *Energy Convers. Mgmt.* **1997,** *38,* S93–S98.

Frazier, H. D.; Kohl, A. L. Selective Absorption of Hydrogen Sulfide from Gas Streams. *Ind. Eng. Chem.* **1950,** *42,* 2288–2292.

Froment, G. F.; Bischoff, K. B. *Chemical Reactor Analysis and Design;* John Wiley & Sons: New York, 1990.

Fürst, W.; Renon, H. Representation of Excess Properties of Electrolyte Solutions Using a New Equation of State. *AIChE J.* **1993,** *39,* 335–343.

Goldman, A. M.; Leibush, A. G. Study of the Equilibrium of Carbon Dioxide Desorption from Monoethanolamine Solutions in the Temperature Range 75–140 °C. *Tr. Gos. Nauchno–Issled. Proeknt. Inst. Azotn. Promsti.* **1959,** *10,* 54–82.

Guggenheim, E. A. The Specific Thermodynamic Properties of Aqueous Solutions of Strong Electrolytes. *Phil. Mag.* **1935,** *19,* 588–643.

Hikita, H.; Asai, S.; Katsu, Y.; Ikuno, S. Absorption of Carbon Dioxide into Aqueous Monoethanolamine Solutions. *AIChE J.* **1979,** *25,* 793–800.

Hoff, K. A. *Modeling and Experimental Study of Carbon Dioxide Absorption in a Membrane Contactor;* Norwegian University of Science and Technology: Trondheim, 2003.

Hook, R. J. An Investigation of Some Sterically Hindered Amines as Potential Carbon Dioxide Scrubbing Compounds. *Ind. Eng. Chem, Res.* **1997,** *36,* 1779–1790

Huang, C. –J.; Kuo, C. –H. Mathematical Models for Mass Transfer Accompanied by Reversible Chemical Reaction. *AIChE J.* **1965,** *11,* 901–910.

Huang, S. H.; Radosz, M. Equation of State for Small, Large, Polydisperse, and Associating Molecules. *Ind. Eng. Chem. Res.* **1990,** *29,* 2284–2294.

Huang, S. H.; Radosz, M. Equation of State for Small, Large, Polydisperse, and Associating Molecules: Extension to Fluid Mixtures. *Ind. Eng. Chem. Res.* **1991,** *30,* 1994–2005.

Jørgensen, E.; Faurholt, C. Reaction between Carbon Dioxide and Amino Alcohols II. Triethanolamine. *Acta Chem. Scand.* **1954,** *8,* 1141–1144.

Jou, F. –Y.; Carroll, J. J.; Mather, A. E.; Otto, F. D. The Solubility of Carbon Dioxide and Hydrogen Sulfide in a 35 wt% Aqueous Solution of Methyldiethanolamine. *Can. J. Chem. Eng.* **1993,** *71,* 264–268.

Jou, F. –Y.; Mather, A. E.; Otto, F. D. Solubility of H_2S and CO_2 in Aqueous Methyldiethanolamine Solutions. *Ind. Eng. Chem. Process Des. Dev.* **1982,** *21,* 539–544.

Jou, F. –Y.; Mather, A. E.; Otto, F. D. The Solubility of CO_2 in a 30 Mass Percent Monoethanolamine Solution. *Can. J. Chem. Eng.* **1995,** *73,* 140–147.

Jou, F. –Y.; Otto, F. D.; Mather, A. E. Vapor–Liquid Equilibrium of Carbon Dioxide in Aqueous Mixtures of Monoethanolamine and Methyldiethanolamine. *Ind. Eng. Chem. Res.* **1994,** *33,* 2002–2005.

Kaewsichan, L.; Al–Bofersen, O.; Yesavage, V. F.; Selim, M. S. Predictions of the Solubility of Acid Gases in Monoethanolamine (MEA) and Methyldiethanolamine (MDEA) Solutions using the Electrolyte–UNIQUAC Model. *Fluid Phase Equilib.* **2001,** *183–184,* 159–171.

Kane, L.; Romanow, S. Solvent Process Removes CO_2 from Natural Gas. *Hydrocarbon Process.* **2003,** *82(3),* 27.

Kent, R. L.; Eisenberg, B. Better Data for Amine Treating. *Hydrocarbon Process.* **1976,** *55(2),* 87–90.

Klyamer, S. D.; Kolesnikova, T. L.; Rodin, Y. A. Equilibrium in Aqueous Solution of Ethanolamine during the Simultaneous Absorption of Hydrogen Sulfide and Carbon Dioxide from Gases. *Gazov. Promst.* **1973,** *18,* 44.

Kohl, A.; Nielsen, R. *Gas Purification;* Gulf Publishing Company: Houston, 1997.

Kritpiphat, W.; Tontiwachwuthikul, P. New Modified Kent–Eisenberg Model for Predicting Carbon Dioxide Solubility in Aqueous 2-Amino-2-Methyl-1-Propanol (AMP) Solutions. *Chem. Eng. Comm.* **1996,** *144,* 73–83.

Kumar, P. S.; Hogendoorn, J. A.; Feron, P. H. M.; Versteeg, G. F. New Absorption Liquids for the Removal of CO_2 from Dilute Gas Streams using Membrane Contactors. *Chem. Eng. Sci.* **2002,** *57,* 1639–1651.

Kumar, P. S.; Hogendoorn, J. A.; Versteeg, G. F.; Feron, P. H. M. Kinetics of the Reaction of CO_2 with Aqueous Potassium Salt of Taurine and Glycine. *AIChE J.* **2003,** *49,* 203–213.

Kuranov, G.; Rumpf, B.; Maurer, G.; Smirnova, N. VLE Modelling for Aqueous Systems Containing Methyldiehanolamine, Carbon Dioxide, and Hydrogen Sulfide. *Fluid Phase Equilib.* **1997,** *136,* 147–162.

Lee, J. I.; Otto, F. D.; Mather, A. E. Equilibrium between Carbon Dioxide and Aqueous Monoethanolamine Solutions. *J. Appl. Chem. Biotechnol.* **1976,** *26,* 541–549.

Lee, J. I.; Otto, F. D.; Mather, A. E. The Solubility of H_2S and CO_2 in Aqueous Monoethanolamine Solutions. *Can. J. Chem. Eng.* **1974,** *52,* 803–805.

Lee, L. –J. B. *A Vapor–Liquid Equilibrium Model for Natural Gas Sweetening Process;* University of Oklahoma: Norman, OK, 1996.

Levenspiel, O. *The Chemical Reactor Omnibook;* OSU Book Stores, Inc.: Oregon, 1996.

Li, Y. –G.; Mather, A. E. Correlation and Prediction of the Solubility of Carbon Dioxide in a Mixed Alkanolamine Solution. *Ind. Eng. Chem. Res.* **1994,** *33,* 2006–2015.

Lide, D. R. *CRC Handbook of Chemistry and Physics 84th ed.*; CRC Press: Boca Raton, Florida, 2003.

Littel, R. J.; Versteeg, G. F.; van Swaaij, W. P. M. Solubility and Diffusivity Data for the Absorption of Carbonyl Sulfide, Carbon Dioxide, and Nitrous Oxide in Amine Solutions. *J. Chem. Eng. Data* **1992,** *37,* 49–55.

Liu, Y.; Zhang, L.; Watanasiri, S. Representing Vapor–Liquid Equilibrium for an Aqueous MEA–CO_2 System using the Electrolyte Nonrandom–Two–Liquid Model. *Ind. Eng. Chem. Res*. **1999,** *38,* 2080–2090.

Lyudkovskaya, M. A.; Leibush, A. G. Solubility of Carbon Dioxide in Solutions of Ethanolamines Under Pressure. *Zhur. Priklad. Khim.* **1949,** *22,* 558–567.

Ma'mun, S.; Nilsen, R.; Svendsen, H. F.; Juliussen, O. Solubility of Carbon Dioxide in 30 mass % Monoethanolamine and 50 mass % Methyldiethanolamine Solutions. *J. Chem. Eng. Data* **2005,** *50,* 630–634.

Ma'mun, S.; Svendsen, H. F.; Hoff, K. A.; Juliussen, O. Selection of New Absorbents for Carbon Dioxide Capture. Proc. of the 7th International Conference on Greenhouse Gas Control Technologies (GHGT–7), 2004, refereed paper no. E3–2, Vancouver, Canada.

Manov, G. G.; Bates, R. G.; Hamer, W. J.; Acree, S. F. Values of the Constants in the Debye–Hückel Equation for Activity Coefficients. *J. Am. Chem. Soc.* **1943**, *65,* 1765–1767.

Mason, J. W.; Dodge, B. F. Equilibrium Absorption of Carbon Dioxide by Solutions of the Ethanolamines. *Trans. Amer. Inst. Chem. Eng.* **1936,** *32,* 27–48.

Mathonat, C.; Majer, V.; Mather, A. E.; Grolier, J. –P. E. Enthalpies of Absorption and Solubility of CO_2 in Aqueous Solutions of Methyldiethanolamine. *Fluid Phase Equilib.* **1997,** *140,* 171–182.

Mimura, T.; Shimojo, S.; Suda, T.; Iijima, M.; Mitsuoka, S. Research and Development on Energy Saving Technology for Flue Gas Carbon Dioxide Recovery and Steam System in Power Plant. *Energy Convers. Mgmt.* **1995,** *36,* 397–400.

Mimura; T.; Simayoshi, H.; Suda, T.; Iijima, M.; Mituoka, S. Development of Energy Saving Technology for Flue Gas Carbon Dioxide Recovery in Power Plant by Chemical Absorption Method and Steam System. *Energy Convers. Mgmt.* **1997,** *38,* Suppl., S57–S62.

Mock, B.; Evans, L. B., Chen, C. –C. Thermodynamic Representation of Phase Equilibria of Mixed–Solvent Electrolyte Systems. *AIChE J.* **1986,** *32,* 1655–1664.

Nasir, P.; Mather, A. E. The Measurement and Prediction of the Solubility of Acid Gases in Monoethanolamine Solutions at Low Partial Pressures. *Can. J. Chem. Eng.* **1977,** *55,* 715–717.

Nilsen, R. *CO_2 Absorption: Equilibrium measurements;* Norwegian University of Science and Technology: Trondheim, 2001.

Nilsen, R. *CO_2 Equilibrium and Kinetic Measurements;* Norwegian University of Science and Technology: Trondheim, 2002.

Olander, D. R. Simultaneous Mass Transfer and Equilibrium Chemical Reaction. *AIChE J.* **1960,** *6*, 233–239.

Olofsson, G.; Hepler, L. G. Thermodynamics of Ionization of Water over Wide Ranges of Temperatures and Pressures. *J. Solution Chem.* **1975,** *4,* 127–143.

Onda, K.; Sada, E.; Kobayashi, T.; Fujine, M. Gas Absorption Accompanied by Complex Chemical Reactions – I Reversible Chemical Reactions. *Chem. Eng. Sci.* **1970,** *25*, 753–760.

Park, M. K.; Sandall, O. C. Solubility of Carbon Dioxide and Nitrous Oxide in 50 mass % Methyldiethanolamine. *J. Chem. Eng. Data* **2001,** *46,* 166–168.

Park, S. –B.; Lee, H. Vapor–Liquid Equilibria for the Binary Monoethanolamine+Water and Monoethanolamine+Ethanol Systems. *Korean J. Chem. Eng.* **1997,** *14,* 146–148.

Peng, D. –Y. ; Robinson, D. B. A New Two–Constant Equation of State. *Ind. Eng. Chem. Fundam.* **1976,** *15,* 59–64.

Perry, R. H.; Pigford, R. L. Kinetics of Gas–Liquid Reactions. *Ind. Eng. Chem.* **1953,** *45*, 1247–1253.

Pitzer, K. S. Electrolytes. From Dilute Solutions to Fused Salts. *J. Am. Chem. Soc.* **1980,** *102,* 2902–2906.

Pitzer, K. S. Thermodynamics of Electrolyte. I. Theoretical Basis and General Equations. *J. Phys. Chem.* **1973,** *77,* 268–277.

Poplsteinova, J. *Absorption of Carbon Dioxide – Modeling and Experimental Characterization;* Norwegian University of Science and Technology: Trondheim, 2004.

Porter, K. E. The Effect of Contact–Time Distribution on Gas Absorption with Chemical Reaction. *Trans. Instn. Chem. Engrs.* **1966,** *44*, T25–T36.

Posey, M. L.; Tapperson, K.G.; Rochelle, G. T. A Simple Model for Prediction of Acid Gas Solubilities in Alkanolamines. *Gas Sep. Purif.* **1996,** *10,* 181–186.

Prausnitz, J. M.; Lichtenthaler, R. N.; de Azevedo, E. G. *Molecular Thermodynamics of Fluid–Phase Equilibria;* Prentice Hall PTR: New Jersey, 1999.

Rao, A. B.; Rubin, E. S. A Technical, Economic, and Environmental Assessment of Amine–Based CO_2 Capture Technology for Power Plant Greenhouse Gas Control. *Environ. Sci. Technol.* **2002,** *36,* 4467–4475.

Reddy, S.; Scherffius, J.; Freguia, S.; Robert, C. Fluor's Econamine FG Plus^{SM} Technology: An Enhanced Amine–based CO_2 Capture Process. The 2nd Annual National Conference on Carbon Sequestration, Alexandria, Virginia, May 5–8, 2003.

Rho, S. –W.; Yoo, K. –P.; Lee, J. S.; Nam, S. C.; Son, J. E.; Min, B. –M. Solubility of CO_2 in Aqueous Methyldiethanolamine Solutions. *J. Chem. Eng. Data* **1997,** *42,* 1161–1164.

Robinson, D. B. *Vapor–Liquid Equilibrium Studies: GRI Project – Acid Gas Absorption;* the University of Oklahoma: Norman, OK, 1993.

Robinson, R. A.; Stokes, R. H. *Electrolyte Solutions: the Measurement and Interpretation of Conductance, Chemical Potential and Diffusion in Solutions of Simple Electrolytes,* 2nd ed.; Butterworth Publication Ltd.: London, 1959.

Rochelle, G. T.; Goff, G. S. ; Cullinane, J. T. ; Freguia, S. Research Results for CO_2 Capture from Flue Gas by Aqueous Absorption/Stripping. Proceeding of the Laurance Reid Gas Conditioning Conference LRGCC, 2002, 131–151, Norman, OK.

Rogers, W. J.; Bullin, J. A.; Davison, R. R. FTIR Measurement of Acid–Gas–Methyldiethanolamine Systems. *AIChE J*. **1998,** *44,* 2423–2430.

Roizard, C.; Wild, G. Mass Transfer with Chemical Reaction: the Slow Reaction Regime Revisited. *Chem. Eng. Sci.* **2002,** *57*, 3479–3484.

Sada, E.; Kumuzawa, H.; Butt, M. A. Gas Absorption with Consecutive Chemical Reaction: Absorption of Carbon Dioxide into Aqueous Amine Solutions. *Can. J. Chem. Eng.* **1976,** *54,* 421–424.

Sander, B.; Fredenslund, A.; Rasmussen, P. Calculation of Vapor–Liquid Equilibria in Mixed Solvent/Salt Systems Using an Extended UNIQUAC Equation. *Chem. Eng. Sci.* **1986,** *41,* 1171–1183.

Secor, R. M.; Beutler, J. A. Penetration Theory for Diffusion Accompanied by a Reversible Chemical Reaction with Generalized Kinetics. *AIChE J.* **1967,** *13*, 365–373.

Shaw, T. P.; Hughes, P. W. Optimize CO_2 Removal. *Hydrocarbon Process.* **2001**, *5,* 53–58.

Shen, K. –P.; Li, M. –H. Solubility of Carbon Dioxide in Aqueous Mixtures of Monoethanolamine with Methyldiethanolamine. *J. Chem. Eng. Data* **1992,** *37,* 96–100.

Smirnova, N. A.; Victorov, A. I. Thermodynamic Properties of Pure Fluids and Solutions from the Hole Group–Contribution Model. *Fluid Phase Equilib.* **1987,** *34,* 235–263

Smith, J. M.; Van Ness, H. C.; Abbott, M. M. *Introduction to Chemical Engineering Thermodynamics;* McGraw–Hill: Boston, 2001.

Solbraa, E. *Equilibrium and Non–Equilibrium Thermodynamics of Natural Gas Processing*; Norwegian University of Science and Technology: Trondheim, 2002.

Stephens, E. J.; Morris, G. A. Determination of Liquid–Film Absorption Coefficient: A New Type of Column and Its Application to Problems of Absorption in Presence of Chemical Reaction. *Chem. Eng. Prog.* **1951,** *47,* 232–242.

Suda, T., Iijima, M.; Tanaka, H. ; Mitsuoka, S.; Iwaki, T. Countercurrent Absorption of CO_2 in a Real Flue Gas into Aqueous Alkanolamine Solutions in a Wetted Wall Column. *Environ. Prog.* **1997,** *16,* 200–207.

Suda, T., Iwaki, T.; Mimura, T. Facile Determination of Dissolved Species in CO_2–Amine–H_2O System by NMR Spectroscopy. *Chem. Lett*. **1996,** *9,* 777–778.

Taylor, R. F.; Roberts, F. The Calibration of Disc Type Laboratory Gas–Absorption Column. *Chem. Eng. Sci.* **1956,** 5, 168–177.

Vallée, G.; Mougin, P.; Jullian, S.; Fürst, W. Representation of CO_2 and H_2S Absorption by Aqueous Solutions of Diethanolamine Using an Electrolyte Equation of State. *Ind. Eng. Chem. Res.* **1999,** *38,* 3473–3480.

van Krevelen, D. W.; Hoftijzer, P. J. Kinetics of Gas–Liquid Reactions. Part I. General Teory. *RECUEIL* **1948,** *7*, 563–586.

Versteeg, G. F.; Kuipers, J. A. M.; van Beckum, F. P. H.; van Saaij, W. P. M. Mass Transfer with Complex Reversible Chemical Reactions – I. Single Reversible Chemical Reaction. *Chem. Eng. Sci.* **1989,** *44*, 2295–2310.

Versteeg, G. F.; van Dijck, L. A. J.; van Swaaij, W. P. M. On the Kinetics between CO_2 and Alkanolamines both in Aqueous and Non–aqueous Solutions. An Overview. *Chem. Eng. Comm.* **1996,** *144,* 113–158.

Versteeg, G. F.; van Swaaij, W. P. M. Solubility and Diffusivity of Acid Gases (CO_2, N_2O) in Aqueous Alkanolamine Solutions. *J. Chem. Eng. Data* **1988,** *33,* 29–34.

Weiland, R. H.; Chakravarty, T.; Mather, A. E. Solubility of Carbon Dioxide and Hydrogen Sulfide in Aqueous Alkanolamines. *Ind. Eng. Chem. Res.* **1993,** *32,* 1419–1430.

Williams, M. *Climate Change: Information Kit;* the United Nations Environment Programme (UNEP) and the United Nations Framework Convention on Climate Change (UNFCCC): Geneva, 2002.

Wilson, G. M. Vapor–Liquid Equilibrium. XI. A New Expression for the Excess Free Energy of Mixing. *J. Am. Chem. Soc.* **1964,** *86,* 127–130.

Wilson, G. M.; VonNiederhausern, D. M.; Giles, N. F. Critical Point and Vapor Pressure Measurement for Nine Compounds by a Low Residence Time Flow Method. *J. Chem. Eng. Data* **2002,** *47,* 761–764.

Wu, H. S.; Sandler, S. I. Use of ab Initio Quantum Mechanics Calculations in Group Contribution Methods. 1. Theory and the Basis for Group Identifications. *Ind. Eng. Chem. Res.* **1991,** *30,* 881–889.

Xu, G. W.; Zhang, C. F.; Qin, S. J.; Wang, Y. W. Kinetics Study on Absorption of Carbon Dioxide into Solutions of Activated Methyldiethanolamine. *Ind. Eng. Chem. Res.* **1992,** *31,* 921–927.

Xu, S.; Qing, S.; Zhen, Z.; Zhang, C.; Carroll, J. J. Vapor Pressure Measurement of Aqueous *N*–Methyldiethanolamine Solutions. *Fluid Phase Equilib.* **1991,** *67,* 197–201.

APPENDIX A

Experimental Data

A.1 Measurements of CO_2 Absorption Rate

Table A.1-1. Absorption rates of CO_2 in 5.0 M MEA for various absorbers at 40 °C.

Absorber 1		Absorber 2		Absorber 3	
α	r_{CO2}	α	r_{CO2}	α	r_{CO2}
0.006	41.8	0.006	42.7	0.006	44.0
0.033	40.1	0.039	42.1	0.040	43.4
0.064	38.9	0.080	41.1	0.082	41.8
0.106	37.5	0.142	39.5	0.145	40.0
0.143	36.5	0.189	37.7	0.192	37.9
0.167	35.5	0.249	35.2	0.253	35.4
0.190	34.5	0.279	33.3	0.283	33.4
0.220	33.0	0.301	32.0	0.305	31.6
0.248	31.6	0.340	28.4	0.345	28.2
0.288	29.1	0.378	24.6	0.382	24.3
0.316	26.9	0.399	21.9	0.403	21.3
0.342	25.1	0.418	18.0	0.422	17.4
0.373	22.1	0.438	12.8	0.442	12.5
0.389	19.8	0.459	6.47	0.462	6.35
0.415	16.0	0.468	3.13	0.472	3.27
0.435	12.1				
0.451	7.94				
0.464	3.95				
0.471	1.71				

α = CO_2 loading [mol CO_2/mol amine]; r_{CO2} = absorption rate $\times 10^5$ [mol L^{-1} s^{-1}])

Table A.1-1. (continued)

Absorber 4		Absorber 5		Absorber 6	
α	r_{CO2}	α	r_{CO2}	α	r_{CO2}
0.006	43.5	0.006	43.5	0.006	42.2
0.025	43.1	0.038	39.6	0.043	41.5
0.058	42.5	0.072	38.4	0.084	40.6
0.109	41.6	0.106	37.7	0.115	39.7
0.145	40.6	0.138	36.4	0.145	38.8
0.181	39.4	0.170	35.1	0.166	37.9
0.219	38.0	0.196	34.0	0.195	37.0
0.263	35.8	0.225	32.9	0.219	35.8
0.294	34.1	0.246	31.4	0.254	34.1
0.323	31.9	0.283	29.3	0.282	31.9
0.353	28.8	0.305	27.9	0.310	29.8
0.386	25.0	0.336	25.3	0.338	27.1
0.411	21.2	0.358	23.1	0.358	25.1
0.430	16.8	0.379	20.9	0.374	22.7
0.444	12.8	0.404	17.2	0.399	18.7
0.456	9.17	0.426	13.1	0.417	14.8
0.468	4.93	0.445	9.03	0.434	11.0
0.474	2.68	0.459	4.96	0.448	6.87
		0.468	2.43	0.460	3.98

Table A.1-2. Absorption rates of CO_2 in various concentrations of MEA at 40 °C.

3.3 M MEA		4.1 M MEA		5.0 M MEA	
α	r_{CO2}	α	r_{CO2}	α	r_{CO2}
0.010	41.7	0.007	42.7	0.006	43.4
0.045	41.4	0.036	42.0	0.039	42.8
0.088	41.0	0.080	41.0	0.081	41.5
0.115	40.6	0.118	40.0	0.144	39.7
0.149	39.7	0.150	38.9	0.191	37.8
0.183	38.4	0.181	37.8	0.251	35.3
0.209	37.5	0.221	36.5	0.281	33.3
0.234	36.4	0.255	35.0	0.303	31.8
0.264	34.9	0.287	32.8	0.343	28.3
0.293	33.1	0.317	31.0	0.380	24.4
0.321	31.2	0.345	29.0	0.401	21.6
0.346	29.1	0.374	26.0	0.420	17.7
0.365	27.2	0.391	23.9	0.440	12.6
0.383	25.2	0.417	19.8	0.460	6.41
0.403	22.3	0.436	15.9	0.470	3.20
0.424	18.3	0.453	11.9		
0.436	15.8	0.467	7.83		
0.450	12.2	0.480	4.06		
0.467	7.93	0.485	2.58		
0.483	3.97				
0.488	2.68				

Table A.1-3. Absorption rates of CO_2 in 30 mass % alkanolamine solutions at 40 °C

5.0 M MEA		4.0 M MMEA		3.3 M EMEA	
α	r_{CO2}	α	r_{CO2}	α	r_{CO2}
0.006	43.4	0.020	43.9	0.009	42.1
0.039	42.8	0.062	43.1	0.044	41.6
0.081	41.5	0.103	42.0	0.085	40.7
0.144	39.7	0.144	41.0	0.125	39.8
0.191	37.8	0.183	39.8	0.164	38.7
0.251	35.3	0.221	38.5	0.202	37.4
0.281	33.3	0.262	36.8	0.244	36.0
0.303	31.8	0.302	34.7	0.279	34.3
0.343	28.3	0.343	31.8	0.323	32.0
0.380	24.4	0.383	27.2	0.362	28.8
0.401	21.6	0.401	24.9	0.402	25.2
0.420	17.7	0.421	21.9	0.441	21.7
0.440	12.6	0.442	17.6	0.461	19.1
0.460	6.41	0.461	13.3	0.500	13.6
0.470	3.20	0.480	9.66	0.541	8.29
		0.500	5.03	0.570	3.48
		0.510	2.83		

Table A.1-3. (continued)

2.6 M MDEA		2.5 M BEA		2.9 M AEEA	
α	r_{CO2}	α	r_{CO2}	α	r_{CO2}
0.013	13.2	0.022	40.2	0.025	40.1
0.020	9.12	0.085	39.2	0.085	40.0
0.041	7.83	0.162	37.3	0.122	39.5
0.080	6.64	0.204	36.1	0.165	38.7
0.121	5.75	0.244	34.5	0.200	38.0
0.161	5.25	0.281	32.7	0.242	37.1
0.200	4.86	0.324	30.1	0.283	36.0
0.241	4.16	0.363	27.2	0.342	35.0
0.280	3.57	0.403	23.7	0.423	32.4
0.291	3.37	0.441	19.4	0.504	29.4
		0.462	16.7	0.562	26.8
		0.482	13.9	0.641	22.9
		0.502	11.0	0.703	18.3
		0.521	8.21	0.761	13.1
		0.541	4.77	0.801	8.14
		0.550	3.15	0.821	5.27

Table A.1-4. Absorption rates of CO_2 in mixtures of MDEA at 40 °C.

2.6 M MDEA + 0.43 M BEA		2.6 M MDEA + 0.86 M BEA		2.6 M MDEA + 0.62 M MEA		2.6 M MDEA + 0.62 M PZ	
α	r_{CO2}	α	r_{CO2}	α	r_{CO2}	α	r_{CO2}
0.003	27.2	0.007	27.9	0.007	26.3	0.010	41.5
0.013	25.3	0.021	26.5	0.030	24.9	0.025	40.7
0.031	23.6	0.042	25.0	0.056	23.1	0.053	39.5
0.049	22.5	0.067	23.2	0.072	21.4	0.081	38.8
0.091	20.5	0.096	21.1	0.087	19.9	0.121	36.8
0.121	18.3	0.123	18.9	0.101	18.6	0.153	34.7
0.141	16.6	0.142	17.6	0.126	16.2	0.189	32.2
0.171	14.2	0.159	16.2	0.158	13.5	0.227	29.3
0.189	12.7	0.178	15.0	0.196	11.0	0.256	26.7
0.215	10.5	0.199	13.7	0.215	9.97	0.279	24.3
0.243	8.53	0.215	12.5	0.231	8.49	0.312	21.4
0.263	6.74	0.231	11.2	0.254	6.99	0.340	18.2
0.282	5.06	0.243	10.0	0.278	5.91	0.369	14.8
0.307	3.37	0.262	8.23	0.300	4.43	0.397	11.7
0.317	2.68			0.325	2.70	0.424	8.43
						0.450	4.98

Table A.1-4. (continued)

2.6 M MDEA + 0.62 M AEEA		3.5 M MDEA + 0.62 M AEEA		4.4 M MDEA + 0.62 M AEEA	
α	r_{CO2}	α	r_{CO2}	α	r_{CO2}
0.009	34.5	0.005	27.7	0.005	28.4
0.015	33.3	0.021	26.5	0.011	26.1
0.038	31.9	0.056	24.6	0.016	23.3
0.066	30.4	0.079	22.7	0.042	21.0
0.102	28.1	0.106	20.4	0.056	19.9
0.136	25.5	0.140	17.8	0.083	17.3
0.166	23.0	0.175	14.7	0.117	14.5
0.193	20.8	0.209	11.9	0.150	11.9
0.224	18.1	0.250	8.60	0.186	9.06
0.246	16.3	0.285	5.71	0.212	7.22
0.278	14.0	0.322	2.15	0.237	5.70
0.309	11.0			0.277	3.95
0.331	9.23				
0.353	7.38				
0.387	3.94				
0.406	2.05				

Table A.1-5. Absorption rates of CO_2 in BEA and its mixtures at 40 °C.

3.3 M BEA		4.1 M BEA		2.5 M BEA + 1.6 M MEA		2.5 M BEA + Foam Inhibitor	
α	r_{CO2}	α	r_{CO2}	α	r_{CO2}	α	r_{CO2}
0.010	42.1	0.008	41.4	0.008	43.1	0.011	37.9
0.045	41.5	0.058	40.5	0.037	42.6	0.054	37.6
0.080	41.2	0.101	39.4	0.071	42.0	0.103	36.5
0.127	40.0	0.132	38.5	0.104	41.5	0.144	35.6
0.161	39.1	0.183	36.5	0.137	40.5	0.191	34.0
0.193	37.9	0.212	34.9	0.175	39.4	0.235	32.1
0.243	36.1	0.231	34.0	0.200	38.5	0.277	30.0
0.272	34.0	0.257	31.9	0.236	37.0	0.316	27.9
0.305	32.1	0.283	29.9	0.274	35.1	0.347	25.8
0.351	27.7	0.324	25.9	0.306	32.9	0.369	24.2
0.385	24.1	0.360	22.0	0.339	29.9	0.395	22.0
0.415	19.9	0.384	18.1	0.359	28.1	0.435	17.9
0.439	16.1	0.405	14.1	0.380	25.9	0.471	14.1
0.459	11.9	0.426	10.0	0.409	22.1	0.506	9.9
0.477	8.0	0.443	6.1	0.430	18.0	0.536	6.1
0.497	4.0	0.458	2.6	0.447	14.0	0.555	4.0
0.504	2.4			0.461	10.0		
				0.474	5.9		
				0.486	1.8		

Table A.1-6. Absorption rates of CO_2 in PT and its mixture at 40 °C.

1.0 M PT		1.0 M PT		1.0 M PT		3.0 M PT + 0.62 M MEA	
α	r_{CO2}	α	r_{CO2}	α	r_{CO2}	α	r_{CO2}
0.025	29.6	0.014	32.5	0.023	34.9	0.008	37.3
0.042	28.0	0.042	31.0	0.065	34.3	0.027	37.0
0.075	27.4	0.069	30.6	0.105	33.4	0.057	36.6
0.123	26.6	0.097	30.1	0.144	32.3	0.093	35.9
0.154	25.6	0.123	29.7	0.182	31.0	0.128	34.5
0.184	24.6	0.150	29.0	0.224	29.3	0.156	33.3
0.226	23.0	0.183	27.7	0.263	27.6	0.188	32.1
0.278	20.2	0.224	26.3	0.305	24.6	0.219	30.7
0.322	17.2	0.261	24.3	0.341	21.5	0.268	28.0
0.365	13.0	0.296	22.1	0.361	19.0	0.311	24.6
0.402	8.56	0.332	18.6	0.381	16.0	0.349	21.0
0.422	5.51	0.362	15.0	0.400	12.4	0.380	16.6
0.443	2.15	0.385	11.3	0.421	7.53	0.401	12.5
		0.406	7.26	0.436	4.46	0.420	7.85
		0.427	2.20			0.434	3.90
						0.438	2.71

Table A.1-7. Absorption rates of CO_2 in PZ, AZ, and K_2CO_3 at 40 °C.

2.5 M PZ		3.2 M AZ		1.7 M K_2CO_3 + 1.9 M MEA		1.7 M K_2CO_3 + 1.0 M MEA	
α	r_{CO2}	α	r_{CO2}	α	r_{CO2}	α	r_{CO2}
0.015	46.7	0.022	33.2	0.007	30.9	0.003	29.0
0.082	46.4	0.065	32.1	0.042	28.5	0.022	26.0
0.159	45.7	0.101	31.2	0.082	26.4	0.060	23.3
0.203	45.2	0.141	29.8	0.120	24.5	0.104	20.0
0.278	44.3	0.185	28.7	0.162	22.1	0.141	17.0
0.362	42.9	0.222	27.3	0.203	19.1	0.163	14.8
0.443	41.2	0.262	25.9	0.241	16.0	0.181	12.8
0.519	38.7	0.301	24.7	0.260	14.0	0.202	10.5
0.599	35.1	0.341	23.4	0.281	11.6	0.221	8.7
0.639	32.0	0.363	22.6	0.301	10.1	0.240	7.8
0.681	27.9	0.424	20.2	0.341	8.2	0.281	6.6
0.723	22.6	0.460	18.6	0.381	6.7	0.320	5.8
0.763	15.5	0.501	17.0	0.420	5.2	0.360	5.1
0.782	11.8	0.543	15.0	0.451	3.6	0.400	4.2
0.800	7.72	0.582	13.1			0.438	3.2
0.820	2.73	0.606	12.1				

A.2 Measurements of CO_2 Solubility in Aqueous MEA, MDEA, and AEEA Solutions

Table A.2-1. Solubilities of CO_2 in 30 mass % MEA solution at 120 °C.

α	p_{CO_2} / kPa
0.1550	7.354
0.1766	9.314
0.1843	9.045
0.2085	15.51
0.2326	19.62
0.2381	25.20
0.2560	27.71
0.2901	39.18
0.2967	40.40
0.3004	43.49
0.3125	51.82
0.3191	58.57
0.3298	62.88
0.3424	77.59
0.3424	74.95
0.3500	83.61
0.3594	92.79
0.3882	137.9
0.4182	191.9

Table A.2-2. Solubilities of CO_2 in 50 mass % MDEA Solution at 55, 70, and 85 °C.

55 °C		70 °C		85 °C	
α	p_{CO_2} / kPa	α	p_{CO_2} / kPa	α	p_{CO_2} / kPa
0.2758	65.75	0.2367	95.70	0.1658	129.7
0.5325	172.8	0.2790	117.7	0.1840	150.6
0.6411	277.4	0.3582	177.2	0.2609	242.9
0.7126	388.8	0.4029	220.9	0.3143	353.1
0.7387	490.5	0.4718	273.6	0.3269	355.6
0.7402	485.1	0.4834	306.7	0.3719	451.5
0.7479	492.3	0.5259	379.1	0.4112	555.7
0.7825	585.1	0.5489	430.4	0.4610	658.6
0.7971	684.9	0.5858	486.7	0.4887	754.9
0.8133	779.8	0.5894	488.3	0.4942	754.6
		0.6058	581.4		
		0.6609	688.1		
		0.6786	776.9		
		0.6898	813.4		

Table A.2-3. Solubilities of CO_2 in aqueous solution of 30 mass % AEEA

40 °C		55 °C		70 °C		95 °C		120 °C	
α	p_{CO2}/kPa	α	p_{CO2}/kPa	α	p_{CO2}/kPa	α	p_{CO2}/kPa	α	p_{CO2}/kPa
0.303	0.0110	0.169	0.0136	0.066	0.0161	0.060	0.1205	0.013	0.0626
0.390	0.0225	0.200	0.0220	0.109	0.0348	0.065	0.1629	0.036	0.2368
0.491	0.0663	0.292	0.0441	0.151	0.0484	0.103	0.2287	0.039	0.3137
0.592	0.1574	0.388	0.1075	0.207	0.0968	0.112	0.3173	0.089	0.9509
0.720	0.5745	0.477	0.2401	0.303	0.2293	0.202	0.6342	0.127	1.761
0.814	2.048	0.564	0.5297	0.397	0.4777	0.312	1.739	0.200	4.289
0.891	8.287	0.688	1.730	0.494	0.9846	0.421	3.908	0.278	8.478
		0.754	3.969	0.587	2.269	0.525	8.712	0.351	14.51
		0.829	12.35	0.677	4.637	0.607	16.65	0.368	17.73
		0.858	14.60	0.771	11.70	0.689	32.97	0.369	17.44
		0.920	41.69	0.872	38.26	0.758	67.32	0.477	34.19
						0.813	128.7	0.549	57.83
						0.841	177.9	0.607	82.58
								0.630	108.5
								0.722	222.4

A.3 Measurements of N_2O Solubility in Aqueous AEEA Solutions

Table A.3-1. Solubilities of N_2O in aqueous solutions of AEEA

T / °C	m / (mol mol^{-1})				
	1.20 M	1.80 M	2.40 M	2.94 M	3.50 M
26.3	0.605				
54.8	0.326				
24.8		0.578			
35.1		0.490			
44.5		0.389			
55.1		0.313			
25.9			0.544		
35.2			0.459		
44.8			0.381		
54.8			0.326		
26.5				0.527	
35.6				0.433	
45.5				0.362	
54.9				0.300	
26.0					0.527
35.2					0.434
44.7					0.355
55.2					0.304

A.4 Measurements of Protonation Constant (pK_a) of Aqueous 30 mass % AEEA Solution

Table A.4-1. pH measurements of 30 mass % AEEA from 20 to 60 °C
(V_{HCl}, volume of 5.0 M HCl [mL]; $W_{2.9M\ AEEA}$ = @ 46.84 g)

20 °C		30 °C		40 °C		50 °C		60 °C	
V_{HCl}	pH	V_{HCl}	pH	V_{HCl}	pH	V_{HCl}	pH	V_{HCl}	pH
0.000	12.54	0.000	12.10	0.000	12.00	0.000	11.70	0.000	11.59
0.250	11.94	0.258	11.56	0.254	11.30	0.502	10.87	0.252	11.05
0.502	11.72	0.500	11.33	0.500	11.13	1.000	10.63	0.500	10.80
1.000	11.46	1.000	11.09	1.000	10.86	2.500	10.23	1.000	10.52
2.500	11.08	2.500	10.71	2.500	10.47	5.000	9.88	2.500	10.11
5.000	10.73	5.002	10.36	5.000	10.13	7.500	9.65	5.002	9.73
7.502	10.50	7.504	10.13	7.500	9.90	10.002	9.45	7.526	9.48
10.000	10.30	10.000	9.93	10.000	9.69	12.500	9.27	10.002	9.27
12.504	10.12	12.506	9.75	12.500	9.51	15.000	9.10	12.500	9.08
15.000	9.95	15.000	9.58	15.000	9.34	17.500	8.91	15.002	8.89
17.500	9.78	17.502	9.40	17.500	9.15	20.000	8.72	17.500	8.70
20.000	9.58	20.000	9.20	20.000	8.95	22.500	8.48	19.002	8.59
22.500	9.34	22.500	8.96	22.502	8.71	24.000	8.31	20.000	8.51
25.000	9.00	25.002	8.63	25.000	8.38	25.000	8.16	21.000	8.42
26.000	8.82	26.000	8.45	26.000	8.20	26.000	7.99	22.060	8.32
27.000	8.61	27.004	8.25	27.000	8.01	27.000	7.81	23.004	8.22
28.000	8.40	28.000	8.06	28.002	7.82	28.002	7.63	24.006	8.10
29.000	8.22	29.002	7.89	29.000	7.65	29.000	7.46	25.004	7.96
30.002	8.07	30.000	7.75	30.000	7.51	30.000	7.32	26.012	7.80
31.000	7.95	31.000	7.63	32.500	7.24	32.500	7.06	27.002	7.62
32.000	7.84	32.500	7.49	35.000	7.04	35.000	6.85	28.000	7.44
33.000	7.75	35.000	7.28	37.502	6.86	37.508	6.68	29.004	7.28
34.000	7.66	37.502	7.11	40.000	6.70	40.000	6.52	30.006	7.15
35.000	7.59	40.000	6.95	42.500	6.54	42.500	6.36	31.002	7.03
36.000	7.51	42.500	6.80	45.002	6.36	45.002	6.19	32.502	6.88
37.008	7.44	45.000	6.63	47.502	6.16	47.502	5.99	35.000	6.68
38.000	7.38	47.500	6.43	50.000	5.89	50.000	5.73	37.502	6.51
39.000	7.31	50.000	6.16	51.002	5.74	51.002	5.58	40.000	6.35
40.000	7.24	51.002	6.02	52.002	5.53	51.502	5.49	42.502	6.19
42.500	7.08	52.000	5.82	52.500	5.39	52.012	5.38	45.002	6.02
45.000	6.90	52.500	5.68	53.000	5.19	52.502	5.25	47.500	5.82
47.500	6.70	53.000	5.49	53.250	5.04	53.000	5.08	50.000	5.56
50.000	6.43	53.254	5.35	53.400	4.93	53.400	4.86	51.000	5.42
52.002	6.06	53.502	5.16	53.600	4.71	53.500	4.79	52.000	5.23
53.000	5.71	53.752	4.84	53.700	4.54	53.600	4.70	52.500	5.10
53.250	5.57	53.802	4.73	53.752	4.42	53.700	4.59	53.000	4.92
53.500	5.36	53.900	4.42	53.800	4.27	53.800	4.45	53.250	4.81
53.750	4.97	53.924	4.28	53.840	4.08	53.902	4.24	53.500	4.65
53.900	4.21	53.950	4.07	53.860	3.96	53.952	4.08	53.750	4.40
53.920	3.85	53.974	3.73	53.880	3.80	54.002	3.83	54.000	3.84
53.940	3.14	53.990	3.34	53.900	3.53	54.050	3.36	54.040	3.63
53.950	2.88	54.000	3.07	53.920	3.13	54.102	2.50	54.060	3.47
53.962	2.65	54.020	2.67	53.940	2.71	54.150	2.11	54.080	3.26
53.972	2.52	54.040	2.43	53.960	2.42	54.200	1.88	54.100	2.97
53.980	2.43	54.060	2.27	53.980	2.24	54.250	1.74	54.120	2.68
53.992	2.33	54.080	2.15	54.000	2.10	54.302	1.62	54.140	2.45

Table A.4-1. (continued)

20 °C		30 °C		40 °C		50 °C		60 °C	
V_{HCl}	pH	V_{HCl}	pH	V_{HCl}	pH	V_{HCl}	pH	V_{HCl}	pH
54.000	2.27	54.100	2.05	54.024	1.97	54.350	1.54	54.160	2.28
54.052	1.99	54.124	1.96	54.050	1.87	54.402	1.46	54.180	2.15
54.100	1.84	54.150	1.88	54.074	1.79	54.500	1.34	54.200	2.05
54.152	1.71	54.200	1.75	54.100	1.71	55.000	1.01	54.224	1.95
54.200	1.62	54.250	1.66	54.152	1.60	55.500	0.82	54.252	1.85
54.302	1.48	54.300	1.58	54.200	1.51	56.000	0.70	54.300	1.73
54.400	1.37	54.400	1.45	54.300	1.37			54.402	1.54
54.600	1.22	54.500	1.35	54.400	1.26			54.500	1.41
54.800	1.10	54.750	1.18	54.502	1.18			54.750	1.20
55.000	1.01	55.002	1.06	54.750	1.02			55.002	1.06
55.250	0.92	55.250	0.96	55.000	0.91			56.000	0.74
55.500	0.85	55.500	0.89	55.502	0.75			57.010	0.57
56.000	0.74	56.000	0.77	56.006	0.63			58.006	0.45
57.000	0.58	56.500	0.68	56.504	0.55			59.002	0.37
58.000	0.47	57.000	0.61	57.000	0.48			60.000	0.29
59.002	0.38	58.000	0.50	58.000	0.37				
60.000	0.32	59.004	0.41						
		60.000	0.35						

A.5 Measurements of Density and Viscosity of Aqueous AEEA Solutions

Table A.5-1. Densities of aqueous solutions of AEEA for different mass fractions and temperatures.

mass fraction	ρ^{a} / kg m^{-3}	T / °C	ρ / kg m^{-3}
0.000	997.05	10.0	1027.2
0.050	1000.3	20.0	1024.2
0.100	1003.5	25.0	1021.1
0.150	1008.3	30.9	1019.0
0.200	1012.1	39.7	1014.2
0.250	1016.7	49.0	1008.5
0.300	1021.1	59.9	1000.6
0.400	1030.8	69.7	993.83
0.483	1038.6	79.5	988.79
0.600	1046.7	89.7	979.03
0.700	1050.3		
0.800	1046.9		
0.900	1039.9		
1.000	1025.0		

[a] at 25 °C

Table A.5-2. Densities of aqueous 30 mass% AEEA solution partially loaded with CO_2 at 25 °C.

mass of CO_2 added / kg m^{-3}	ρ / kg m^{-3}	mass of CO_2 added / kg m^{-3}	ρ / kg m^{-3}
0.000	1021.1	50.27	1062.9
3.690	1024.4	51.15	1065.2
4.593	1025.1	53.80	1062.9
5.002	1026.1	61.40	1071.8
6.554	1027.1	63.31	1074.4
7.628	1026.0	63.62	1074.8
11.31	1028.6	66.07	1073.7
13.05	1030.6	69.53	1080.5
14.47	1034.0	72.62	1082.2
14.09	1033.8	75.61	1085.6
15.95	1031.4	77.84	1087.7
21.73	1037.4	76.20	1085.5
25.04	1040.4	80.58	1091.5
25.62	1040.8	86.93	1096.7
25.74	1037.7	87.20	1096.6
26.72	1042.4	88.63	1095.4
27.21	1042.6	92.70	1099.6
34.37	1049.9	95.96	1103.1
37.57	1052.4	97.06	1103.8
38.99	1053.4	99.32	1107.7
40.06	1053.5	104.9	1110.0
39.08	1053.4	105.5	1108.0
43.79	1057.5	106.8	1115.9
45.03	1061.0	112.3	1117.0
46.15	1061.5	114.7	1119.7
49.92	1061.2	118.5	1124.0

Table A.5-3. Viscosities of aqueous AEEA solutions

T / °C	1000μ / Pa s				
	1.20 M	1.80 M	2.40 M	2.94 M	3.50 M
20	1.738	2.327	3.208	4.525	6.250
30	1.356	1.785	2.356	3.260	4.332
40	1.143	1.501	2.006	2.714	3.573
50	1.072	1.425	1.986	2.623	3.403

A.6 Measurements of the Reaction Rate Constant

Table A.6-1. The observed pseudo–first order reaction rate constants, k_{obs}, of the CO_2–AEEA–H_2O system

T / °C	k_{obs} / s^{-1}				
	1.20 M	1.80 M	2.40 M	2.94 M	3.50 M
31.7	16383				
34.3	18522				
39.1	23581				
44.3	28834				
49.6	35296				
31.4		26678			
34.6		30798			
38.9		36712			
43.6		47256			
47.7		56274			
32.9			46682		
34.7			48419		
39.5			57180		
44.0			67128		
48.4			78745		
31.6				53857	
36.0				66876	
40.6				78878	
45.0				99128	
49.3				116593	
32.6					77815
35.1					81900
39.6					103522
44.1					122273
49.0					145905

APPENDIX B

PAPER I

Selection of NEW Absorbents for Carbon Dioxide Capture

Sholeh Ma'mun, Hallvard F. Svendsen, and Karl A. Hoff
Department of Chemical Engineering, Norwegian University of Science and Technology
N-7491 Trondheim, Norway

Olav Juliussen
SINTEF Materials and Chemistry, N-7465 Trondheim, Norway

Presented at The 7th International Conference on Greenhouse Gas Control Technologies (GHGT–7), Vancouver, Canada, September 5–9, 2004;
Refereed Paper E3–2

SELECTION OF NEW ABSORBENTS FOR CARBON DIOXIDE CAPTURE

Sholeh Ma'mun[1,†], Hallvard F. Svendsen[1,*], Karl A. Hoff[2] & Olav Juliussen[2]

[1]Department of Chemical Engineering, Norwegian University of Science and Technology
N-7491 Trondheim, Norway
[2]SINTEF Materials and Chemistry, N-7465 Trondheim, Norway

Abstract

This work focuses on selecting new absorbents for CO_2 capture. Absorption of CO_2 was studied at 40 °C using both single and mixed amine-based absorbents. The experimental results show that most absorbents tested have a poorer performance than MEA, but that aqueous AEEA might be a possible contender. In addition to the absorption measurements, the VLE of CO_2 in the selected absorbent, the aqueous 2.9M AEEA, were studied at 40 and 120 °C. The equilibrium partial pressures of CO_2 in the aqueous 2.9M AEEA at the temperature of the removal (40 °C) and that of regeneration (120 °C) are lower than for aqueous 5.0 M MEA, but the maximum net cyclic capacity is somewhat higher.

Introduction

Removal of acidic gases, e.g., carbon dioxide (CO_2), is an important industrial operation. Carbon dioxide is produced in large quantities by many important industries such as fossil-fuel-fired power plants, steel production, chemical and petrochemical manufacturing, cement production, and natural gas purification. The reasons for the CO_2 removal are traditionally technical and economical concerns. Carbon dioxide present in natural gas will reduce the heating value of the gas and as an acid component it has the potential to cause corrosion in pipes and process equipment and also to cause catalyst poisoning in ammonia synthesis [1]. Natural gas pipe lines usually permit from 1 to 2 percent CO_2 and sometimes as high as 5 percent [2]. In the past decades, CO_2 removal from flue gas streams started as a potentially economic source of CO_2, mainly for enhanced oil recovery (EOR) operations. Moreover, CO_2 was also produced for other industrial applications such as carbonation of brine, welding as an inert gas, food and beverage carbonation, dry ice, urea production, and soda ash industry [3, 4]. However, environmental concerns, such as the global climate change, are now focused as one of the most important and challenging environmental issues facing the world community, and have motivated intensive research on CO_2 capture and sequestration. Carbon dioxide as one of the greenhouse gases (GHG) is currently responsible for over 60% of the enhanced greenhouse effect, methane (CH_4) contributes 20%, and the remaining 20% is caused by nitrous oxide (N_2O), a number of industrial gases, and ozone. Scientific evidence now strongly suggests that increased levels of GHG may lead to higher temperature, and cause climate change on a global scale. Various climate models estimate that the global average temperature may rise by about 1.4–5.8 °C by the year 2100 [5].

A wide range of technologies currently exists for separation and capture of CO_2 from gas streams as given in [3]. Such systems have been used in the chemical industry and in the production of technical gases for industrial and laboratory use [6]. Absorption with amine-based absorbents is the most common technology for CO_2 removal today. It is a process with considerable inherent problems, particularly when used on large gas flows,

* Corresponding author: Tel. +47-735 94100, Fax. +47-735 94080, Email: hallvard.svendsen@chemeng.ntnu.no
† Permanent address: Department of Chemical Engineering, Gadjah Mada University, Jl. Grafika 2 Jogjakarta, Indonesia 55281

e.g., exhaust resulted from fossil-fuel-fired power stations. The processes are bulky, leading to large investment costs, high-energy consumption, and the absorbents in use to day are not stable and form degradation products that need to be handled.

A chemical that is to be used as a new commercial absorbent for removal of CO_2 will require both a high net cyclic capacity and high reaction/absorption rate for CO_2, as well as high chemical stability, low vapor pressure, and low corrosiveness. Aqueous solutions of alkanolamines are the most commonly used chemical absorbents for the removal of acidic gases (CO_2 and H_2S) from natural, refinery, and synthesis gas streams. Among them, aqueous monoethanolamine (MEA) as a primary amine has been used extensively for this purpose especially for removal of CO_2. It has several advantages over other commercial alkanolamines, such as high reactivity, low solvent cost, low molecular weight and thus the high absorbing capacity on a weight basis, reasonable thermal stability and thermal degradation rate. The disadvantages of MEA include high enthalpy of reaction with CO_2 leading to higher desorber energy consumption, the formation of a stable carbamate and also the formation of degradation products with COS or oxygen-bearing gases, inability to remove mercaptans, vaporization losses because of high vapor pressure, and more corrosive than many other alkanolamines and thus needs corrosion inhibitors when used in higher concentration [7-10]. Due to its wide use and advantages compared to other alkanolamines, MEA is set as a base case in this work. The parameters evaluated here are the absorption rate and the cyclic capacity.

This work focuses on selecting new absorbents for CO_2 capture using a screening method giving the absorption rate as function of loading, a molar ratio between CO_2 absorbed and absorbent used. The vapor-liquid equilibria (VLE) of CO_2 in a selected absorbent at temperature of removal (40 °C) and that of regeneration (120 °C) were also studied. The objective of the work described here is to select new and more acceptable absorbents or absorbent mixtures whose absorption rate and net cyclic capacity are higher than the existing ones, thereby reducing the energy consumption of the removal process.

Materials and Methods

Materials

The CO_2 (min. 99.99%) and N_2 (min. 99.6 and 99.999%) gases used were obtained from AGA Gas GmbH. The alkanolamines were obtained from Acros Organics and used without further purification. Those selected were monoethanolamine (MEA) – [$H_2N(CH_2)_2OH$], 2-(butylamino)ethanol (BEA) – [$CH_3(CH_2)_3NH(CH_2)_2OH$], N-methyl-diethanolamine (MDEA) – [$CH_3N(CH_2CH_2OH)_2$], 2-(methylamino)ethanol (MMEA)– [$CH_3NH(CH_2)_2OH$], 2-(ethylamino)ethanol (EMEA) – [$CH_3CH_2NH(CH_2)_2OH$], 2-(2-aminoethyl-amino)ethanol (AEEA) – [$H_2N(CH_2)_2NH(CH_2)_2OH$] and reported purities were not less than 99, 98, 98.5, 99, 98, and 97%, respectively. Other absorbent chemicals tested were piperazine (PZ) – [-$NH(CH_2)_2NH(CH_2)_2$-] (Acros Organics, min. 99%) and potassium salt of taurine (PT) which was prepared by neutralizing taurine [2-aminoethanesulfonic acid – $H_2N(CH_2)_2SO_3H$] (Acros Organics, 99%) with an equimolar amount of potassium hydroxide (KOH) (Merck, p.a.).

Screening Apparatus

The absorbent selection experiments were carried out in a screening apparatus as shown in Figure 1. The apparatus designed to operate at atmospheric pressure and temperatures up to 80 °C consists of six 1-liter glass absorbers, six K-type thermocouples,

a HETO circulating heater (Type 02 T 623), a Hartmann & Braun Uras 3G IR CO_2 analyzer, and a BRONKHORST HI-TEC $N_2/CO_2/H_2S$ mass flow controller (Type E-7100). The data acquisition system uses LabVIEW. Before starting the experiment, a CO_2-N_2 gas mixture containing 10 vol% CO_2 with flowrate of 5 $NL.min^{-1}$ was circulated through a by-pass valve to calibrate the analyzer. As the process started the by-pass valve closed automatically. The gas mixture was passed through a water saturator and then to the absorber containing 750 mL of absorbent, being either a single or mixed absorbent. The gas phase leaving the absorber was cooled and the CO_2 content directly determined by IR analysis. The temperature of water bath was maintained at 40 ± 0.1 °C. The gas CO_2 content, the temperatures, and the gas flow rates were collected by the LabVIEW data acquisition system. The process automatically terminated when the concentration of CO_2 in the outlet reached 9.5 vol% (9.5 kPa CO_2 partial pressure). After terminating the experiment, a liquid sample was then analyzed by the barium chloride method. The amount of HCl not used to dissolve $BaCO_3$ was titrated with 0.1M ($mol.L^{-1}$) NaOH carried out with an automatic titrator (Metrohm 702 SM Titrino) with end point pH 5.2.

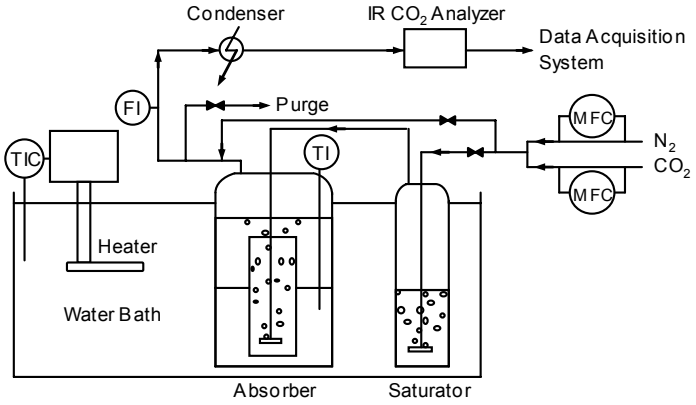

Figure 1: Screening apparatus for CO_2 capture

VLE Apparatuses

The equilibrium measurements were carried out in the VLE apparatuses for atmospheric and medium pressures as shown in Figures 2 and 3. The VLE apparatus for atmospheric pressure designed to operate at temperatures up to 80 °C consists of four 360-cm^3 glass flasks, a Fisher-Rosemount BINOS® 100 NDIR CO_2 analyzer, a BÜHLER pump (Type P2), and two K-type thermocouples. A preloaded amine solution of 150 cm^3 was fed into flask 2. The same amount was also fed into flasks 3 and 4 while flask 1 was used as gas stabilizer. The flasks were heated by water and placed in thermostated box with temperature measured to within ±0.1 °C. The gas phase was circulated as the temperature reached the desired temperature. Equilibrium was obtained when the analyzer showed a constant value. This took approximately 30 to 60 minutes. A liquid sample was then withdrawn from the flask 4 to be analyzed.

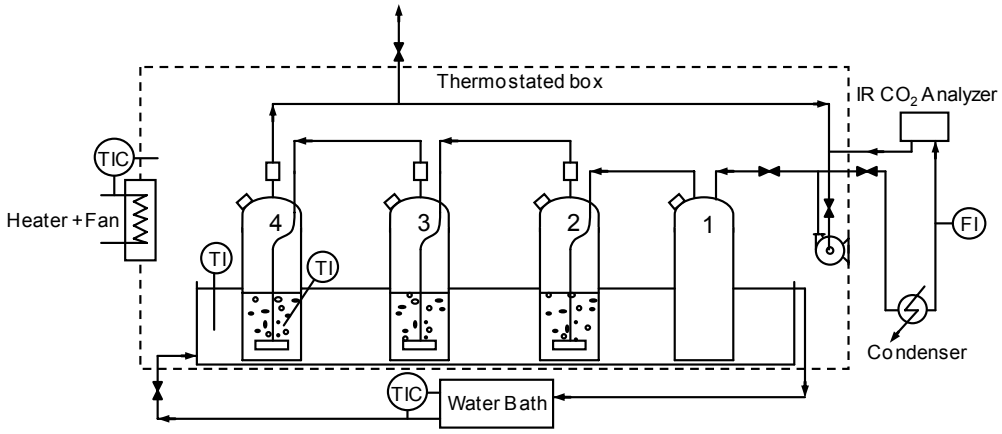

Figure 2: Vapor-liquid equilibrium apparatus for atmospheric pressure

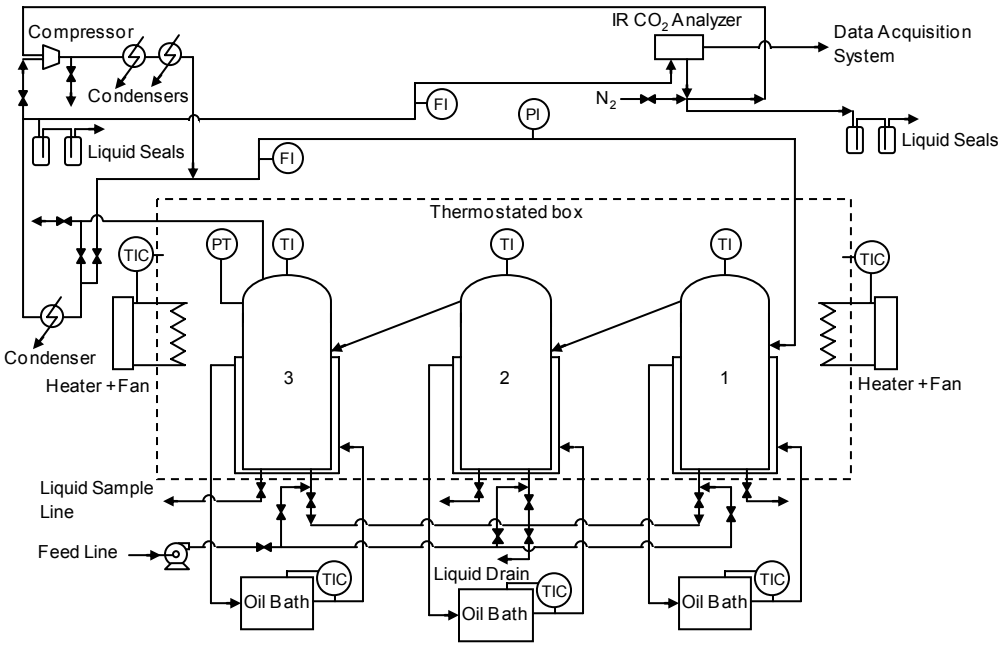

Figure 3: Vapor-liquid equilibrium apparatus for medium pressure

The VLE apparatus for medium pressure is designed to operate at pressures up to 7 bara and temperatures up to 130 °C. It consists of three 300-cm^3 stainless steel cylindrical tanks, a SERA (Seybert & Rahier GmbH) diaphragm pump (Model ZR 408W), a KNF Neuberger compressor (Model PM 15785-145), a Bourdon pressure gauge, a Druck PTX 610 pressure transducer with accuracy ±0.3% of full scale, four K-type thermocouples, and a Fisher-Rosemount BINOS® 100 NDIR CO_2 analyzer. The data acquisition uses FieldPoint™ FP-1000 and FP-AI-110. The cylinders placed in thermostated box were heated by oil baths and the temperatures were measured to within ±0.1 °C. Before starting the experiment, N_2 was flushed through the apparatus to purge out the air within the cylinders. A preloaded amine solution of 200 cm^3 was then fed into the cylinder 1 while cylinder 2 and cylinder 3 held 150 cm^3 each. To prevent boiling and vaporization of the absorbent during the heating up, the minimum initial pressure in the cylinders was set to 2 barg. As the temperature reached the desired temperature the compressor increased the

pressure up to 6 barg and circulated the vapor. A backpressure valve was used to maintain the pressure at 6 barg. Equilibrium was obtained when the temperature was established at a constant value. This took about 2 to 3 hours. After equilibrium was obtained, a liquid sample was withdrawn from cylinder 3 into a 75-cm^3 evacuated sampling cylinder such that the cylinder was always completely filled by the liquid sample. The cylinder containing the sample was then cooled to ambient temperature.

The liquid analysis procedures for both the VLE apparatuses were the same as mentioned before. Due to absorbent losses during the process at high operating temperature, the amine concentrations were then determined by titration. The liquid sample of 0.5 cm^3 was diluted into deionized water of 75 cm^3 and titrated with 0.1M H_2SO_4 (Metrohm 702 SM Titrino). The end point was obtained at pH about 4 to 5.

Results and Discussion

Screening Tests

Absorption rates of CO_2 in amine-based absorbents and their mixtures were measured at 40 °C. To evaluate the absorption rates of CO_2 in single amine-based absorbents, BEA, MDEA, EMEA, AEEA, and MMEA, a constant weight basis, 30wt%, was used for all absorbents. This implies that the molar concentrations (M) were not the same, and generally lower than that of MEA. However, the optimal operational concentrations for these absorbents are not known a priori so a comparison based on weight fraction might be as good as one based on constant molarity. The absorption rates of CO_2 in Piperazine (PZ) and some mixtures of MDEA were also measured. In addition to the amine-based absorbents, the potassium salt of taurine (PT) was also tested at a concentration of 2.0M. All the absorbents tested have good solubility in water. MEA, MMEA, and AEEA are miscible and the rest of the absorbents are very soluble in water. The absorption rate can be calculated by the following formula:

$$r_{CO_2}\left[\frac{\text{mol CO}_2\text{ absorbed}}{\text{L solution}.\text{s}}\right]=\frac{1}{V\left[\text{L solution}\right]}\left(n_{CO_2}^{in}\left[\frac{\text{mol CO}_2}{\text{s}}\right]-\frac{x_{CO_2}^{out}\left[\text{mole fraction}\right]n_{N_2}\left[\frac{\text{mol N}_2}{\text{s}}\right]}{\left(1\text{-}x_{CO_2}^{out}\right)\left[\text{mole fraction}\right]}\right) \quad (1)$$

The relative performance of the amines can be evaluated from Table 1 or Figures 4 and 5. It should be noted that the comparison is semi-quantitative, in the sense that there is no guarantee that the bubble structure, and therefore the gas-liquid interfacial area was exactly the same during all experiments. However, the superficial gas velocity was the same, so differences would arise mainly due to variations in interfacial tension, bubble coalescence properties, and viscosity.

In the loading range lower than 0.18 the absorption rates of CO_2 into aqueous 5.0 M MEA is generally higher than into all the other absorbents except for aqueous 2.5 M PZ and 4.0 M MMEA. Above about 0.32 in loading, however, the absorption rates into MEA are lower than into the other absorbents except for aqueous 2.0 M PT, aqueous 2.6 M MDEA (Figure 4), and the MDEA mixtures with MEA, AEEA, and PZ (Figure 5). It is also clearly shown that the absorption rates of CO_2 into MDEA is by far the lowest compared to all absorbents tested over the whole loading range. As a tertiary amine, MDEA lacks the extra hydrogen atom and does not form carbamate which contributes to increase the overall rate of absorption.

The series of secondary amines, MMEA, EMEA, and BEA, all perform very well. MMEA has even a slightly higher absorption rates than MEA at low loadings and continues to outperform MEA also for higher loadings. One should keep in mind, however, that MMEA has a somewhat higher molecular weight (75 versus 61), and therefore a lower molar concentration. In addition, MMEA has moderate carbamate stability resulting in increased absorbed amounts of CO_2 at low partial pressure [11]. Both MMEA and BEA are foaming and MMEA is in this respect much worse than BEA. A foam inhibitor DREW 210-667 modification 1 (AMEREL 2000) was therefore added in this work at a quantity of 50 ppm into aqueous MMEA. Normally, a foam inhibitor will have a negative impact on the mass transfer characteristics, both by reducing the interfacial area and possibly by increasing the surface resistance. MMEA could thus have an even greater potential than shown here when used in contactors where the two phases are separated, like in membrane contactors.

TABLE 1: ABSORPTION RATES OF CO_2 IN AMINE-BASED ABSORBENTS AND THEIR MIXTURES

(α, CO_2 loading [mol CO_2/mol amine]; r_{CO2}, absorption rate x10^5 [mol.L^{-1}.s^{-1}])

5.0 M MEA		2.5 M BEA		2.6 M MDEA		3.3 M EMEA		2.9 M AEEA		4.0 M MMEA[a)]	
α	r_{CO2}	α	r_{CO2}	α	r_{CO2}	α	r_{CO2}	α	r_{CO2}	α	r_{CO2}
0.0063	43.4	0.0217	40.2	0.0134	13.2	0.0095	42.1	0.0250	40.1	0.0204	43.9
0.0394	42.8	0.0845	39.2	0.0205	9.12	0.0440	41.6	0.0848	40.0	0.0623	43.1
0.0811	41.5	0.1623	37.3	0.0411	7.83	0.0848	40.7	0.1216	39.5	0.1035	42.0
0.1437	39.7	0.2037	36.1	0.0802	6.64	0.1249	39.8	0.1650	38.7	0.1437	41.0
0.1906	37.8	0.2436	34.5	0.1205	5.75	0.1638	38.7	0.2004	38.0	0.1829	39.8
0.2511	35.3	0.2815	32.7	0.1605	5.25	0.2018	37.4	0.2421	37.1	0.2207	38.5
0.2812	33.3	0.3239	30.1	0.2003	4.86	0.2444	36.0	0.2829	36.0	0.2622	36.8
0.3027	31.8	0.3627	27.2	0.2405	4.16	0.2791	34.3	0.3418	35.0	0.3017	34.7
0.3426	28.3	0.4027	23.7	0.2802	3.57	0.3227	32.0	0.4235	32.4	0.3429	31.8
0.3803	24.4	0.4413	19.4	0.2906	3.37	0.3623	28.8	0.5041	29.4	0.3834	27.2
0.4006	21.6	0.4615	16.7			0.4025	25.2	0.5620	26.8	0.4014	24.9
0.4200	17.7	0.4821	13.9			0.4408	21.7	0.6409	22.9	0.4206	21.9
0.4400	12.6	0.5016	11.0			0.4606	19.1	0.7027	18.3	0.4423	17.6
0.4605	6.41	0.5210	8.21			0.5005	13.6	0.7614	13.1	0.4612	13.3
0.4701	3.20	0.5408	4.77			0.5407	8.29	0.8010	8.14	0.4800	9.66
		0.5505	3.15			0.5702	3.48	0.8205	5.27	0.5004	5.03
										0.5100	2.83

2.0 M PT		2.5 M PZ		2.6 M MDEA + 0.62 M MEA		2.6 M MDEA + 0.62 M AEEA		2.6 M MDEA + 0.62 M PZ	
α	r_{CO2}	α	r_{CO2}	α	r_{CO2}	α	r_{CO2}	α	r_{CO2}
0.0136	32.5	0.0153	46.7	0.0067	26.3	0.0086	34.5	0.0100	41.5
0.0416	31.0	0.0822	46.4	0.0299	24.9	0.0146	33.3	0.0246	40.7
0.0693	30.6	0.1595	45.7	0.0558	23.1	0.0379	31.9	0.0533	39.5
0.0965	30.1	0.2031	45.2	0.0718	21.4	0.0657	30.4	0.0812	38.8
0.1234	29.7	0.2783	44.3	0.0868	19.9	0.1025	28.1	0.1214	36.8
0.1496	29.0	0.3619	42.9	0.1007	18.6	0.1357	25.5	0.1532	34.7
0.1834	27.7	0.4425	41.2	0.1259	16.2	0.1658	23.0	0.1888	32.2
0.2236	26.3	0.5191	38.7	0.1581	13.5	0.1932	20.8	0.2269	29.3
0.2612	24.3	0.5986	35.1	0.1957	11.0	0.2245	18.1	0.2565	26.7
0.2957	22.1	0.6386	32.0	0.2146	9.97	0.2460	16.3	0.2790	24.3
0.3320	18.6	0.6811	27.9	0.2314	8.49	0.2782	14.0	0.3115	21.4
0.3618	15.0	0.7229	22.6	0.2543	6.99	0.3092	11.0	0.3395	18.2
0.3849	11.3	0.7630	15.5	0.2779	5.91	0.3314	9.23	0.3687	14.8
0.4065	7.26	0.7821	11.8	0.2999	4.43	0.3528	7.38	0.3968	11.7
0.4265	2.20	0.8002	7.72	0.3251	2.70	0.3870	3.94	0.4236	8.43
		0.8202	2.73			0.4061	2.05	0.4497	4.98

[a)] plus 50 ppm foam inhibitor

It is also clearly seen that aqueous 2.5 M PZ gives the highest absorption rates among all the absorbents tested, and has about the same absorption capacity for CO_2 (loading 0.82) as aqueous 2.9 M AEEA used in this work. BASF has successfully used PZ as a promotor in MDEA systems for high-capacity CO_2 removal in ammonia plants and in natural gas processing, and patented it [12]. However, some environmental concerns have been raised about PZ based on its slow biodegradability. PZ is a diamine with two secondary amine groups. This explains its readiness to exceed 0.50 in loading. The low biodegradability, on the other hand, probably stems from its ring structure. AEEA is also a diamine, with one secondary and one primary amine group. It is a chain molecule and should therefore be an environmentally relatively acceptable absorbent. It is also among the amines with better absorption characteristics as it has a relatively high absorption rates (maximum rate of 40.1×10^{-5} mol.L^{-1}.s^{-1}) at low loadings combined with a high absorption capacity for CO_2 (loading 0.82 at 9.5 kPa CO_2 partial pressure). In addition, the vapor pressure of AEEA is much lower than that of MEA, e.g., P^o_{MEA} = 15.9 kPa [13] and P^o_{AEEA} = 0.969 kPa [14] at 120 °C. However, as MEA, AEEA is also corrosive [4] and this may limit its usefulness.

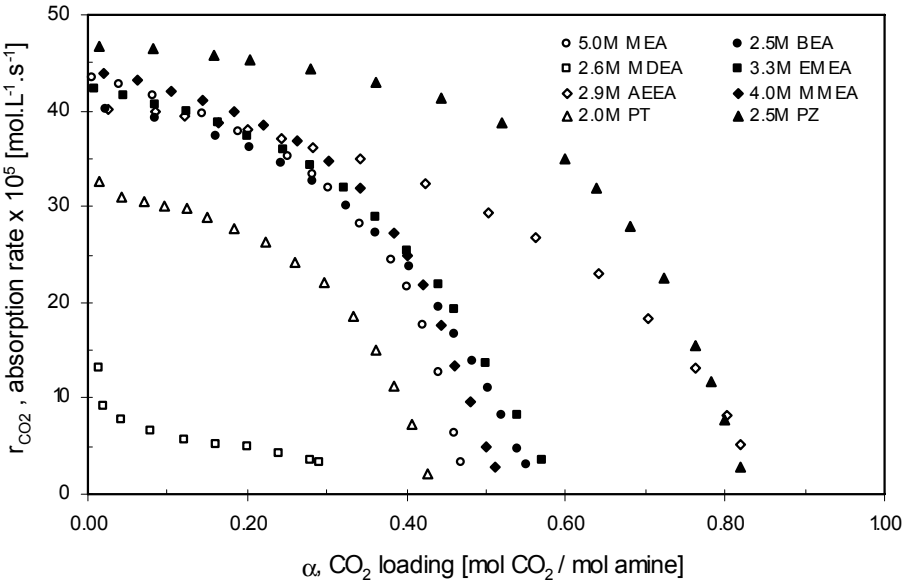

Figure 4: Absorption rates of CO_2 in amine-based absorbents at 40 °C

The absorption rates of CO_2 in several mixtures of MDEA can also be seen in Figure 5. At the same concentration of 2.6 M MDEA and 0.62 M of promotors, aqueous MDEA-PZ mixture gives the highest absorption rates compared to aqueous MDEA-AEEA and aqueous MDEA-MEA mixtures. The mixture MDEA-PZ almost has the same absorption rates as aqueous 5 M MEA at low loadings. This underlines the strong effect of PZ as a promotor.

TNO has developed and patented a range of absorbents based on amino acid salts and given them the trade name CORAL (CO_2 Removal Absorption Liquid). These liquids offer similar absorption characteristics as aqueous alkanolamine solutions, e.g., energy consumption and cyclic loading, better mass transfer and degradation properties, and do not wet polyolefin microporous membranes [15-17]. PT as one of the suggested amino acid salts was also tested in this work at a concentration of 2.0 M. The absorption rates of CO_2

into aqueous PT were found to be lower than into aqueous 5.0 M MEA. Increasing the concentration of PT to above 3 M was found to lead to precipitation at higher loadings.

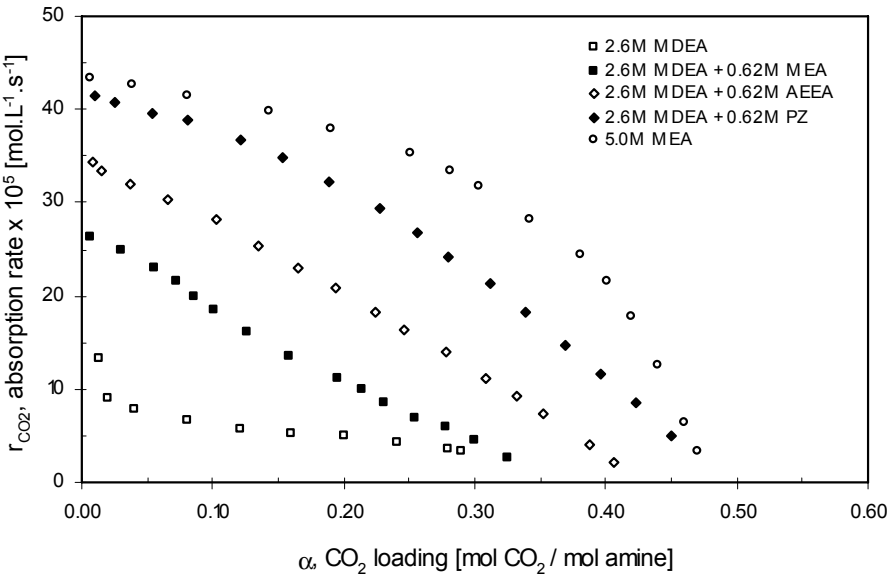

Figure 5: Absorption rates of CO_2 in amine blends at 40 °C

Vapor-Liquid Equilibria and Cyclic Capacity

From the screening test results, AEEA seems to offer somewhat better absorption characteristics than the other absorbents tested as it shows a relatively high absorption rate combined with a high absorption capacity of CO_2. To test the absorbent further, the VLE of CO_2 into aqueous 2.9 M AEEA were therefore studied and measured at the temperature of removal (40 °C) and that typical of the regeneration (120 °C) processes. In addition, the VLE of CO_2 in aqueous 5.0M MEA were also measured at 120 °C in a loading range between 0.18 and 0.42. The results are presented in Figure 6. From this figure it is clear that the cyclic capacities of MEA and AEEA are rather similar, but with a somewhat higher capacity for AEEA.

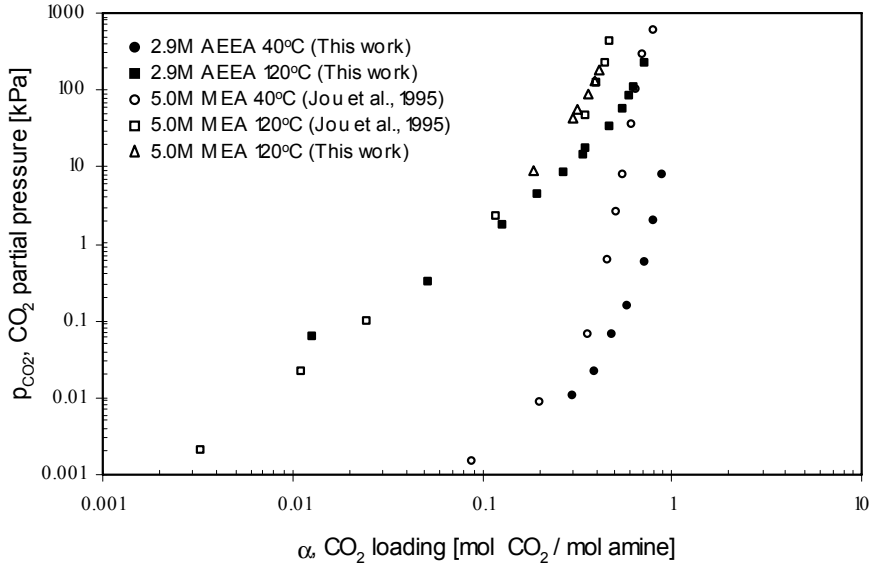

Figure 6: Equilibrium partial pressures of CO_2 in 5.0 M MEA and 2.9 M AEEA solutions

New Method for Comparison of Absorbent Performance

As noted above the difference between AEEA and MEA is not very clear, and a better way of comparing the absorbents is needed. A comparison AEEA and MEA for CO_2 recovery can be made by using a combination of the VLE data in Figure 6 together with the rate data from Figure 4. If, as a first order estimate, it is assumed that equilibrium is attained in both the absorption and stripping steps, the net cyclic capacity (Q) can then be defined as:

$$Q\left[\frac{\text{mol CO}_2\text{ absorbed}}{\text{L solution}}\right] = C_{\text{Amine}}\left[\frac{\text{mol amine}}{\text{L solution}}\right](\alpha - \alpha_{\text{lean}})\left[\frac{\text{mol CO}_2\text{ absorbed}}{\text{mol amine}}\right] \quad (2)$$

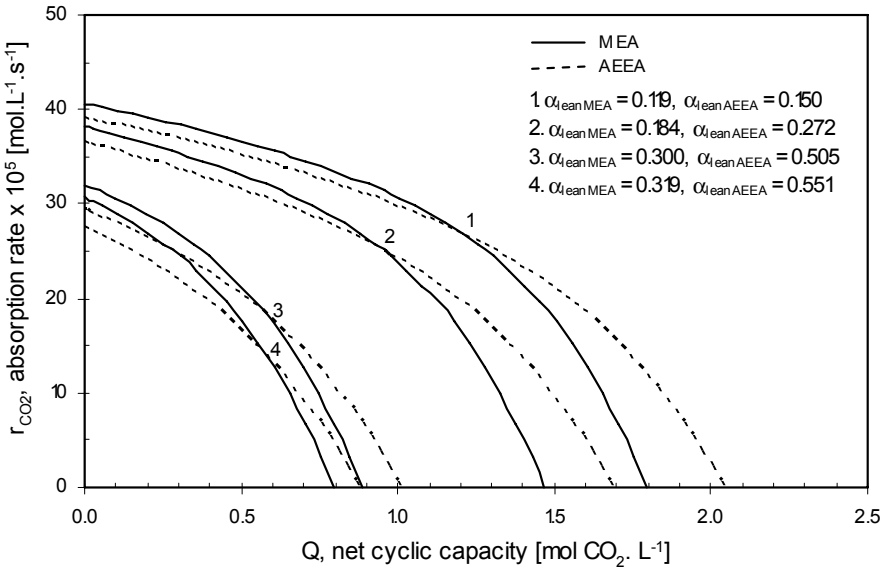

Figure 7: Relationship between absorption rate of CO_2 and net cyclic capacity in 5.0 M MEA and 2.9 M AEEA solutions

The highest difference in net cyclic capacity between AEEA and MEA is obtained as the loading reaches its maximum (α_{max}) in which the absorption rate of CO_2 equals zero as shown in Figure 4. The maximum net cyclic capacity can then be calculated as a function of lean amine loading. The lean amine loading for the two absorbents is determined at a set partial pressure of CO_2. As an example, a maximum net CO_2 pickup of 1.47 M CO_2 absorbed is given by a lean MEA at loading of 0.184 which gives a CO_2 partial pressure of 9.04 kPa at 120 °C. At the same CO_2 partial pressure and temperature, the loading of lean AEEA is 0.272 with a maximum net CO_2 pickup of 1.69 M CO_2 absorbed. The difference in maximum net cyclic capacity between AEEA and MEA is therefore 0.22 M CO_2 absorbed for this case. This has been done for several lean amine loadings as seen in Figure 8 where the maximum net cyclic capacity is given together with the difference in cyclic capacity as a function of lean loading in one of the absorbents (MEA).

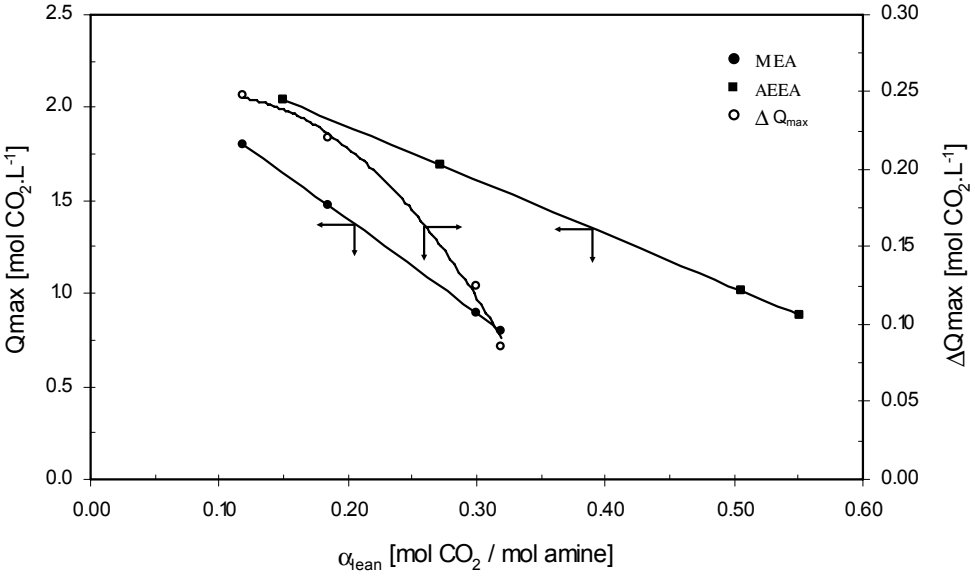

Figure 8: Comparison of maximum net cyclic capacity in 5.0 M MEA and 2.9 M AEEA solutions

In Figure 7, the CO_2 absorption rate is shown as function of the net cyclic capacity for the two absorbents. The results indicate that at high cyclic capacities, as is normally desired in absorption processes, AEEA seems to have better characteristics than MEA. At lower cyclic capacities, MEA is then the better choice. The region where AEEA outperforms MEA seems to increase with decreasing lean loading. In a real process, the loading of rich amine (α_{rich}) is equal to or less than α_{max}. The difference in maximum net cyclic capacity at the same absorption rate will be negative at a rich amine loadings of MEA below 0.38 and those of AEEA below 0.60 for the example mentioned above. This is because the absorption rate of CO_2 in MEA is higher than for AEEA at the observed loadings. It should be noted that increasing the AEEA concentration will strengthen its case even more.

Conclusions

An apparatus for rapid screening of CO_2 absorption chemicals has been developed and a range of absorbents was tested. In general, the main absorption characteristics of absorbents for CO_2 removal are the absorption rate and the absorption capacity of CO_2. The experimental results show that AEEA seems to be a potentially good absorbent for capturing CO_2 from low pressure gases according to the above criteria. It offers high absorption rate combined with high absorption capacity compared to the other absorbents used in this work. In addition, the vapor pressure of AEEA is much lower compared to that of MEA. The maximum net cyclic capacity of AEEA is somewhat higher than that of MEA and maintains its absorption power at higher loadings. A method for comparing absorbents based on a combination of cyclic capacity and absorption rate is proposed and used on an example. In addition to AEEA, MMEA also needs to be considered. It could have a greater potential than indicated here when used in contactors where the two phases are separated, like in membrane contactors.

Acknowledgement

This research was supported financially by the Norwegian Research Council "Klimatek Programme" through the SINTEF Project 661292.01.

References

1. Astarita, G., D.W. Savage, and A. Bisio. 1983. *Gas Treating with Chemical Solvents*. New York: John Wiley & Sons.
2. Buckingham, P.A. 1964. Fluor Solvent Process Plants: How They are Working. *Hydrocarbon Process*. 43, 4: 113-116
3. Rao, A.B. and E.S. Rubin. 2002. A Technical, Economic, and Environmental Assessment of Amine-Based CO_2 Capture Technology for Power Plant Greenhouse Gas Control. *Environ. Sci. Technol.* 36, 20: 4467-4475
4. Suda, T., M. Iijima, H. Tanaka, S. Mitsuoka, and T. Iwaki. 1997. Countercurrent Absorption of CO_2 in a Real Flue Gas into Aqueous Alkanolamine Solutions in a Wetted Wall Column. *Environ. Prog.* 16, 3: 200-207
5. Williams, M. 2002. *Climate Change: Information Kit.* Geneva: the United Nations Environment Programme (UNEP) and the United Nations Framework Convention on Climate Change (UNFCCC).
6. Desideri, U. and R. Corbelli. 1998. CO_2 Capture in Small Size Cogeneration Plants: Technical and Economical Considerations. *Energy Convers. Mgmt.* 39, 9: 857-867
7. Bucklin, R.W. 1982. DGA – A Workhorse for Gas Sweetening. *Oil Gas J.,* 204-210
8. Li, Y.-G. and A.E. Mather. 1994. Correlation and Prediction of the Solubility of Carbon Dioxide in a Mixed Alkanolamine Solution. *Ind. Eng. Chem. Res.* 33, 8: 2006-2015
9. Jou, F.-Y., A.E. Mather, and F.D. Otto. 1995. The Solubility of CO_2 in a 30 Mass Percent Monoethanolamine Solution. *Can. J. Chem. Eng.* 73, 140-147
10. Liu, Y., L. Zhang, and S. Watanasiri. 1999. Representing Vapor-Liquid Equilibrium for an Aqueous MEA-CO_2 System using the Electrolyte Nonrandom-Two-Liquid Model. *Ind. Eng. Chem. Res*. 38, 5: 2080-2090
11. Suda, T., T. Iwaki, and T. Mimura. 1996. Facile Determination of Dissolved Species in CO_2-Amine-H_2O System by NMR Spectroscopy. *Chem. Lett*. 9, 777-778
12. Bishnoi, S. and G.T. Rochelle. 2000. Absorption of Carbon Dioxide into Aqueous Piperazine: Reaction Kinetics, Mass Transfer and Solubility. *Chem. Eng. Sci.* 55, 5531-5543
13. Austgen, D.M. 1989. *A Model of Vapor-Liquid Equilibria for Acid Gas-Alkanolamine-Water Systems*. Ph.D. dissertation, The University of Texas at Austin.
14. Wilson, G.M., D.M. VonNiederhausern, and N.F. Giles. 2002. Critical Point and Vapor Pressure Measurement for Nine Compounds by a Low Residence Time Flow Method. *J. Chem. Eng. Data* 47, 4: 761-764
15. Feron, P.H.M. and A.E. Jansen. 1995. Capture of Carbon Dioxide using Membrane Gas Absorption and Reuse in the Horticultural Industry. *Energy Convers. Mgmt.* 36, 6-9: 411-414
16. Feron, P.H.M. and A.E. Jansen. 1997. The Production of Carbon Dioxide from Flue Gas by Membrane Gas Absorption. *Energy Convers. Mgmt.* 38, Suppl.: S93-S98
17. Kumar, P.S., J.A. Hogendoorn, P.H.M. Feron, and G.F. Versteeg. 2002. New Absorption Liquids for the Removal of CO_2 from Dilute Gas Streams using Membrane Contactors. *Chem. Eng. Sci.* 57, 1639-1651

PAPER II

Solubility of Carbon Dioxide in 30 mass % Monoethanolamine and 50 mass % Methyldiethanolamine Solutions

Sholeh Ma'mun, Roger Nilsen, and Hallvard F. Svendsen
Department of Chemical Engineering, Norwegian University of Science and Technology N-7491 Trondheim, Norway

Olav Juliussen
SINTEF Materials and Chemistry, N-7465 Trondheim, Norway

J. Chem. Eng. Data **2005,** *50,* 630–634

Paper II is not included due to copyright.

PAPER III

Experimental and Modeling Study of the Solubility of Carbon Dioxide in Aqueous 30 Mass % 2-(2-Aminoethyl-amino)ethanol Solution

Sholeh Ma'mun, Jana P. Jakobsen, and Hallvard F. Svendsen
Department of Chemical Engineering, Norwegian University of Science and Technology
N-7491 Trondheim, Norway

Olav Juliussen
SINTEF Materials and Chemistry, N-7465 Trondheim, Norway

Accepted in *Ind. Eng. Chem. Res.* for the CO_2 Capture Special Issue, April 2006

Paper III is not included due to copyright.